CENTRIFUGE MODELING AND NUMERICAL ANALYSIS OF THE BEHAVIOUR OF SUCTION CAISSONS IN CLAY

JIANCHUN CAO

CENTRIFUGE MODELING AND NUMERICAL ANALYSIS OF THE BEHAVIOUR OF SUCTION CAISSONS IN CLAY

By

© Jianchun Cao

B. Eng., M. Eng.

A thesis submitted to the School of Graduate Studies
in partial fulfillment of the requirements for
the degree of Doctor Philosophy

Faculty of Engineering and Applied Science
Memorial University of Newfoundland
December, 2003

St. John's Newfoundland Canada

ABSTRACT

Although suction caissons have been used as mooring systems for offshore structures since 1980s, the working principles of caissons installed in clay and subjected to uplift loading have not been fully understood. Those phenomena include (1) installation resistance during both self-weight and suction penetration; (2) distribution of excess pore pressures, EPPs induced by installation in the soil and their dissipation after installation; (3) setup development; (4) failure mechanism and corresponding appropriate parameters for reasonable prediction of pullout capacity; and (5) distribution of EPPs in soil during pullout of a suction caisson. This study was to investigate these phenomena using both centrifuge modeling and finite element analysis (FEA).

The first part of this study focuses on centrifuge modeling on the behavior of suction caissons in normally consolidated (NC) or slightly overconsolidated (SOC) clay. All caissons were installed in-flight by both self-weight and active suction. The undrained shear strength profile, the penetration resistance profile, the distribution and dissipation of the EPPs in clay during both installation and pullout phases, the passive suction, and the pullout capacity were measured.

Centrifuge test results indicated that the penetration resistance depended not only on the soil properties but also on the effective stress in soil which was influenced by the EPPs. The initial EPPs in the soil induced by installation of a suction caisson can be

described using cylindrical cavity expansion theory. The consolidation time of EPPs can be reasonably predicted using two methods: (1) radial consolidation theory (initially developed for driven piles) through adjusting the radius by the annular base of the caisson wall; and (2) modified Bogard and Matlock method (originally derived for driven piles) by adjusting the diameter or the wall thickness of the caisson to keep the D/Δ ratio (diameter/wall thickness) to a maximum value of 48.

A confined general shear (CGS) failure mechanism is appropriate to describe the soil failure for sealed suction caissons in clay under fast upward loading. A displacement of 4 to 10% of caisson's diameter is required to mobilize maximum reverse end bearing (*REB*). The *REB* is in range 40 to 60% of the total pullout capacity, resulting in a *REB* factor in the range of 6.5 to 10.8. Moreover, a setup curve used to predict the wall skin friction resistance of the caisson at different times after installation is also proposed.

The second part of this study focuses on the numerical investigation of the behavior of suction caissons subjected to vertical loading. A finite element model based on centrifuge model test SAT06 was developed. The caisson-soil interaction was simulated using interface elements. A new method, in which the water inside the caisson is simulated by a very soft porous-elastic material, was introduced to simulate the development of passive suction. This numerical model was validated using the centrifuge experimental results.

Finite element analysis (FEA) results confirmed the failure mechanism of suction caisson in clay observed in the centrifuge tests. Although the passive suction versus

pullout displacement curve obtained using the FEA was slightly different from that obtained from the centrifuge tests, the maximum suction was almost the same, and the pullout force versus displacement curve obtained using FEA was close to that obtained from the centrifuge tests. FEA results also indicated that the distribution of the EPPs in the soil inside the caisson is different from that in the outside soil during pullout of a suction caisson.

In summary, this study has combined centrifuge modeling and finite element analysis to investigate the performance of suction caissons in clay. The study presented in this thesis clarifies several working principles of suction caissons to provide better understanding. They include the friction coefficients for predicting the installation resistance during both self-weight and suction penetration, the distribution of EPPs in clay induced by installation and their dissipation with time, the setup development, the failure mechanism with corresponding parameters, the EPPs in clay during pullout of the caisson, and the simulation of passive suction using FEA.

ACKNOWLEDGMENTS

I would like to express my sincere thanks to my supervisor, Dr. Ryan Phillips, for his guidance, encouragement, and financial support throughout my time at Memorial University of Newfoundland (MUN). I am grateful to my co-supervisor, Dr. Radu Popescu, for providing me detailed guidance and help on Finite Element Analysis in this research. I also wish to thank Dr. A.S.J. Swamidas, a member of my supervisor committee, for his enthusiastic guidance of my research.

I am especially thankful to Dr. Dave Walter for teaching me to carry out centrifuge tests. His work was very helpful. I am very grateful for the help provided by the C-CORE staff members, particularly Mr. Don Cameron, Dr. Paul Barrette, Mr. Tony King, Mr. Richard Hanke, Mr. Karl Tuff, Mr. Steve Smyth, Mr. Ian Durdle and Dr. Fanyu Zhu, in the centrifuge tests. Centrifuge modeling also involved a lot of technical assistance. Mr. Jerry Smith, a member of machine shop of MUN, gave unstinting help during the preparation of the centrifuge test set-up and suction caissons. Special thanks also are due to Dr. Mahmoud Haddara and Mrs. Moya Crocker for their help in my graduate studies.

I greatly appreciate both C-CORE for providing an excellent research environment and Faculty of Engineering and Applied Science of MUN for providing ABAQUS software.

Finally, I would like to express my thanks to my wife, Linghui, for her patience and encouragement, and to my daughter, Yuanxue, for giving me so much happiness during this time.

TABLE OF CONTENTS

LIST OF TABLES

LIST OF FIGURES

NOMENCLATURE

Roman Letters

a	cross-sectional area of standpipe, mm^2
a_0	initial overconsolidation parameter of Cam-Clay Model
A	cross-sectional area of soil sample, m^2
A_{base}	cross section area of caisson including areas of soil plug cross section and annular area of caisson wall, m^2
A_s	combination of internal and external wall skin areas of caisson, m^2
A_{se}	external wall skin area of caisson, m^2
A_{si}	internal wall skin area of caisson, m^2
A_{sp}	internal cross section area of caisson or cross-sectional area of soil plug, m^2
A_{tip}	annular area of caisson wall, m^2
B	bulk modulus, kPa
c_h	coefficient of horizontal consolidation of soil, mm^2/s
CFT	concrete foundation template
CPT	cone penetration test
c_v	coefficient of vertical consolidation of soil, mm^2/s
d	pullout displacement, m
D	caisson diameter, m
$DDCV$	deep draft caisson vessel
DHG	downward hydraulic gradient
D_i	internal diameter of caisson, m
D_o	external diameter of caisson, m
DSS	direct simple shear test
e	void ratio of soil
e_0	initial void ratio of soil
E	Young's (elastic) modulus, kPa
EPP	excess pore pressure, kPa
f_s	unit wall skin friction, kPa
F_{asu}	active suction force, kN
FEA	finite element analysis
F_{ef}	external wall skin friction, kN
F_{if}	internal wall skin friction, kN
F_{psu}	passive suction force, kN
F_{pu}	total pullout force, kN
F_{sf}	combination of internal and external skin frictions, kN
F_{uh}	lateral capacity of suction caisson, kN
g	acceleration of gravity, m/s^2

G shear modulus of soil, *kPa*
Gs specific gravity
h penetration depth, *m*
h_1 hydraulic head across sample at beginning of test ($t=0$) , *m*
h_2 hydraulic head across sample at end of test ($t=t_{test}$), *m*
h_h heave of plug, *m*
H embedment depth, *m*
H_s thickness of clay sample during consolidation, *m*
I_r rigidity index of soil
k permeability, *cm/s*
K third stress invariant parameter
k_h horizontal permeability, *cm/s*
k_τ stress transfer between caisson wall (pile) and soil, *kPa*
k_v vertical permeability, *cm/s*
k_0 coefficient of lateral pressure at rest
L sample length, *m*
LCR load cell reading
LL liquid limit
LVDT linear variable differential transformer
M slope of critical line of Cam-Clay Model
MIT Massachusetts Institute of Technology
I/N scale factor of centrifuge test
N_c bearing capacity factor of clay
NC normally consolidated clay
N_E reverse end bearing factor
N_h lateral bearing capacity factor
N_k an empirical cone factor for evaluating *CPT* results
N_q factor of bearing capacity of sand
NGI Norwegian Geotechnical Institute
OCR overconsolidated ratio
p water pressure in soil, *kPa*
p' mean effective stress, *kPa*
p_i pressure inside caisson top, *kPa*
PI plastic index
PL plastic limit
p_o pressure outside caisson top, *kPa*
PPT pore pressure transducer
q Mises equivalent stress, *kPa*
q_c cone tip resistance, *kPa*
r radius at this point the pore pressure is calculated, *m, or* third stress invariant
r_0 external radius of caisson, *m*
r_i internal radius of caisson, *m*
r_{mas} radius of massive open ended piles, *m*
r_p pile radius or equivalent radius, *m*

R_p radius of plastic zone, *m*
REB reverse end bearing, *kN*
R_{pe} penetration resistance, *kN*
R_{sf} wall skin (shaft) friction resistance, *kN*
R_{tip} tip resistance, *kN*
S devitoric stress tensor
S_t sensitivity of clay
SOC slightly overconsolidated clay
s_u undrained shear strength of clay, *kPa*
$\bar{s}_u$ average undrained shear strength of clay in contact with caisson walls, *kPa*
SDU sustainable development units
SUC slightly underconsolidated clay
$\tilde{s}_u$ average undrained shear strength of clay from mudline to caisson's tip, *kPa*
t time, *second,*
t_m a measure of deviatoric stress at failure of Cam-Clay Model
t_{50} consolidation time at which excess pore pressures were reduced to half of its initial maximum values, *second*
t_{90} consolidation time of 90% degree of consolidation, *second*
T time factor
T_{90} a non-dimensional time factor of soil at 90% degree of consolidation
TLP tension leg platform
T_k non-dimensional parameter
u excess pore water pressure in soil, *kPa*
u_0 initial excess pore pressure in soil, *kPa*
u_{0m} total *in-situ* vertical stress from water column above mudline, *kPa*
u_{tip} pore water pressure in soil at caisson tip, *kPa*
U degree of consolidation
UTA umbilical termination assembles
v pulled out velocity of caisson, *mm/s*
V_0 initial specific volume of soil
W_c submerged (buoyant) weight of caisson, *kN*
WC water content, %
W_s submerged (buoyant) weight of soil plug, *kN*
W_T total submerged (buoyant) weight of caisson and additional dead-weight or ballast that can be added on top of caisson, *kN*
W_w weight of water above caisson, *kN*
z depth below mudline, *m*
z_p vertical distance from mudline to load attachment point (padeye), *m*

Greek Letters

δ_v vertical displacement at laboratory consolidation, *m*

Δ wall thickness, *m*

$\Delta\sigma_m$ increase in mean total stress, *kPa*

$\Delta\sigma_r$ increase of mean stress in *r*-direction, *kPa*

$\Delta p'$ change in mean effective stress due to shearing and remolding of soil

ΔH thickness change of clay sample in laboratory consolidation, *m*

$\Delta\sigma_z$ increase of mean stress in *z*-direction, *kPa*

$\Delta\sigma_\theta$ increase of mean stress in θ-direction, *kPa*

α coefficient for evaluating undrained shear strength of clay

α_f friction coefficient at caisson-soil interface

α_{pe} friction coefficient during installation of suction caisson

α_{pd} friction coefficient of driven pile

α_{pu} friction coefficient during pullout of suction caisson

β coefficient for evaluating undrained shear strength of clay

β_A displacement ratio

β_l wet cap parameter of Cam-Clay Model

γ_w unit weight of water, kN/m^3

γ' submerged (buoyant) unit weight of soil , kN/m^3

δ_v vertical displacement of clay slurry during consolidation, *cm*

ϕ' effective friction angle of sand, *degree*

κ logarithmic elastic bulk modulus

λ logarithmic hardening modulus

ν Poisson's ratio

σ'_h effective horizontal stress, *kPa*

σ'_n effective normal stress, *kPa*

σ_t total tension stress across the base of clay plug, *kPa*

σ_v total vertical stress, *kPa*

σ'_v effective vertical stress, *kPa*

$\sigma'_{v,average}$ average effective vertical stress, *kPa*

σ'_{vb} vertical effective stress in soil at caisson's tip, *kPa*

σ_{v0} total *in-situ* vertical stress, *kPa*

τ_{ad} adhesion between caisson skin and soil, *kPa*

Chapter 1
Introduction

1.1 Suction Caissons

Suction caissons are also known as suction anchors, skirted foundations and bucket piles. They are large cylindrical, triangular or polygonal shape tubular foundations made of steel or concrete. These foundations are open at the bottom and closed with a lid at the top. They are an anchoring mechanism used in marine environments (typical for offshore operations). As more hydrocarbon exploration and development are being carried out in deep waters, floating platforms are frequently being used for both drilling and production. Suction caissons provide an alternative efficient means of tethering various types of floaters and tension leg platforms to the seafloor (e.g., SPARs, deep draft caisson vessels (DDCVs), and semis) or support seabed founded systems (e.g., well heads, sustainable development units (SDUs), and umbilical termination assemblies (UTAs)), and have gained popularity in recent years. They are set in place by both self-weight and active suction induced by pumping the water out of the caisson to create an internal under-pressure relative to the outside water pressure.

Suction caissons have several advantages compared to other mooring systems: (1) the installation of these devices, by both self-weight and active suction, does not require heavy machinery, resulting in lower costs and shorter time for installation; (2) when a vertical or an inclined uplift force is applied by the floating structure, an under-pressure

(passive suction) in the soil inside and at the bottom of the caisson is generated. The resulting combination of passive suction, additional dead-weight or ballast and the soil friction along the outside wall of the caisson, collectively defined as the pullout capacity, reacts to keep the structure in place; (3) there is a large area on top of the caisson where ballast can be stored; (4) suction caissons can achieve substantial horizontal holding capacity or mobilize significant pullout load capacity; and (5) they have a high positioning accuracy, and require no drag-in operations or proof-loading tests. As a result, this type of mooring system is significantly less expensive than other traditional foundations and anchors.

There are generally three kinds of loads acting on suction caissons and the structures they support (Clukey & Morrison, 1993): permanent (static), low frequency cyclic, and cyclic loads. Permanent loads are those that are applied permanently throughout the design life of the floater/platform. They are compensated by self-weight, ballast, and external wall friction of the caisson. Low frequency cyclic loads are loads varying in periods from hours to days and are induced by wind, current, wave drift, and tides. Most of these loads are compensated by dead-weight, and a small component is compensated by passive suction. Cyclic loads are high frequency loads (seconds to minutes). They are generally compensated by reverse end bearing (*REB*) carried through passive suction through the soil at the caisson to its bottom.

Although suction caissons have several operational and logistical advantages over other types of mooring structures, their working principles are still not fully understood.

Firstly, the friction resistance coefficient of the caisson in suction penetration phase is different from that in self-weight penetration phase because of the different "soil flow" pattern due to the application of active suction in the soil inside the caisson. So, more investigations are required on this aspect, especially when the caisson is installed in normally consolidated or slightly overconsolidated clay. Most suction caissons have been used in this kind soil. Secondly, the undrained shear strength of the clay along the wall skin (skirt) of the caisson is reduced due to the remolding of clay during installation of a caisson. This shear strength recovers with time after installation. The regain of the shear strength with time is defined as setup effect and influences the external wall skin friction force, one of the components contributing to the total capacity of suction caissons. More studies are needed to understand both how large the regained shear strength can be and how fast this regain occurs. Thirdly, the installation of a suction caisson induces excess pore pressures (EPPs) in the soil around the caisson. These EPPs which dissipate with time affect the setup effect and the pullout capacity of the caisson. Also, different EPPs are generated in the soil during the pullout of the caisson. The understanding on the distribution of the EPPs in clay when a suction caisson is subjected to an uplift load contributes to the design of suction caissons. Therefore, the EPPs in soil induced during both installation and pullout phases also require further investigations. Fourthly, the increasing use of suction caissons in clay requires a reliable prediction method of the pullout capacity. An appropriate failure mechanism for suction caissons in clay is needed. These are important considerations for designers and operators.

Suction caissons are generally subjected to inclined cyclic loading. The load attachment (padeye) of a suction caisson is usually located at a position about two-thirds of its embedment below mudline, and the chain angle at the attachment point ranges 30° to 50° from horizontal direction. Studies (Deng and Carter, 2000b and 2002, Randolph and House, 2002, and Clukey and Phillips, 2002) indicated that, for a suction caisson having loading angle ranging 30° to 50° from horizontal direction, its vertical capacity still controls its failure mechanism. Previous studies (El-Gharbawy and Olson, 1998, House and Randolph, 2001, and Randolph and House, 2002) showed that the degradation of a caisson capacity from cyclic loading could be as high as 15 to 25%. The maximum capacity of a suction caisson can be determined according to its behavior under a static load. Therefore, more studies on suction caissons subjected to a static vertical load can help designers and users better understand the working principles.

1.2 Objectives and Scope of Present Research

The behavior of a suction caisson is partially affected by the loading condition applied on the caisson. For example, reverse end bearing (REB) can be mobilized when a caisson is under an undrained loading condition (i.e., large loading rate). Combining with external skin friction and caisson submerged weight, a relatively large pullout capacity can be achieved. When a caisson is under a drained loading condition, REB can not be efficiently mobilized, and the combination of external skin friction, internal skin friction and submerged caisson weight gives its capacity. Therefore, the loading condition on a caisson should be taken into consideration for a practical design.

The focus of this research is to investigate the behavior of suction caissons installed in normally consolidated or slightly overconsolidated clay, especially under an undrained loading condition. Its main objectives and scope are as follows:

- Investigation on penetration resistance

The penetration resistance of suction caissons can be evaluated through the sum of the internal and the external wall skin frictions and the tip resistance. Usually, the wall skin friction resistance can be calculated by the product of the average undrained shear strength of the soil near the wall skin (skirt) from mudline to the tip of the caisson, the wall skin area, and the friction coefficient. The friction coefficient, α_{pe}, defined as the ratio of the unit wall skin friction resistance to the undrained shear strength in the soil near the caisson wall skin, is different in self-weight penetration and suction penetration phases. This difference comes from both the soil properties and the effective stress of the soil which is affected by the excess pore pressures (EPPs) induced by installation. In self-weight penetration phase, the EPPs in the soil increase with depth and the rate of the effective stress increase decreases with depth. In suction penetration phase, the effective stress in the soil increases due to the application of the active suction. Moreover, the installation process, such as continuous or staged penetration and the duration of any pauses, also influences the effective stress in the soil. In order to better understand the influence of the effective stress to the penetration resistance, more investigations are required. Therefore, the first objective of this study is to investigate the penetration resistance (friction coefficient, α_{pe}) in self-weight and suction penetration phases.

- Investigation on the setup development along the external wall skin (skirt)

The undrained shear strength of the clay along the wall skin (skirt) of the caisson is reduced to its remolded shear strength, which is the original undrained shear strength, s_u, divided by the sensitivity, S_t. After installation, the remolded shear strength of the soil along the wall skin (skirt) of the caisson will increase with time due to the dissipation of the EPPs, the increasing horizontal effective stress, and the thixotropy (Andersen and Jostad, 2002), resulting in an increase of wall skin friction. This phenomenon is defined as setup development. Since different loads will be applied on the caisson at different times after installation (i.e., hook-up phase, and operation phase), the prediction of the setup effect (i.e., the increase in friction resistance with time) plays a very important role in the design of suction caissons. However, to what magnitude and how fast the setup develops with time is still not fully understood, and very limited studies were carried out. The second objective of this study is to investigate the setup development with time.

- Investigation on the distribution and dissipation of the EPPs

As observed with driven pile foundations, the installation of suction caissons induces the EPPs in the soil around the caisson. These EPPs which dissipate with time affect the setup development. Even though some studies were carried out on the distribution and dissipation of the EPPs, studies on their influence on setup development are required. Also, the pullout of the caisson induces the EPPs (passive suction) in clay. Those EPPs affect the effective stress in the soil, resulting in an influence on the wall skin friction resistance, one of the components contributing to the total pullout capacity of a caisson.

The understanding on the distribution of the EPPs in clay during pullout of a caisson contributes to the design of suction caissons. Therefore, the third objective of this study is to investigate the EPPs in the soil induced during both installation and pullout phases.

- Investigation on failure mechanism of suction caissons in normally consolidated (NC) and slightly overconsolidated (SOC) clay

It is very important for designers and operators to understand the failure mechanism and to use the most appropriate one to predict the pullout capacity. The fourth objective of this study is to investigate the failure mechanism, to develop a simple and reasonable equation for predicting the pullout capacity, and to determine the factors used in the equation.

- Numerical simulation of passive suction using finite element analysis

Finite element analysis (FEA) has been used to simulate the behavior of suction caissons. However, numerical simulation of passive suction is still a challenging problem, which is not fully solved at the present time. Another objective of this study is to simulate the development of passive suction and to investigate the behavior of suction caissons during pullout using FEA.

1.3 Methodology

In this study, a detailed literature review on the studies of suction caissons was first conducted. Based on the literature review and the industrial requirements, the research

objectives mentioned in Section 1.2 were determined. A series of centrifuge model tests were designed to investigate the behavior of suction caissons in clay, and limit equilibrium theory was used to analyze the test data. Finite element analysis (FEA) was carried out to numerically simulate the passive suction and the pullout behavior of suction caissons. The centrifuge test results were compared with those from both FEA and literature.

Centrifuge model tests were the main approach in this study. The model caissons were installed into kaolin clay testbeds with the aid of an actuator. The in-flight installation simulated the correct profiling of the effective stress as that may be encountered in a field installation of suction caissons. A total of eight different clay testbeds (soil samples) were prepared. These testbeds were used to investigate the penetration resistance of suction caissons, the excess pore pressures (EPPs) in the soil during installation and pullout phases, the setup development, and the failure mechanism. Each test package (sample) consisted of a cone penetration test (CPT) and up to three caisson tests. Each caisson test included in-flight caisson installation by both self-weight and active suction and single caisson uplift loading test.

Another method used in this study was finite element analysis (FEA). Based on one of the centrifuge models, a finite element model was developed. The axisymmetric assumption was used, and the stress-strain behavior of the porous soil material (clay) was simulated using Modified Cam-Clay model. The caisson-soil interaction (interface) was simulated by two pairs of surfaces, using Coulomb friction contact. Passive suction

during pullout of the caisson was numerically simulated by replacing the water inside caisson top with a soft porous-elastic material and allowing negative pore water pressures to develop in this soft material. The total pullout force versus the pullout displacement curve, the failure mechanism, the passive suction development, the EPPs in the soil during pullout of a suction caisson obtained from FEA were then compared with the experimental results.

1.4 Major Contributions

The major contributions of this thesis are:

1. The penetration resistance of suction caissons in clay in self-weight penetration and suction penetration phases was confirmed to depend on the effective stress in the soil.

2. The centrifuge tests confirmed that cylindrical cavity expansion theory can also be used to describe the distribution of the EPPs in the soil induced by installation of suction caissons.

3. Both radial consolidation theory and modified Bogard and Matlock's method can be used to predict the dissipation of the EPPs in the soil after installation.

4. A setup curve with time was obtained.

5. The distribution of the EPPs in the soil during pullout of a caisson was found by centrifuge tests and simulated by finite element analysis.

6. Based on both centrifuge test and FEA results, a confined general shear (CGS) failure mechanism was verified to be the most appropriate one to describe the failure of a sealed suction caisson in clay under an undrained loading condition (fast loading rate). An equation was derived to reasonably predict the pullout capacity, and appropriate parameters were determined.

7. Passive suction was numerically simulated using finite element analysis. The caisson-soil interaction was well modeled by contact surfaces.

1.5 Organization of the Thesis

This thesis includes six chapters, the first being the Introduction. Chapter 2 presents the literature review related to the research area covered in this study. The review consists of development and application of suction caissons and previous research work, including design of suction caissons, prediction of penetration resistance, excess pore pressure development due to caisson installation, typical failure mechanism, characteristics of pullout load versus displacement curve, passive suction development during pullout, effect of loading characteristics, numerical investigation on the behavior of suction caissons, and considerations from related pile researches. Published information on laboratory, centrifuge and field testing, in addition to the theoretical and numerical analyses pertinent to the present study, has been reviewed.

Chapter 3 presents the scaling principles and laws, and scaling effects and errors relevant for the centrifuge modeling of suction caissons. This chapter also describes a

detailed discussion on the design of centrifuge tests, preparation of clay testbeds, centrifuge facility and test equipment, and centrifuge test procedure. Details of various laboratory tests performed to estimate the undrained shear strength profile, coefficient of consolidation, and permeability of clay testbed are discussed. The in-flight cone penetration tests conducted to obtain the undrained shear strength (s_u) profiles of testbeds to check with the design s_u profiles in this study are also presented.

The centrifuge test results of installation and pullout testing are presented and analyzed in Chapter 4, including penetration resistance, distribution and dissipation of excess pore pressures (EPP) in clay induced during installation phase, failure mechanism, reverse end bearing (*REB*) and friction development, setup development, and EPP distribution in clay during pullout phase of suction caissons. Those centrifuge results are then compared with the literature documentations.

Chapter 5 describes the numerical analysis on the behavior of suction caissons in clay. A detailed description on the development of the finite element model is presented, including FEA mesh and element type, boundary conditions, soil model and simulation of passive suction. The characteristics of pullout load versus displacement curve and passive suction generated from FEA are discussed and compared with the centrifuge test results.

Finally, the conclusions drawn from the present research are presented in Chapter 6. This chapter also includes recommendations for the future work.

Chapter 2
Literature Review

2.1 History of Suction Caissons

2.1.1 Development

Several types of anchoring systems are currently used in deepwater offshore structures. These anchoring systems include dead-weight anchors, pile anchors, drag anchors, embedded anchors, and suction anchors (Albertsen and Beard, 1982). They are all known as high capacity systems.

Drag embedment anchors have high holding capacity. However, they do not work on rock seafloors. Their behavior is erratic in layered seafloors and their capacity decreases as the cable angle increases from horizontal direction. They also need to be embedded significantly on site to develop their holding capacity. Anchor piles are usually driven into the seafloor by a hammer or a vibrodriver. They develop their holding capacities by mobilizing the lateral earth pressure and wall skin friction in the surrounding seafloor soils. They can resist both lateral and vertical loads. The main disadvantages are that they require large specialized installation equipment and a more comprehensive site survey. The installation costs increase rapidly in deepwater or in exposed locations. Baseplate-dead-weight anchors depend primarily on their own weights to resist the external loads. They have the ability to resist the uplift forces. Their main disadvantages are their

relatively large size and weight compared to other types of anchors and the difficulty of transportation to their operational site.

The principle of a suction caisson was introduced in the 1950's. However, before 1970, suction was only used for the purpose of installation (Hogervorst, 1980, and Senpere and Auvergne, 1982), and only a few laboratory model tests were conducted. After 1970, the research and application of suction caissons developed rapidly, and suction, both active and passive, was used for the installation and the operational phases, respectively. Studies on the behavior of suction caissons have been carried out in the laboratory, field and centrifuge. Numerical and analytical analyses were also conducted. The most important year in the history of suction caisson development was 1979. During that year, twelve large capacity suction anchor piles made from pipes were installed in the North Sea (Senpere and Auvergne, 1982). It was the first commercial application of this technique. In 1989, the Gullfaks C concrete platform, consisting of 16 large diameter skirt piles penetrating 22 meters into the seabed for a gravity base structure stand, was the first application of the concrete suction caisson anchoring system (Tjelta et al., 1990). The application range of suction caissons has since been extended. Table 2.1 shows some key data for suction caissons used in major permanent mooring systems from 1995 to 1998 (Sparrevik, 1998). One recently successful suction caisson installation was completed for BP's Horn Mountain SPAR in Blocks 126/127, Mississippi Canyon Area, Gulf of Mexico (Audibert et al., 2003). Nine caissons, 5.5 m in diameter and 27.7 to 29.3 m in length each, were penetrated into a very soft to soft clay. The caissons were designed to resist the "100-year hurricane, one-line damaged" load. For each line, the

maximum environmental load was 1062 tones with a 41.3° from horizontal direction at mudline. The design ultimate pullout capacity of each caisson was 1355 tones. The water depth on the site was about 1662 m.

Table 2.1: Summary of key data for suction caissons used in major permanent mooring system 1995 - 1998

Field name	Year	Water depth (m)	Mooring system	No of anchors	Soil conditions	Design load (ton)	Load angle	Skirt depth (m)	Dia-meter (m)	Weight (ton)
Nkossa prod. Barge (Elf)	95	180	catenary	14	soft clay	600	15°	12.5	4.5-5	40[1)]
Harding EPSO (BP)	95	110	catenary	8	layered clay/sand	-	-	8-10	5	40
YME FPSO (Statoil)	95	100	catenary	8	layered clay/sand	900	15°	7	5	40
Nome FPSO (Statoil)	96	350	catenary	12	layered clay	-	-	10	5	-
Balder FPSO (Esso)	97	350	riser base	8	layered clay	160	85°	7	5	100[2)]
Njord Semi /FPU(Hydro)	97	330	catenary	20	layered clay	800	15°	7-11	5	40
Curlew FPSU (Shell)	97	90	catenary	9	layered clay/sand	-	15°	9-12	5-7	60-80
Marlim P.19 /26 Semis	97	700-1000	fibre rope taut leg	32	very soft clay	650	40°	13	4.7	80[2)]
Schiehallion FPSO(BP)	97	350	catenary	12	layered clay	1200	15°	12	6.5	130
Visund Semi (Hydro)	97	350	catenary	16	soft/med. clay	800	15°	11[3)]	5[4)]	50
Lufeng FPSO (Statoil)	97	-	catenary	8	soft clay	700	10°	10	5	40
Aquila FPSO (Agip)	97	850	catenary	9	very soft clay	700	15°	16	5	70
Laminaria FPS O(woodside)	98	400	catenary	9	soft clay	-	-	13	5.5	-
Marlim p33/35 FPSO's(Pet.)	98	600	catenary	16	layered clay/sand	1100	15°	17	4.7	75
Asgard A FPSO(Statoil)	98	350	catenary	12	soft clay	-	-	11	5	-
Troll C Semi (Hydro)	98	330	catenary	16	soft clay	800	15°	15	5	70

Notice: 1) without top lid, 2) including ballast, 3) installed by follower with anchor top 2.5 m below mudline, and 4) excluding fins each protruding 1.7 m.

In a nutshell, suction caissons have been used in more than 36 fields with water depth as deep as 1650 m during the last decade (Andersen and Jostad, 2002). These structures have been installed in different types of seabed soil conditions, such as very soft and soft

clay, soft/medium clay, layered clay, and layered clay/sand. The largest design load of a single suction caisson is more than 1200 tons. Suction caissons have the ability to withstand external loads of different angles from the horizontal direction.

Different designs of suction caissons are used for different soil conditions and mooring structures. Caissons with long and slender "stiff pipe" are used for deep penetration in soft clay. Caissons with triangular or squared shape are used for horizontal stability during transportation to prevent desk skidding. Caissons with full-length stiffener plates to increase the vertical friction, and caissons with external wings to increase the projected area, were also developed.

2.1.2 Applications

Suction caissons can be used for both fixed and floating platforms, including floaters, Tension Leg Platforms (TLPs), steel jackets, jack-up rigs, subsea systems, and other offshore structures. They replace conventional mooring systems such as drag anchors, anchor piles, and baseplate and deadweight anchors (Lacasse, 1999, and Sparrevik, 1998). These platforms are usually subjected to permanent, low frequency cyclic, and cyclic loads. Bucket foundations have frequently been used in the North Sea as foundations for jackets or small platforms. A top loaded circular suction anchor is suitable for single anchor buoy moorings as it can be loaded in any direction. These structures can also be used for discrete pipeline supports, and they may work in combination with piles.

Four typical applications of suction caissons are presented here to exemplify their range of suitability.

The first successful commercial application of suction caissons was performed in the North Sea in 1980 (Senpere and Auvergne, 1982). One Catenary Anchor Leg Mooring and twelve anchor points were designed and delivered by Single Buoy Moorings, Inc., to meet the specific requirements and environmental conditions in this area. The twelve suction piles, each composed of a steel cylinder with a diameter of 3.5 m, a length of 8.5 to 9.0 m, and a wall thickness of 25 mm, were embedded in the seabed under 40 m water depth by means of suction. On the site, the top 6 m thick sand layer was underlain by a soft clay with thickness of 1 to 2 m, over a thick stiff clay. The installation time of the twelve suction piles was 18 days which included the time for load testing. The average installation time for each pile was approximately two hours. Even though the design capacity of each pile was as large as 200 tones, suction was only used in the installation phase, and not considered in the operational phase.

The second application of suction caissons, also the first successful application with very deep concrete skirts, was performed in May 1989 in the Gullfaks C concrete platform (Tjelta et al., 1990). This platform was designed for 220 m water depth, and supported by 16 large diameter skirt piles penetrating 22 m into the seabed. The upper 45 m of seabed soils mainly consisted of normally consolidated soft clay, loose clayey and silty sands with interbedded dense sand layers. The skirt penetration resistance, foundation stability, foundation load distribution, and platform settlement were

considered in the design. After a lot of in-situ testing, this example demonstrated that a skirt piled gravity base structure can be successfully installed and operated safely on a soft clay.

The third application was the Snorre TLP in June 1991 (Stove et al., 1992). The Snorre TLP was anchored by four Concrete Foundation Templates (CFT). Each CFT was a three-celled concrete structure with a 720 m^2 base area, and every individual cell had a 17 m diameter and a 35 mm wall thickness. These CFTs were penetrated 12 m into the seabed, located at 300 m depth of water. A clay of 8 m in thickness varying from very soft to soft on the top of the seabed was underlain by a clay of 9 m in thickness varying from medium to stiff and a very stiff clay 9 m in thickness. Before these Concrete Foundation Templates (CFTs) were installed, a detailed study on the foundation design and four Concrete Foundation Templates (CFT) scale model tests (scale ratio 1/13) subjected to different kinds of loads were conducted (Fines et al., 1991).

The fourth application was at the Nkossa field, located in the Gulf of Guinea (Colliat et al., 1996). There were twelve mooring lines. Each line was equipped with a steel suction pile 4.5 m in diameter and 11.25 m in length. The soils under 150 to 170 m depth of water at the site generally consisted of soft normally consolidated clays. The design capacity of each suction pile was 5790 kN.

The examples described above are the early typical applications of suction caissons. They indicated the development of this technique. Additional applications are shown in Table 2.1, and the latest ones are introduced in recent literatures (Erbrich and Hefer,

2002, Sparrevik, 2002, Kolk and Kay, 2002, Dendani and Colliat, 2002, and Audibert et al., 2003).

2.2 Previous Work

As the advantages of this mooring system became better known, further investigations were carried out, including study of various designs, the installation in various soil conditions, and the behavior of the caissons when subjected to different loading conditions such as static, low frequency, and dynamic loads. The behavior of suction caissons, including the magnitude of suction and the characteristics of the bearing capacity with pullout displacement, soil properties and pullout velocity were also studied. These investigations included theoretical analyses, laboratory tests, centrifuge model tests, field (prototype) tests, and finite element analyses.

2.2.1 Designs of Suction Caissons

Suction caissons made of different materials such as steel, concrete, and reinforced concrete have been developed. Suction caissons with permanent top, retrievable top and follower top are used for different in-place conditions. Even though the geotechnical consequences of the internal stiffeners are one of the design issues which are not fully understood (House and Randolph, 2001), long and slender "stiff pipe" caissons or caissons with internal ring stiffeners for deep penetration are still often used due to the increasing soil strength and holding capacity with depth when caissons are installed in

soft clays and suction penetration is available. On the other hand, short and stubby suction caissons are used in dense sand to resist large horizontal loads because of the limited driving depth by active suction. Suction caissons may also be single-celled to multi-celled structures. For example, when the caisson supports a pipe, only one caisson, called a single-celled structure, is needed. When a very big platform is supported by suction caissons, a structure combined of several caissons as a whole, defined as multi-celled structure, is often used

2.2.2 Penetration Resistance

Suction caissons are penetrated into the soil by self-weight and active suction. Generally, the penetration resistance (R_{pe}) consists of wall skin friction resistance (R_{sf}) and tip resistance (R_{tip}). This resistance can be expressed by

$$R_{pe} = R_{sf} + R_{tip} \tag{2.1}$$

For clays, the penetration resistance (Renzi et al., 1991) increases with penetration depth, and the combination of both self-weight and suction is sufficient for penetrating the caisson to the required depth. When limit equilibrium theory is used, Eq. 2.1 can be rewritten as (Renzi et al., 1991)

$$R_{pe} = \alpha_{pe} A_s \bar{s}_u + (s_u N_c + \gamma' h) A_{tip} \tag{2.2}$$

where γ' is the buoyant unit weight of the soil, h is the penetration depth below the mudline, A_{tip} is the base area of the caisson wall, A_s is the combination of the internal and external wall skin areas of the caisson, α_{pe} is an empirical value called friction

coefficient, N_c is a bearing capacity factor, ranging 5 to 9 with depth; s_u is the undrained strength of the clay at the caisson's tip, and $\bar{s}_u$ is the average undrained shear strength of the soil in contact with the caisson walls.

Tjelta et al. (1986) carried out a field test for the design of the Gullfaks C fixed concrete platform. The caisson consisted of two steel cylinders with an outside diameter of 6.5 m, a length of 23 m, and a wall thickness of 35 mm. The soil in the top 45 m was normally consolidated clay and relatively loose clayey and silty sands. They found that the friction coefficient α_{pe} in clay was 0.15, and was not influenced by suction. Andréasson et al. (1988) conducted five model tests with a seven-cell foundation on a soft clay site in the vicinity of Gothenburg. Each cell was a pipe with a diameter of 0.6 m, a height of 0.6 m, and a wall thickness of 4 or 5 mm. The undrained shear strength of the clay on the site was determined as 15 kPa from fall cone and vane shear tests and 12 kPa from triaxial and direct simple shear tests. The sensitivity of the clay is approximately 15. The test results showed that the value of α_{pe} was 0.2 to 0.4 in soft clay when the bearing capacity factor N_c was assumed as 7.

Renzi et al. (1991) performed four centrifuge model tests in soft normally consolidated clays, at a scale factor of 1:100. The model caisson represented a prototype with a diameter of 15 m, a length of 21 m, and a wall thickness of 0.4 m. The test results indicated that α_{pe} was 0.25-0.30 for self-weight penetration and 0.35-0.40 for suction penetration, respectively. House and Randolph (2001) and Randolph and House (2002) carried out four centrifuge model tests at the University of Western Australia, with an

embedment ratio (embedment depth to diameter) of about 4 and at a scale factor of 1:120. Three model caissons were fabricated from aluminum with a semi-rough surface. Model A was a smooth walled caisson, and Model B and Model D were stiffened caissons. Those caissons were used to investigate the influence of the stiffeners on the total penetration resistance of the caissons. A normally consolidated kaolin clay sample was used, and its undrained shear strength profile was $s_u = 1.125$ kPa/m depth with 0 kPa at the mudline. The caissons were subjected to jacked installation at a model rate of 1 mm/s. The test results indicated that the resistance friction coefficient α_{pe} ranged from 0.35 to 0.4.

The friction coefficient α_{pe} depends on both the soil properties and the effective stress in the soil during installation. In a given soil, the distribution and magnitude of the excess pore pressures (EPPs) in the soil are different during self-weight and suction penetration phases respectively, which leads to different friction coefficients. For the same clay, different s_u values can be obtained using different experiment methods, such as direct simple shear test (DSS) and triaxial test, resulting in different α_{pe} values. Also, different tip resistance assumptions (N_c ranges from 5 to 9 and is a function of embedment depth) can derive different penetration friction coefficients. Moreover, the roughness of the caisson wall surface and the area of stiffeners influence the friction coefficient.

There are two more aspects which may affect the friction coefficient in the installation of suction caissons: (1) the ratio of diameter to wall thickness of a caisson; and (2) the setup effect. The clay is partially or fully disturbed by the caisson wall during

installation, the larger the wall thickness, the bigger the disturbed radial range of the clay around the caisson's wall. Therefore, caissons with different ratio of diameter to wall thickness (D/Δ) may have different friction coefficients during installation. As mentioned in Chapter 1, the clay may regain its shear strength from the remolded shear strength due to the dissipation of EPPs, the increased horizontal effective stress, and the thixotropy when there is a stopping during the installation. The regain of shear strength of the soil leads to an increase in the penetration resistance.

For sands, Eq. 2.1, is similar to that used for driving piles and can be rewritten as (Jones et al., 1994)

$$R_{pe} = \pi(D_O + D_i)\int_0^h f_s dz + A_{tip}\sigma'_{vb}N_q \tag{2.3}$$

where D_o and D_i are outside and inside diameters of the caisson, h is the penetration depth of the caisson, A_{tip} is the tip area of the caisson wall, σ'_{vb} is the vertical effective stress in the soil at tip, N_q is a bearing capacity factor, and f_s is the unit wall friction and can be determined by (Jones et al., 1994)

$$f_s = k_0\sigma'_v \tan\phi' \tag{2.4}$$

where k_0 is the coefficient of lateral pressure at rest, σ'_v is effective vertical stress along the wall of the caisson, ϕ' is the effective friction angle of sand along the wall of the caisson.

Piping of sand can also be induced during suction penetration causing the sand surface inside the caisson to rise. The penetration resistance can also be significantly

reduced by the application of suction pressure compared to that for piles driven into the sand. Therefore, the calculated penetration resistance by Eq. 2.3 can be an overestimate (Jones et al., 1994).

The tip resistance can also be evaluated from cone penetration resistance. However, Tjelta et al. (1986) found that the tip resistance in a dense sand layer was 20 to 25% lower than the *in-situ* Dutch cone penetration resistance.

The penetration resistance of suction caissons in sand is large so it can be difficult to penetrate them to the design depth. Some special methods for reducing penetration resistance may be applied. One of these methods is water injection at the caisson's tip. It induces excess pore pressures (EPPs) and reduces the effective stress in the sands at the tip and along the wall skins (skirts) of the caisson. Therefore, both the tip resistance and the wall friction resistance are reduced. Theoretically, a reduction of up to 70% of the wall friction may be achieved by water injection at the tip of the caisson (Rognlien et al., 1991).

2.2.3 Excess Pore Pressures in Soil during Installation

As observed for driven pile foundations, the installation of suction caissons induces excess pore pressures in the soil. The distribution and dissipation of these excess pore pressures determine the pullout capacity development of a suction caisson. It is relatively difficult to investigate the excess pore pressures for suction caissons due to their application environment; and very few people have attempted it. Centrifuge model tests

were used to simulate this behavior of suction caissons in clay (Hjortnaes-Pedersen and Bezuijen, 1992). The modeled prototype, a pipe with a length of 36 m, an inside diameter of 10.5 m, and a wall thickness of 1.27 m, was scaled at both 1:150 and 1:300. The clay testbeds were constructed in four containers by both pre-consolidation in laboratory with different vertical stresses and centrifuge consolidation at 150 g and 300 g, respectively. An in-flight cone penetration test was carried out in each testbed to measure the undrained shear strength profile. The measured s_u profile increased with depth according to s_u / σ_v' (a ratio of undrained shear strength to vertical effective stress) of 0.19 for the 150 g tests and 0.26 for the 300 g tests. They found that, using the cylindrical cavity expansion theory as for driven piles, the initial excess pore pressures u in clay can be described by

$$u = \Delta\sigma_m = \begin{cases} 2s_u \ln(R_p / r) & r_0 \le r \le R_p \\ 0 & r > R_p \end{cases} \tag{2.5}$$

where $\Delta\sigma_m = \dfrac{\Delta\sigma_z + \Delta\sigma_r + \Delta\sigma_\theta}{3}$ is the increase in mean total stress, R_p is the extent of the plastic zone and is equal to $r_0\sqrt{G/s_u}$, G is the shear modulus and G/s_u is the rigidity index I_r, r is a radius, r_0 is the outer radius of the caisson, which, for the skirt of massive open ended piles (caisson), is $r_{mas} = r_0\sqrt{\beta_A}$, where β_A is the displacement ratio $\dfrac{r_0^2 - r_i^2}{r_0^2}$.

After penetration, the excess pore pressures (EPPs) at a depth z can be expressed by Eq. 2.6, Eq. 2.7, and Eq. 2.8 (Hjortnaes-Pedersen and Bezuijen, 1992).

Inside the skirt

$$u = \frac{2(1-k_0)\sigma_v^{'} + 4s_u}{3} + h_h \gamma' Ng + \int_0^z \frac{2}{r_i}\tau_{ad}(z)dz \tag{2.6}$$

Outside the skirt

$$u = s_u \ln(\beta_A G / s_u) + 1/3 \int_0^z \frac{2}{r_r}\tau_{ad}(z)dz \tag{2.7}$$

Near the tip

$$u = \Delta u_{inside} + s_u \ln(G / s_u) \tag{2.8}$$

where h_h is the heave, γ' is the submerged density of the clay, g is the acceleration of gravity, N is the factor by which the acceleration of gravity is increased in the centrifuge, τ_{ad} is the unit adhesion between caisson wall and soil.

The test results also showed that the dissipation time of the excess pore pressures (EPPs) in clay at an acceleration 150 times that of gravity ($N = 150$) was between 2.2 to 2.8 hours, representing 5.5 to 7.2 years in the prototype.

Renzi et al. (1991) conducted four centrifuge model tests in clays (as mentioned in Section 2.2.2). The prototype caisson of 15 m diameter, 21 m length, and 0.4 m wall thickness was scaled at 1/100. The testbed was a normally consolidated clay. The capacity development with time after installation was investigated. The test results indicated that the capacity increased with time after installation due to the dissipation of the excess pore pressures (EPPs), and three to four years were needed after the installation to achieve the ultimate capacity at prototype.

Cylindrical cavity expansion theory can be well used to describe the distribution of the EPPs in clay for driven piles. It has been adopted for suction caissons after some adjustments (Hjortnaes-Pedersen and Bezuijen, 1992). More studies are required to confirm this theory and those adjustments. Otherwise, investigations on the EPPs in soil are needed, so that the dissipation of the EPPs and their influence on the setup effect can be better understood.

2.2.4 Failure Modes

The failure of a suction caisson occurs when the load applied to the caisson exceeds its ultimate pullout capacity (the failure being discussed in this research) or the structure of the caisson is damaged by the applied load and/or soil pressures. The failure mode depends on soil properties, caisson dimensions, and characteristics of the environmental loads. Local shear failure, local tension failure, general shear failure and other failure mechanisms are usually considered in the analysis of pullout capacity.

Eq. 2.9 was used to evaluate the pullout capacity of a suction caisson (Brown and Nacci, 1971, Das et al., 1994, and Datta and Kumar, 1996). This equation is based on the limit equilibrium theory and it takes into consideration the dead weight, self-weight of the caisson, soil plug weight, skin friction and passive suction.

$$F_{pu} = W_T + F_{sf} + F_{psu} \tag{2.9}$$

where F_{pu} is the pullout capacity, W_T is the total buoyant weight of the caisson and additional dead-weight or ballast that can be added on the top of the caisson, F_{sf} is the

combination of the outside skin friction and inside skin frictions and the inside skin friction is limited to the soil plug weight, and F_{psu} is the passive suction force. Hogervorst (1980) used the pile foundation formula to calculate the pullout capacity, and only the total buoyant weight and wall skin frictions were considered. Clukey and Morrison (1993) extended Hogervorst's result to account for caisson shape, load inclination and embedded depth factors.

Fuglsang and Steensen-Bach (1991) and Christensen et al. (1991) in their centrifuge model tests, and Rao et al. (1997) in their laboratory tests on suction caissons in clay found that local shear failure, local tension failure and general shear failure are the most common failure modes of suction caissons under different conditions. These three failure modes are shown in Figure 2.1, and three corresponding equations 2.10 through 2.12 were used to calculate the associated pullout capacities (Fuglsang and Steensen-Bach, 1991, and Christensen et al., 1991).

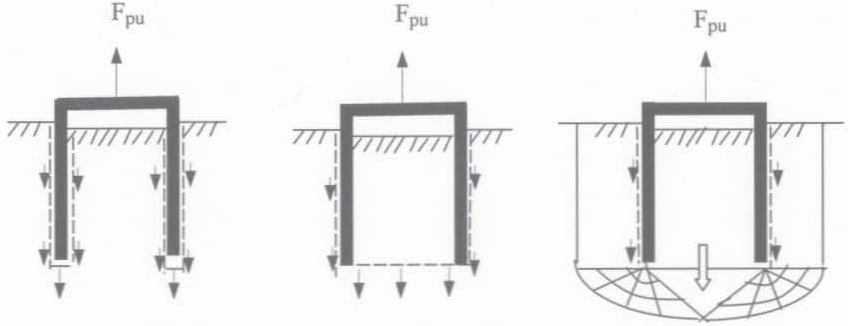

a) Local Shear Failure b) Local Tension Failure c) General Shear Failure

Figure 2.1 Failure mechanisms

For local shear failure

$$F_{pu} = \alpha_{pu} \bar{s}_u A_s + W_c + W_w + A_{tip} u_{tip} \tag{2.10}$$

For local tension failure

$$F_{pu} = W_c + W_s + W_w + \alpha_{pu} \bar{s}_u A_{se} + \sigma_t A_{sp} \tag{2.11}$$

For general shear failure

$$F_{pu} = W_c + W_s + W_w + \alpha_{pu} \bar{s}_u A_{se} + (N_c s_u - u_{tip}) A_{base} \tag{2.12}$$

where F_{pu} is the pullout capacity, W_c , W_s and W_w are the buoyant weights of the caisson, soil plug and water above the caisson respectively, α_{pu} is a non-dimensional friction coefficient, $\bar{s}_u$ is the mean undrained shear strength of the clay along the caisson skin, s_u is the undrained shear strength of the clay at the tip of the caisson, A_{se} is the external skin area of the caisson, A_s is the combination of the internal and external wall skin areas, A_{base} is the cross section area of the caisson including the areas of soil plug and the annular base area, A_{sp} is the internal cross section area of the caisson, A_{tip} is the annular area of the caisson wall, σ_t is the total tension stress across the base of the clay plug, and u_{tip} is the pore water pressure in the soil at the caisson tip.

Christensen et al. (1991) also found that the pullout capacity of a suction caisson can be calculated according to the drained state or transient (partially undrained) state when the caisson was installed in sand. The difference between these two states was that passive suction was taken into consideration in the calculation of pullout capacity for the second state while it was not for the first state.

Several different failure modes may occur when a suction caisson is subjected to inclined loads as indicated in Figure 2.2 (Sparrevik, 1998).

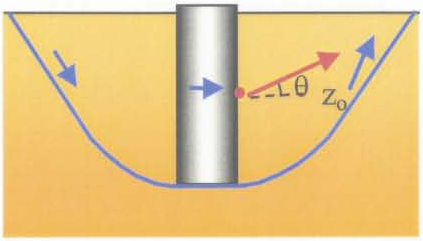

a) optimal location of mooring line for pre-dominantly horizontal loads (translation)

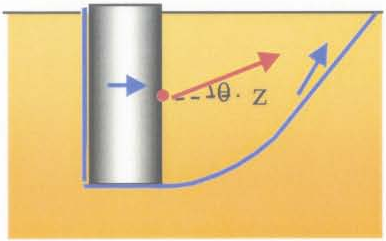

b) same as a) but tension crack form--ing at back of the caisson

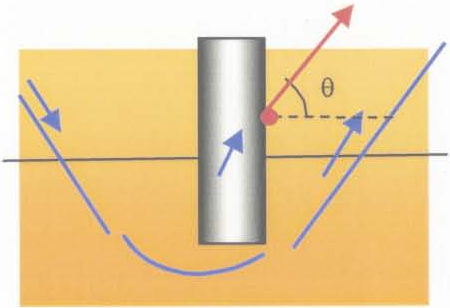

c) optimal location of mooring line for loads with large vertical components (translation)

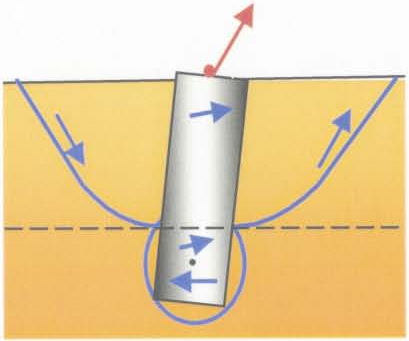

d) same load angle as c) but applied on top of the caisson (translation and rotation failure)

(continued on the next page)

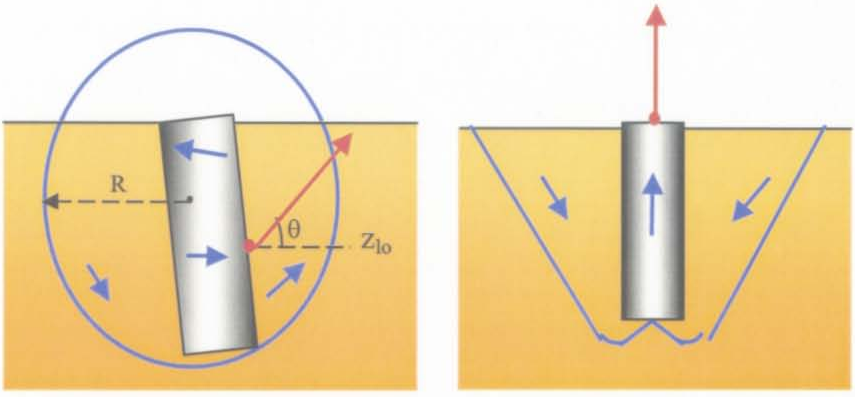

e) mooring line located slightly below optimal position (reversed rotation, large failure surface and no tension crack)

f) optimum location of mooring line for vertical loads (unloading failure)

Figure 2.2 Failure modes for suction caissons (Sparrevik, 1998)

The modes mentioned above can be used in the design of suction caissons. However, which model is the most appropriate when the caissons are installed in normally consolidated or slightly overconsolidated clay? What values of parameters should be used in the design corresponding the selected model? No details were available on these issues in the literature, and more studies are required.

2.2.5 Characteristics of Pullout Load-Displacement Curve

The pullout load versus displacement (F_{pu}-d) curves of suction caissons installed in clays are very different from those of piles or pipes with open tops. This difference was investigated using laboratory and centrifuge model tests in speswhite kaolin clay (Fuglsang and Steensen-Back, 1991). Three types of tests, each one with two piles of 65

mm and 80 mm in diameter respectively, were carried out. Type A was the suction pile, a pipe with a closed top. Type B was a pipe with an open top and a soil plug. Type C was also a pipe with an open top but no soil plug. They found that, for type A, the displacement at failure was relatively large: 10 to 20 mm, exceeding 15% of the diameter. For types B and C, the displacement when the pile achieved its maximum pullout capacity was small. The values ranged from 2 to 4 mm, corresponding to 2% to 4% of the diameter. The total pullout capacity for type A caissons, due to the reverse end bearing, was much bigger than that for type B and type C caissons.

Rao et al. (1997) carried out laboratory tests in soft marine clays to investigate the characteristic of F_{pu}-d curve of suction caissons. Caissons with and without suction and suction caissons with embedment ratio, the ratio of penetration depth to diameter, of 2, 4 and 8 and pullout rate of 0.32, 1.6 and 8.0 mm/min were examined. They observed that, for caissons without suction, the F_{pu}-d curves showed a peak at very small displacement, and that rate did not significantly change the F_{pu}-d behavior. For caissons with suction, the F_{pu}-d curves showed a sharp peak at small displacement corresponding to a maximum wall skin friction force and a mild peak at large displacement showing the full development of suction.

The pullout characteristics of the F_{pu}-d curves of suction caissons depend on both the pullout velocity and the density of the soil when they are used in sands. Generally, the vertical pullout distance at peak tensile load for fully drained tests was less than that for partially drained tests (Jones et al., 1994).

2.2.6 Passive Suction

When a vertical or an inclined load is applied to the platform, an under-pressure is generated in the soil inside and at the bottom of a sealed caisson. This is referred to as passive suction and is one of the principal characteristics of suction caissons. It is normally used to counteract environmental cyclic loads. All previous investigations showed that passive suction depended on soil properties, caisson dimensions, embedment depth and environmental load characteristics.

When suction caissons are installed in clays, a reverse end bearing factor also called suction breakout factor, N_E is used to quantify the effect of passive suction. N_E = suction force/$(A_{sp}s_u)$, where A_{sp} is the cross area of the soil plug at the caisson base and s_u is the undrained shear strength of clay at the base. N_E was found to decrease from 4.5 to 1.5 with an increase of H/D, a ratio of embedment depth to diameter, from 1 to 5 (Das et al., 1994), and a range from 3.5 to 7.5 was obtained by Datta and Kumar (1996). A change in N_E from 2 to 5 was reported by Rao et al. (1997). Those values were obtained through laboratory tests on clay. Both laboratory and centrifuge model tests were used to investigate the reverse end bearing factor with speswhite kaolin clay (Fuglsang and Steensen-Bach, 1991). The suction breakout factor was found to change with embedment ratio, pullout rate, and caisson dimensions in those tests. The value of N_E ranged from 4.7 to 11.3.

When suction caissons were used in sands, passive suction can also be produced in soils inside and below the caisson. The magnitude and duration of this suction depends on both the pullout velocity and the soil permeability. The greater the ratio of pullout velocity to permeability was, the larger the suction was up to a point. At the beginning of pullout, the soil inside the caisson moved with the caisson. With the increase of the pullout, piping in soil plug occurred. When the pullout velocity was increased and equaled to or exceeded a critical value, the soil plug failed in tension at the caisson base and moved upwards with the caisson. Then a state of cavitation was developed along the whole soil plug, and passive suction reached its peak (Christensen and Haahr, 1992, Jones et al., 1994).

2.2.7 Effect of Loading Characteristics

The behavior of a suction caisson also depends on the loading characteristics and pullout velocity. For example, in the laboratory tests, the ultimate pullout capacity was found to be of the same magnitude for both static and oscillating loads in dense sand (Larsen, 1989). However, the capacity to oscillating loads was 1/2 to 2/3 times the static ultimate pullout for normally consolidated clay. Several centrifuge tests (Clukey and Morrison, 1993) showed that the pullout capacity of a suction caisson can be determined using traditional prediction methods for a pile under compressive loading by considering a suction efficiency coefficient in the reverse end bearing. This coefficient was 80% for high frequency loading and 61% for slow rate of loading. Other laboratory tests were used to investigate the behavior of suction caissons in the Gulf of Mexico (El-Gharbawy

and Olson, 1998). The soil used was normally consolidated clay, and both static and cyclic loading conditions on the caisson were simulated. Their work indicated that the pullout capacity of a caisson under long-term conditions was about 2/3 of the pullout capacity of the caisson under short-term conditions. Recent centrifuge tests carried out at University of Western Australia (House and Randolph, 2001 and Randolph and House, 2002), mentioned in detail in Section 2.2.2, showed that the pullout friction resistance, when the caisson is pulled out under drained condition (open lid) immediately after its installation, was about 20% larger than the penetration friction resistance calculated using the friction coefficient in range 0.35 to 0.4. The long term capacity of a suction caisson under sustained axial loading can be at least 75% of the immediate ultimate capacity.

2.2.8 Numerical Investigations

Finite element analyses (FEA) may be used to numerically simulate the behavior of suction caissons. However, these analyses are complex and difficult to apply as they should take into account the penetration by self-weight and suction, pullout, and environmental loading characteristics.

The first finite element model for suction caissons was developed to investigate the pullout behavior of a long-skirted foundation (suction caisson) installed in a soft clay site in the vicinity of Gothenburg (Andréasson et al., 1988). The 3-dimensional foundation was simplified as a plane strain footing. A Duncan and Chang type hyperbolic stress-strain relationship was used to simulate the nonlinear behavior of the clay. This model

was used to predict the deformation behavior and static capacity of suction caissons and the failure surface of the soil when the caisson was subjected to an inclined load. For example, the analytical results indicated that the failure mode of the caisson was a rotational type of failure, with the center of rotation at a depth below surface in the order of 70 to 80% of the skirt length. The prediction results had a good agreement with their small-scale field model tests done in parallel with the FEA study.

FEA were also carried out to investigate the load-transfer mechanisms in deep skirted gravity foundations and potential failure mechanisms for the site specific case of the Gullfaks C gravity base platform, with 16 suction caissons embedded 22 m into the seabed (Hight et al., 1988). Axi-symmetric and plane strain simplifications were made, and soils were represented by an elastic-plastic model with strain hardening/softening. The analyses indicated that the soil contained within the caissons had a significant influence on the behavior of the foundations, and the overall mechanisms were in good agreement with those adopted by the NGI (Norwegian Geotechnical Institute) in their limit equilibrium analysis of the foundation.

Clukey and Morrison (1993) performed a series of FEA to simulate their pullout tests. Eight-noded quadrilateral axi-symmetric elements with reduced integration were used. These FEA were carried out with ABAQUS software. The non-linear soil response was represented by a tri-linear stress-strain curve. A von Mises yield failure criterion was used to approximate the soil response under varying stress conditions. Passive suction was simulated in the analysis by maintaining contact between soil and caisson nodes at

the top of the caisson during loading. The FEA results showed that the uplift tests had an overall suction efficiency of 92.3%. These analyses and the centrifuge tests were in good agreement to about 0.6 m displacement on the curve of load-vertical displacement.

Based on the same conditions of two laboratory tests done by Massachusetts Institute of Technology (MIT) and University of Texas (Austin), a finite element model for simulating the behavior of suction foundations under both vertical and inclined pullout loads was developed by Handayanu et al. (2000). A Modified Cam-Clay model was selected to simulate the nonlinear response behavior of the soil. Eight-noded axisymmetric elements, with pore pressure degrees of freedom and contact surface along the caisson-soil interface, were used. The analysis results and the laboratory test results had reasonable agreement.

A series of finite element analyses were performed to investigate the behavior of suction caissons in sand and clay by Deng and Carter (2000a, 2000b, and 2002) and Deng et al. (2000). An elastoplastic soil model was used to simulate the stress-strain relationship of sand (Deng and Carter, 2000a). An elastic, perfectly plastic soil model and Modified Cam-Clay model were used to represent the stress-strain behavior of clay, and undrained, partially drained, and drained conditions, were considered through a non-dimensional parameter, T_k (Deng and Carter, 2002)

$$T_k = \frac{c_v}{vD} \tag{2.13}$$

where c_v is the coefficient of vertical consolidation of the soil, v is the constant velocity at which the caisson is pulled out of the soil, and D is the caisson diameter. Whenever T_k is bigger than a critical value (Deng and Carter, 2002), the behavior of the foundation soil can be assumed as drained, i.e., undrained behavior was observed when the velocity (v) was greater than 10^{-5} m/s, and whenever T_k is smaller than another critical value, the behavior of the foundation soil can be considered as undrained, i.e., undrained behavior could be predicted when the velocity (v) was less than 10^{-8} m/s. The vertical uplift loading capacity was investigated with embedment ratios, H/D, from 0.15 to 3.0 (Deng and Carter, 2002). The inclined uplift loading capacity of suction caissons in sand (Deng and Carter, 2000a) and the horizontal loading capacity of suction caissons in clay (Deng et al., 2000) were also investigated. The pullout capacity depended greatly on the load attachment point position when the caisson was subjected to an inclined load. The relationship between the pullout capacity and the load attachment point position was determined and the optimal load attachment point was found. Different ratios of embedment to caisson diameter from 1.0 to 2.5 were used in the analyses of horizontal loading capacity (Deng et al., 2000). The ultimate horizontal load for a suction caisson, F_{uh}, was defined as

$$F_{uh} = N_h H D s_u \tag{2.14}$$

where N_h is the lateral capacity factor, H is the embedment depth, D is the diameter of the caisson, and s_u is the undrained shear strength of the clay.

It was found that N_h can be described by

$$N_h = \frac{3.6}{\sqrt{(0.75 - (\frac{Z_p}{H}))^2 + (0.45(\frac{Z_p}{H}))^2}} \tag{2.15}$$

where Z_p is the distance from the mudline to the load attachment point. The relationship between the lateral capacity, N_h, and the load attainment point position, Z_p/H, is shown in Figure 2.3. The optimal load attachment position was at Z_p/H=0.63, at a maximum normalized horizontal capacity $F_{uh}/(HDs_u)$ of 11.7.

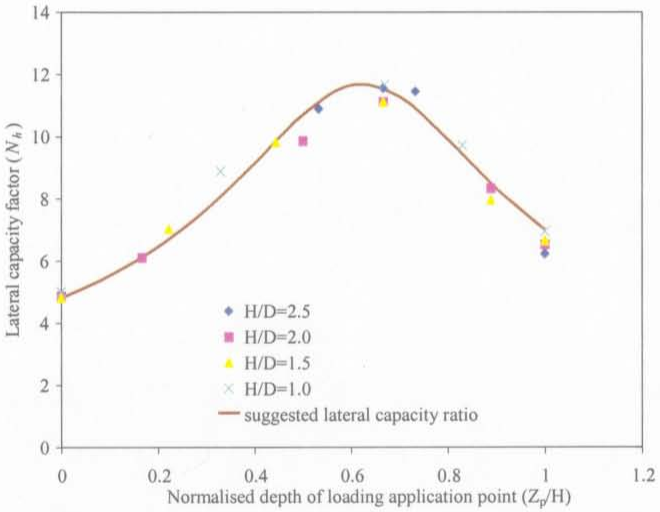

Figure 2.3: Lateral capacity against load attachment point (Deng and Charter, 2000b)

Finite element analyses have been used in the investigations on the behavior of suction caissons, especially in the load-displacement behavior, interaction of caisson-soil, padeye (load attachment) position optimization, and passive suction. However, numerical simulation of passive suction is still a challenging problem, which is not fully solved at

the present time. The finite element analysis is experiencing increased use in offshore suction foundation engineering (Templeton, 2002). Correctly simulating the generation of passive suction using FEA can help designers and users better understand the working principle of suction caissons.

2.2.9 Considerations from Related Pile Research

Both suction caissons and driven piles have been used as offshore foundations. They have some common characteristics: (1) some soil is displaced by the caisson wall or the pile; (2) the installation of these foundations induces excess pore pressures in the soil, resulting in a reduction in the effective stress; and (3), their capacities increase with time after installation due to setup development. So, the analysis approaches and theories used for driven pile design may also be useful for suction caisson design. However, some adjustments should be considered due to the different installation process. A suction caisson is penetrated to the design depth by both its own self-weight and active suction. Studies (Renzi et al., 1991, NGI, 1999, and Andersen and Jostad, 2002) indicated that only about a half volume of the soil displaced by the caisson's wall goes inside the caisson during self-weight penetration phase, and most of the soil displaced by the caisson's wall goes inside the caisson during suction penetration phase. For driven piles, the soil displaced by the pile goes outside of the pile. Moreover, the effective stress in the soil for suction caissons, due to the use of active suction in their installation, is different from those for driven piles.

In order to compare the centrifuge test and finite element analysis results obtained in this study with the performance of piles, this section provides some of the parameters related with these structures.

The maximum axial unit skin resistance of a driven pile is generally expressed as (Audibert et al., 1984)

$$f_s = \alpha_{pd} s_u \tag{2.16}$$

where s_u is the undrained shear strength of the soil and α_{pd} is an empirical coefficient varying with s_u . Figure 2.4 shows the relationship between α_{pd} and s_u (Audibert et al., 1984), which was obtained from the field studies by Tomlinson (1957) and Stas and Kulhawy (1983). This relationship was based on total stress and usually recommended for imposed displacement problems. However, the installation of a pile or a suction caisson induces excess pore pressures (EPPs) in the clay. These excess pore pressures induce a reduction of the effective stress in the clay, resulting in a decrease of the empirical penetration friction coefficient $\alpha_{pd.}$ Hence, effective stress in the soil during installation should be considered when Eq. 2.16 is used to calculate the penetration resistance.

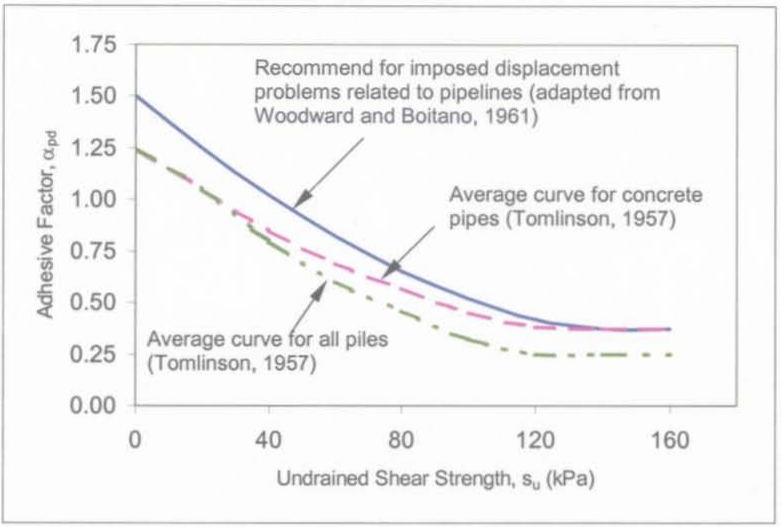

Figure 2.4: Relationship between α_{pd} and s_u for driven piles in clay (Audibert et al., 1984)

Several studies on the excess pore pressures induced by the installation of driven piles and the bearing capacity development of piles in clay have been carried out. For example, Randolph et al. (1979) suggested that the excess pore pressures, u, close to a driven pile may be estimated from

$$u = 4s_u - \Delta p' \tag{2.17}$$

where s_u is the undrained shear strength, and $\Delta p'$ is the change in mean effective stress due to shearing and remolding of the soil. In normally consolidated (NC) or slightly overconsolidated (SOC) clay, $\Delta p'$ will be negative and its magnitude may be as high as $2\text{-}3s_u$ for sensitive clays. In more heavily overconsolidated clay, $\Delta p'$ will become positive as the clay attempts to dilate upon shearing. The centrifuge test results on the distribution of the excess pore pressures in the clay induced by the penetration of a suction caisson

and the pullout capacity development in this study will be compared to the response of driven pile foundations in clay. Figure 2.5 shows typical field measurements of the excess pore pressures due to pile installation. Those results are in good agreement with Eq. 2.17.

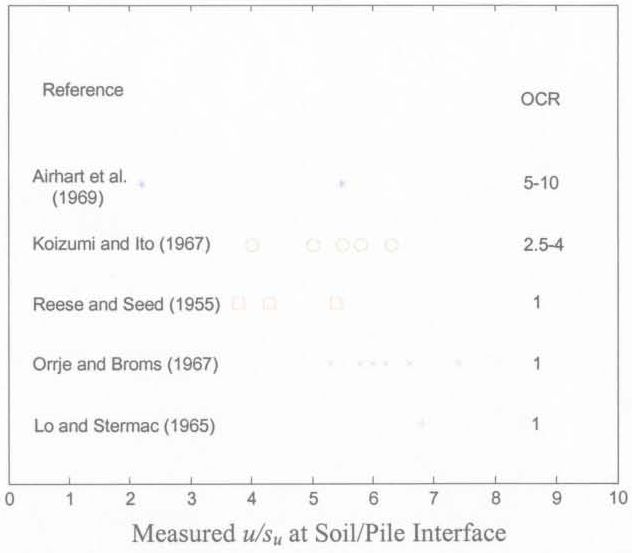

Figure 2.5: Field measurements of the excess pore pressures due to installation

The cylindrical cavity expansion theory was used to describe the excess pore pressures in clay (Randolph et al., 1979). They found that the excess pore pressures induced by the installation of driven piles can be evaluated from

$$u = 2s_u \ln(R_p / r) \qquad \text{for } r_0 \le r \le R_p \tag{2.18}$$

where $R_p{}^2 = (G/s_u)r_0^2$, G is the shear modulus, r_0 is the radius of the pile, r is the distance from the location of interest in the clay to the center of the pile.

The maximum excess pore pressures at the pile face were

$$u = s_u \ln(G / S_u) \tag{2.19}$$

This theory can also be used for suction caissons when installed in clay (Hjortneas-Pedersen and Bezuijen, 1992, see 2.2.3).

2.3 Summary

Suction caissons have been widely used in recent years for operations in the offshore environment. Studies on the behavior of suction caissons have been carried out using theoretical analyses, laboratory tests, centrifuge tests, field tests, and finite element analyses since 1960s. The following conclusions may be derived:

1. Suction caissons are a feasible and efficient mooring system. They can be used in deep water, in different types of soils, and can handle static and cyclic loads at various angles from the vertical.

2. Suction caissons can be installed using self-weight, dead weight, and active suction. The pullout capacity collectively consists of the buoyant weight of the anchor and ballast, the outside friction, the inside friction or the weight of the plug, and the passive suction.

3. Limit equilibrium theory, assuming local shear failure, local tension failure, or general shear failure is often used in the analysis and design of suction caissons.

4. The pullout capacity of suction caissons depends not only on the dimensions, but also on the pullout velocity and the soil properties such as undrained shear strength and permeability.

5. Like driven pile foundations, the installation of suction caissons induces excess pore pressures in the soil. For soils with low permeability, the excess pore pressures affect the pullout capacity of the caissons.

Even though suction caissons have become the foundation of choice for anchoring deepwater floating structures or supporting seabed systems, their working principles have not been fully understood.

Suction caissons are widely installed in normally consolidated and slightly overconsolidated clay, such as in the seafloors of Gulf of Mexico, Africa, and North Sea. In the field, they are generally subjected to an inclined cyclic load. For most suction caissons, their chain angles range between 30^{o} to 50^{o} from horizontal direction, and the pullout capacity is mainly controlled by the uplift capacity. It is necessary to understand the behavior of suction caissons under static uplift loading. Moreover, the external wall skin friction, one of the components contributing to the capacity, increases with setup after installation. As different loads will be applied on the caisson at different times after installation (i.e., hook-up phase, and operation phase), it is very important for designers and operators to reasonably predict the setup, so that the required wait time for applying the loads at different phases can be correctly evaluated.

Based on the literature review and the industrial requirements of suction caissons, this study focuses on: (1) investigation on the friction coefficient along suction caisson walls during installation; (2) investigation on the development of setup after the installation of the caisson; (3) confirmation of the application of cylindrical cavity expansion theory to the distribution of EPPs in soil induced by installation of suction caissons; (4) investigation on the dissipation of these EPPs; (5) investigation on the EPP development in soil during pullout of a suction caisson; (6) verification of the failure mechanism of suction caissons in normally consolidated and slightly overconsolidated clay and providing reasonable parameters; and (7) numerical investigation on the behavior of suction caissons during pullout using finite element analysis, including failure mechanism and simulation of passive suction.

Chapter 3
Centrifuge Model Tests

3.1 Centrifuge Modeling Technique

3.1.1 Introduction

Physical modeling plays an important role in geotechnical engineering. It usually consists of laboratory model tests, large scale field tests, and centrifuge model tests. Laboratory model tests are cost-effective and easiest to carry out because of a better control of the test parameters. However, the vertical effective stress profile in the prototype cannot easily be represented satisfactorily in the model. The stress-strain behavior and the patterns of deformation of the soil in the model can be quite different from those of the soil in the field. Large scale field tests can overcome these disadvantages, but they are expensive and time-consuming. In centrifuge testing, if the soil in the model is representative of the soil in the prototype, the vertical effective stress at corresponding points in the model and the prototype are similar, so that the soil behavior both in terms of strength and stiffness should be equivalent in the model and the prototype. Centrifuge technology thus combines advantages from the two other approaches: a better representation of effective stress and better control of test parameters at low cost.

The idea of centrifuge modeling and its potential use was first proposed in 1869 by Edouard Phillips (Taylor, 1995), a French engineer and a teacher at both École Centrale and the École Polytechnique. Its first recorded practical use was in 1931 by Philip Bucky and in 1932 by Davidenkov and Pokrovskii (Taylor, 1995). In the 1940s and 1950s, it was mostly used for military applications. It has only become a common tool for civil engineers since the 1960s. Since then, it has been used to study such issues as foundations, slope stability, hazardous waste disposal, cold regions phenomena, earthquake hazard mitigation, explosions and excavation performance (Taylor, 1995). Centrifuge model testing has also been used to investigate the behavior of suction caissons (Fuglsang and Steensen-Bach, 1991, Renzi et al., 1991, Bezuijen and Hjortnaes-Pedersen, 1992, and Morrison and Clukey 1994), and some examples have already been described in Chapter 2.

3.1.2 Scaling Principles and Laws

A geotechnical centrifuge is a device which applies an inertial (centrifugal) acceleration to a model by spinning the model about a central axis at a given angular velocity. The most important aspect in geotechnical centrifuge modeling is correct scaling of relevant parameters. Scaling laws can be derived from the use of both dimensionless analysis and consideration of governing differential equations. The principles and relevant scaling laws on centrifuge model testing were discussed in detail by Schofield (1980) and Taylor (1995). The scaling laws relevant to the centrifuge tests carried out in this study are presented in Table 3.1. When the same soil is used in model

and prototype, the time scale factor for consolidation is derived as $1/N^2$ ($N = 100$ in this study) through dimensional analysis (Taylor, 1995).

Table 3.1: Scaling factors in centrifuge tests

Parameter Modeled	Scale factor (Prototype: Model at Ng)
Acceleration	1:N
Model dimension	N:1
Soil density	1:1
Soil unit weight	1:N
Stress	1:1
Strain	1:1
Force	N^2:1
Displacement	N:1
Void ratio	1:1
Time (Inertial events)	N:1
Time (Consolidation and diffusion)	N^2:1
Time (Viscous flow)	1:1

3.1.3 Scaling Effects and Errors

The earth's gravitational field is uniform in the range of soil depths, that is of interest to geotechnical engineers. However, there is a slight variation in acceleration with depth in the model as high acceleration field is required in the centrifuge testing. An exact representation of the prototype cannot usually be fully achieved, and three fundamental principles are used in the design of the models: (1) the most significant effects should be modeled in similarity; (2) those that are not modeled should be considered; and (3) any

unknown influence should be revealed by experimental results. Inaccuracies and errors also exist. The rotational acceleration field effect and the soil particle size effect are examples. Some methods to reduce these errors are discussed by Schofield (1980), Taylor (1995), and Zhu (1998).

There are four main undesirable effects produced by the rotational acceleration field in centrifuge testing (Schofield, 1980, Taylor, 1995):

The inertial radial acceleration is proportional to the radius which leads to the effective stress in the model of a non-linear profile, rather than the linear variation existing in the field. This effect can be minimized by considering the relative magnitudes of under- and over-stress in the model (Schofield, 1980). When the effective centrifuge radius is taken as the distance from its axis to the position of one third of the model depth, there exists exact correspondence in stress between model and prototype at two thirds model depth and the maximum difference at any depth in the model is less than 3% (Schofield, 1980, Taylor, 1995).

There exists an acceleration component normal to the model (a lateral component of inertial acceleration) due to the geometry of the radial acceleration field. This lateral component increases towards the edges of the test package (Taylor, 1995). An effective practice used in this study to minimize it is that the major events should be designed to occur near the central region of the model.

The Coriolis acceleration occurs when there is a movement of the model in the plane of rotation also affects centrifuge test results. Its value is related to both the angular velocity of the centrifuge and the velocity of a mass within the model. This error can be negligible when the ratio of Coriolis acceleration to the inertial acceleration is less then 10% (Taylor, 1995).

If the similarity law were employed for particle size, a clay in a model at 100 g could be thought of as representing a fine sand. This is clearly flawed because of their very different stress-strain and permeability characteristics (Taylor, 1995). In order to maintain the mechanical behavior of the soil, care should be taken before scaling down the particle size in the model. It is found that the observed behavior represents the prototype behavior when the ratio of a major dimension of the model to the mean particle size is larger than 30 (Taylor, 1995). Since the particle size of fine speswhite kaolin clay is very small, the scale effect is considered to be marginal and the error due to scale effect can be considered insignificant in this study.

3.2 Design of Centrifuge Tests

3.2.1 Introduction

The focus of this study was to investigate the penetration resistance, the excess pore pressures (EPPs) in clay during both installation and pullout phases, the setup development, the failure mechanism, and the EPPs in the soil during pullout of a suction caisson. Eight centrifuge tests with three sizes of caissons were carried out in normally

consolidated (NC) or slightly overconsolidated (SOC) clays. Each centrifuge test consisted of clay testbed consolidation, a cone penetration test (CPT) and up to three caisson tests.

This section presents the design of these centrifuge tests, including the parameters of testbeds, preparation and check of undrained shear strength profiles of testbeds, caisson geometries, loading conditions, dissipation time of EPPs from the end of installation to the beginning of pullout test, and pullout velocity.

3.2.2 A Typical Suction Caisson Prototype

A typical prototype suction caisson, based on the typical shape of caissons used in Gulf of Mexico, was used to build the model caisson for both centrifuge tests and finite element analysis in this study. The main prototype caisson had a length of 24.5 m, diameter of 5.17 m, wall thickness of 65 mm and submerged weight of 500 kN. The wall of the caisson was relatively smooth, and no stiffeners were considered. The soils were highly plastic clays, normally consolidated or slightly overconsolidated. The undrained shear strength profile was linearly increasing from zero at the mudline at a rate of 1.14 kPa/m depth. In order to investigate the effect of the ratio D/Δ (diameter to wall thickness) to penetration resistance, two more caissons of different D/Δ ratios were also used.

3.2.3 Description of Model Caissons

The centrifuge tests were performed at a scale factor (a linear dimension ratio of model to prototype) of 1:100. Three model caissons were designed. The main model caisson SC #1, based on the typical prototype described in Section 3.2.2, was fabricated from a copper tube, a top plate made of brass, and some brass fittings. It had a 245 mm length, 51.7 mm outside diameter, and 0.65 mm wall thickness. This model caisson was used to investigate the penetration resistance, the excess pore pressures in clay, the setup development and the pullout behavior of suction caissons. Two more model caissons, SC #2 and SC #3, were also designed to investigate the behavior of suction caissons with different embedment ratios (a ratio of embedment to diameter, H/D). They were also constructed using the same materials and with a same length as SC #1. SC #2 simulated a prototype caisson characterized by an outside diameter of 10.3 m and wall thickness of 165 mm, and was only used to investigate the penetration resistance. SC #3 represented a prototype caisson with an outside diameter of 2.87 m and wall thickness of 100 mm, and was used to investigate both the penetration resistance and pullout behavior of open topped caissons/piles.

In order to simulate a prototype with an approximate buoyant self-weight of 500 kN, 800 kN and 300 kN with SC #1, SC #2 and SC #3 respectively, a piece of Styrofoam (50 mm thick) was fastened to the top of each model caisson to reduce the buoyant weight of the caisson. Two ports were drilled at the top plate of each caisson for two 1/4″ NPT brass fittings. One of the ports was used for a 1/4″ diameter tubing connection to an

external overflow through two three-way valves and was used to carry out self-weight penetration, suction penetration, and the pullout test. The second port was used to mount a miniature pore pressure transducer (PPT) inside the caisson top in order to measure the water pressure change during the test. Parameters of the models and their prototypes are listed in Table 3.2. Figure 3.1 shows the details of model caisson SC #1.

Table 3.2: Parameters of model caissons and the corresponding prototypes

Items	SC #1	Prototype 1	SC #2	Prototype 2	SC #3	Prototype 3
O.D.	51.7 mm	5.17 m	103.4 mm	10.34 m	28.7 mm	2.87 m
I.D.	50.4 mm	5.04 m	100.2 mm	10.02 m	26.7 mm	2.67 m
W.T.	0.65 mm	65.0 mm	1.6 mm	160 mm	1.0 mm	100 mm
Length	245.0 mm	24.5 m	245.0 mm	24.5 m	245.0 mm	24.5 m
M.P.D.	195.0 mm	19.5 m	195.0mm	19.5 m	19.5 mm	19.5 m
B.S.W.	0.491 N	500 kN	0.785 N	800 kN	0.294 N	300 kN

Note: O.D.– outside diameter, I.D.– Inside diameter, W.T.– wall thickness, M.P.D.– maximum penetration depth, B.S.W. – buyant self-weight

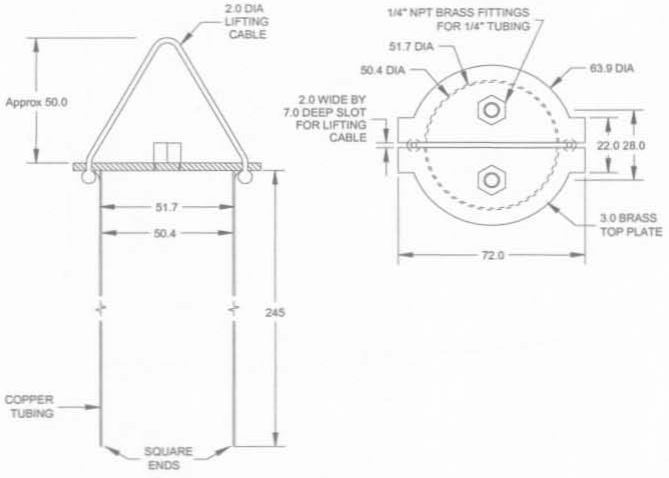

Figure 3.1: Model caisson SC #1

3.2.4 Testing Program

In order to investigate the behavior of suction caissons in NC or SOC clay, a series of centrifuge modeling tests were carried out, as described in Table 3.3,

Table 3.3: Test Design

Test ID	Model Caisson	D/Δ	Su Profile	Investigation Purposes
SAT01, SAT02 and SAT05	SC #1	79	*SOC*	Penetration resistance
SAT04	SC #1	79	*SUC*	Penetration resistance, REB and setup development
SAT06 and SAT08	SC #1	79	*NC*	Penetration resistance, EPPs, REB and setup development
SAT09	SC #2	64	*NC*	Penetration resistance
SAT10	SC #3	28	*NC*	Penetration resistance

Notes: SOC – slightly overconsolidated clay, NC – normally consolidated clay, SUC – slightly underconsolidated clay, and REB – reverse end bearing, and D/Δ - ratio of caisson diameter to wall thickness.

The influence of the effective stress in the soil to the penetration resistance was analyzed using the test data. The effect of the D/Δ ratio of caissons to the penetration resistance could be achieved by comparing the results of Tests SAT06, SAT08, SAT09, and SAT10. The distribution and dissipation of the EPPs were monitored by several miniature pore pressure transducers (PPT) embedded in the clay testbed at various elevations outside the caisson during the testing. The development of setup could be determined through analyzing development of external wall skin friction resistance from a series of caisson pullout tests with several pre-determined time intervals from the end of installation to the beginning of pullout test. The *REB* factors of suction caissons were

measured through the pressure differential between inside and outside caisson top. Moreover, the undrained shear strength of each testbed was measured by performing an in-flight cone penetration test (CPT) before the caisson tests.

3.2.5 Design of Testbeds

Fine speswhite kaolin processed by English China Clays, Lovering Pochrin & Co. Ltd. (ECLP) of Cornwall, England, was purchased through their US distributor Hamill & Gilespie. It is used for the clayey soil in the model. This material has a relatively high permeability, which reduces the time it requires to consolidate. It also has consistent properties, having provided excellent repeatability between models over the last decade. This clay has been used extensively by C-CORE and its properties are documented in Phillips (1989) and Springman (1993). The main geotechnical properties assumed for construction of the testbed are summarized in Table 3.4.

The testbeds were intended to be normally consolidated or slightly overconsolidated. The targeted undrained shear strength (s_u) profile was approximately 1.14 kPa/m depth with $s_u = 0$ at the surface of the clay. In order to reduce the consolidation time in the centrifuge prior to centrifuge testing, the samples were pre-consolidated in the laboratory using a downward hydraulic gradient (DHG) technique (Phillips, 1995).

Table 3.4: Speswhite kaolin parameters determined by C-CORE and others

Property	Value
Material	Speswhite kaolin
Specific gravity (*Gs*)	2.61
Coefficient of earth pressure at rest for normally consolidated clay (k_0)	0.64
Liquid limit (*LL*)	69%
Plastic limit (*PL*)	38%
Plastic index (*PI*)	31%
Vertical permeability (k_v)	2 to 3 x 10^{-6} mm/second
Horizontal permeability (k_h)	3 to 5 x 10^{-6} mm/second
Coefficient of virgin consolidation (c_v)	~0.1 mm^2/second
Coefficient of virgin compressibility, $\lambda\ (e - \ln p')$	0.26
Coefficient of rebound compressibility, $\kappa\ (e - \ln p')$	0.01~0.05
Vane shear stress, s_u/σ'	0.19 $OCR^{0.59}$
Sensitivity at 58% water content	1.3
Initial specific volume V (@ p'=1 kPa)	3.58

The undrained shear strength of a clay testbed, s_u, can be calculated by

$$s_u = \alpha\sigma'_v(OCR)^{\beta} \tag{3.1}$$

where σ'_v is the effective vertical stress, OCR is the overconsolidated ratio, α and β are coefficients listed in Table 3.5.

Table 3.5: Values of α and β for speswhite kaolin clay

Reference	α	β	Remark
Nunez (1989)	0.22	0.62	In-flight vane shear test
Bolton et al. (1993)	0.19	0.67	In-flight vane shear test
Springman (1989)	0.22	0.706	In-flight vane shear test
Poorooshasb (1991)	0.19	0.59	In-flight vane shear test

In this study, the targeted undrained shear strength profile is linear from zero at the mudline increasing at 1.14 kPa/m depth (using Eq. 3.1 for $OCR = 1$ and $\alpha = 0.19$, $\beta = 0.59$ (Poorooshasb, 1991)). Based on the soil parameters, the targeted effective vertical stress profile for normally consolidated clay was $\sigma'_v = 6.0$ kPa/m depth.

Figure 3.2 presents the change of soil properties such as saturated density, water content and void ratio with depth. The design undrained shear strength and effective vertical stress profiles are also presented.

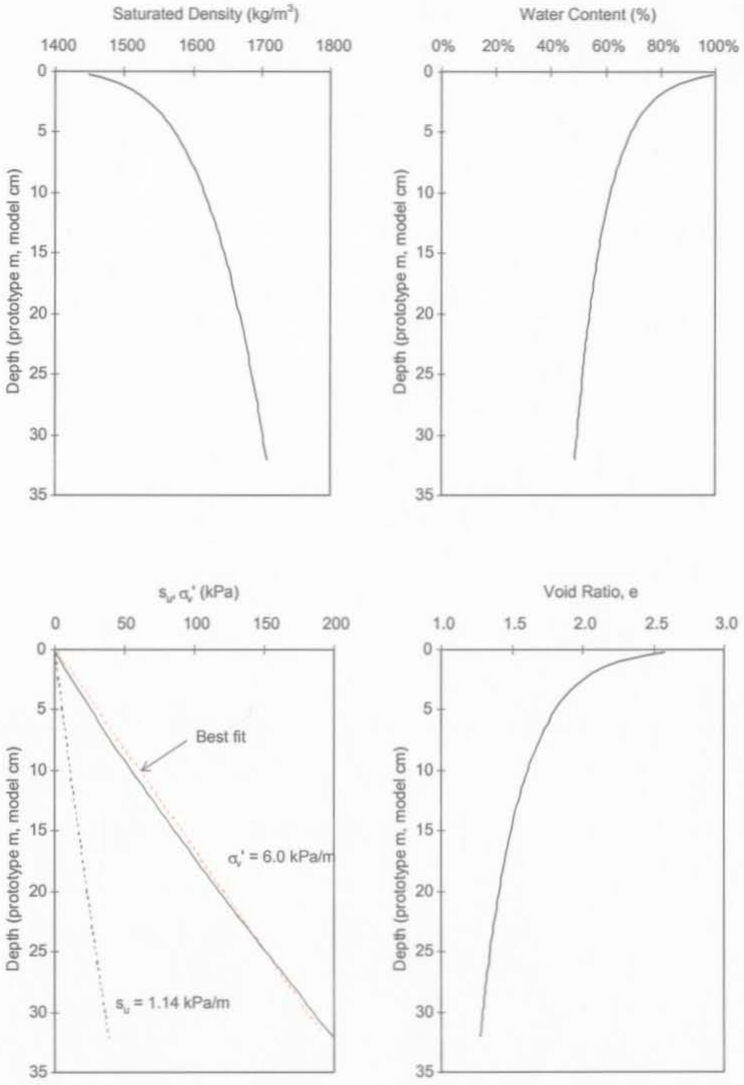

Figure 3.2: Variation of design geotechnical parameters with depth for NC kaolin clay

3.3 Preparation of Clay Testbeds and Laboratory Tests

3.3.1 Introduction

This section describes both the preparation of normally consolidated (NC) or slightly overconsolidated (SOC) clay testbeds and laboratory tests. All testbeds were consolidated in the laboratory with a downward hydraulic gradient technique (DHG) to minimize the centrifuge consolidation time.

Soil parameters used for finite element analysis including logarithmic elastic bulk modulus (κ) and logarithmic hardening modulus (λ) were obtained using laboratory consolidation tests. The coefficient of permeability of the testbed clay was measured using falling-head method.

Fall cone and mini-vane shear tests were carried out to measure the undrained shear strength profile and the sensitivity of the clay testbed. These results were used to check the in-flight cone penetration test (CPT) results.

3.3.2 Preparation of Clay Testbeds

3.3.2.1 General

All clay testbeds were constructed in a 904 mm diameter by 900 mm height deep extended container. Compared to the caisson sizes, the boundary effects can be neglected

when a series of caisson tests were carried out in one soil sample. Each testbed consisted of three lifts of speswhite kaolin clay. Three drainage layers were placed on the top, middle and bottom of Lifts #1 and #2 to accelerate the consolidation in the laboratory. Figure 3.3 shows the strongbox (container) with the completed testbed. Figure 3.4 indicates the distribution of the 5 mm fine sand drainage layer in the middle of the testbed. Detail design of testbeds is presented in Section 3.3.2.3.

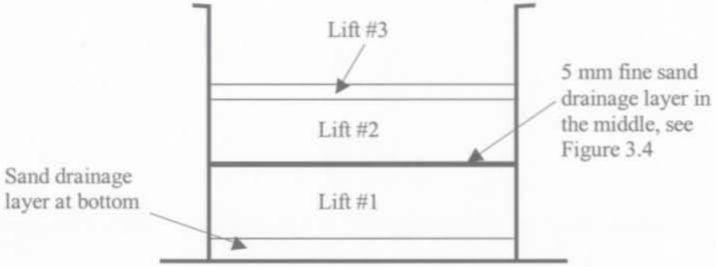

Figure 3.3: Positions of clay lifts in consolidometer

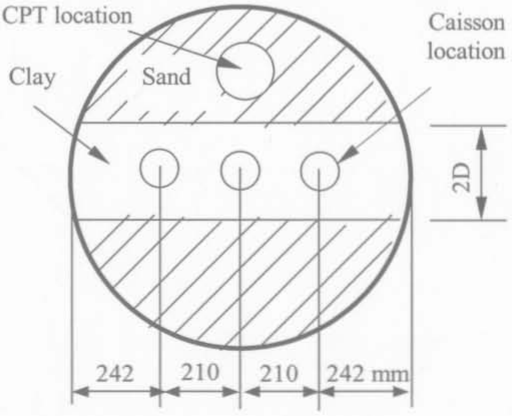

Figure 3.4: Middle 5 mm fine sand drainage layer in the testbed

3.3.2.2 Consolidation Equipment

A special consolidation apparatus with a downward hydraulic gradient (DHG) technique, shown on Figure 3.5, was developed (Phillips, 1995) and established (Walter and Phillips, 1998 and Cao et al., 2002) to obtain a normally consolidated (NC) clay profile for centrifuge experiments. This apparatus consisted of four parts: a large diameter consolidometer with an extension, a ram, a high pressure air supply with a air/water interface, a pore water pressure controller and data acquisition system with a PC computer. The consolidometer was a cylindrical structure made of steel by 904 mm in diameter and 500 mm in depth. The extension, also made of steel, was 500 mm in diameter and 400 mm in height. This extension was placed on the top of the consolidometer. When downward hydraulic gradient (DHG) technique was applied, a specially designed piston with a seal formed by two "O" rings along its side was used. A uniform total vertical stress was applied to the clay slurry by the self-weight of the ram and piston through the hydraulic pressure acting on the ram (i.e., piston pressure). A water pressure, 20 kPa less than the piston pressure, was applied on the top of the clay slurry under the piston using an air/water steel container connected to a high pressure air supply. A valve located at the bottom of the consolidometer connecting with the bottom drainage layer was opened to atmospheric pressure to allow drainage during consolidation. The pore water pressure on top of the clay was controlled by a PC computer through a pore pressure transducer (PPT) embedded at the center of the clay top surface. All data including force from the ram for total stress, pore water pressure on the

top of the clay, the compression of the clay (through the movement of the piston) and the water pressure inside the air/water steel container were recorded at 0.05 Hz.

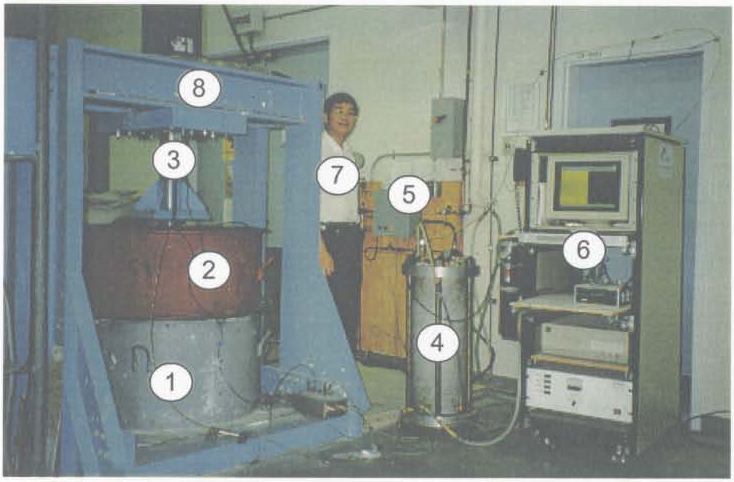

Figure 3.5: Laboratory consolidometer with DHG system

On Figure 3.5, 1 is the strongbox (consolidometer) containing slurry clay, 2 is the extension containing the piston, 3 is the ram, 4 is the air/water interface, 5 is the hydraulic system controller, 6 is the data acquisition system, 7 is the author for scale, and 8 is the reaction frame.

3.3.2.3 Procedure of Testbed Preparation

Each clay testbed was constructed in three lifts. Lifts #1 and #2 were pre-consolidated in laboratory. The typical design lift thickness and material requirements for one testbed are listed in Table 3.6.

Table 3.6: Design lift thickness and material requirement for construction of a testbed

Lift No.	Item	Value	Remark
Lift #1	Initial mass kaolin	117.0 kg	Constructed in consolidometer, Lift #2 was placed on it after 90% consolidation under 50 kPa.
	Initial mass water	140.4 kg	
	Initial water content	120%	
	Initial sample thickness	280 mm	
	Design final sample thickness	160 mm	
Lift #2	Initial mass kaolin	73.8 kg	Constructed in consolidatometer in steps, DHG technique was used.
	Initial mass water	88.6 kg	
	Initial water content	120%	
	Initial sample thickness	180 mm	
	Design final sample thickness	105 mm	
Lift #3	Initial mass kaolin	27.7 kg	Consolidated in centrifuge
	Initial mass water	33.2 kg	
	Initial water content	120%	
	Initial sample thickness	76 mm	
	Design final sample thickness	55 mm	
Design final thickness of total sample		320 mm	

The preparation procedure of a testbed is following:

Step 1, preparation of Lift #1: Dry speswhite kaolin clay powder was placed into a mixer and tap water was added to obtain a water content of approximately 120%. The mixing lasted about 12 hours under a vacuum of approximately 0.5 atm. During this time, a steel plate was placed at the bottom of the consolidometer to allow extrusion of the clay after the test. A 50 mm thick granular drainage layer was placed on the bottom inside the consolidometer to accelerate the consolidation of the clay slurry. The drainage sand was covered with a geotextile filter and saturated with water. The inside walls of the consolidometer and the extension were coated with a film of grease to minimize the

sidewall friction. Once 280 mm clay slurry was transferred into the consolidometer and a layer of saturated drainage gravel and a piston were placed on the top of the slurry, the consolidometer was placed under a frame for the purpose of consolidation. The clay slurry was subjected to a final vertical stress of 50 kPa in two stages (25 kPa at stage 1) until it achieved 90% degree of consolidation at each staged stress level. At the same time, a second mix of clay slurry for Lift #2 was prepared.

Step 2, preparation of middle sand drainage layer and Lift #2: After Lift #1 was unloaded, a fine sand layer 5mm in thickness (Figure 3.4) was placed on the top of Lift #1 to reduce the drainage distance and accelerate the consolidation process in the centrifuge. Then, Lift #2, 180 mm of clay slurry, was poured onto the top of the sand. The height of the consolidometer was extended to facilitate the operation. In order to obtain a uniform hydrostatic water pressure across the entire area of the clay surface, six alternating layers of sand and gravel with a total thickness of 250 mm were placed on the top of the clay. A filter geotextile was used at each interface of sand/gravel or sand/clay. The whole package including Lifts #1 and #2 was then transferred to the consolidation frame.

Step 3, laboratory consolidation: The clay Lifts #1 and #2 were subjected to a vertical pressure of 20 kPa until 90% consolidation in the first stage. Then, a downward hydraulic gradient (DHG) technique was used to develop the desired effective vertical stress profile of the clay. The clay testbed was consolidated in three additional stages until it reached 90% at each stage.

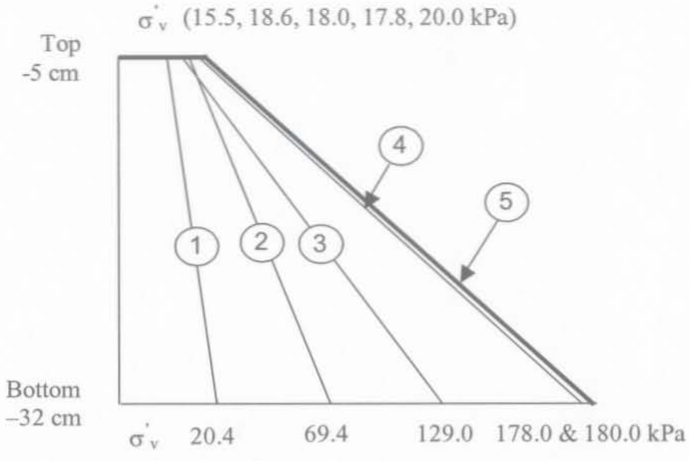

Figure 3.6: Effective vertical stress profile at each stage in NC clay (SAT06)
(1-stage 1, 2-stage 2, 3-stage 3, 4-stage 4, 5-design stress profile)

The effective vertical stress profile of the clay varied linearly with depth. The vertical effective stresses at the top and bottom were 20 kPa and 70 kPa for stage 2, 20 kPa and 120 kPa for stage 3, and 20 kPa and 180 kPa for stage 4. To avoid overconsolidation in each stage, the total vertical stress from ram (σ_v) and the pore water pressure on the clay (u) controlled by the air/water interface steel container were increased in 10 kPa intervals. Figure 3.6 presents the effective vertical stresses along the depth of the clay sample at different stages of Test SAT06.

Step 4, access to the middle drainage layer and Lift #3: The base valve was closed and the package was then incrementally unloaded by gradually decreasing the applied total vertical stress. After the free water and the drainage sand on the top of the clay were removed, Lift #3, a clay slurry of 70 mm in thickness, was placed on the top of Lift #2.

The fine sand layer in the middle of the sample was connected to the clay surface by three plastic tubes of 6.35 mm (0.25 inch) in diameter as shown on Figure 3.7, and about 560 mm water was immediately added on the surface of Lift #3. Care was taken to prevent air entry into this drainage layer. The testbed was loaded into the centrifuge after the instrumentations, test set-up, pore pressure transducers (PPTs), load cells and linear variable differential transformer (LVDT), were installed.

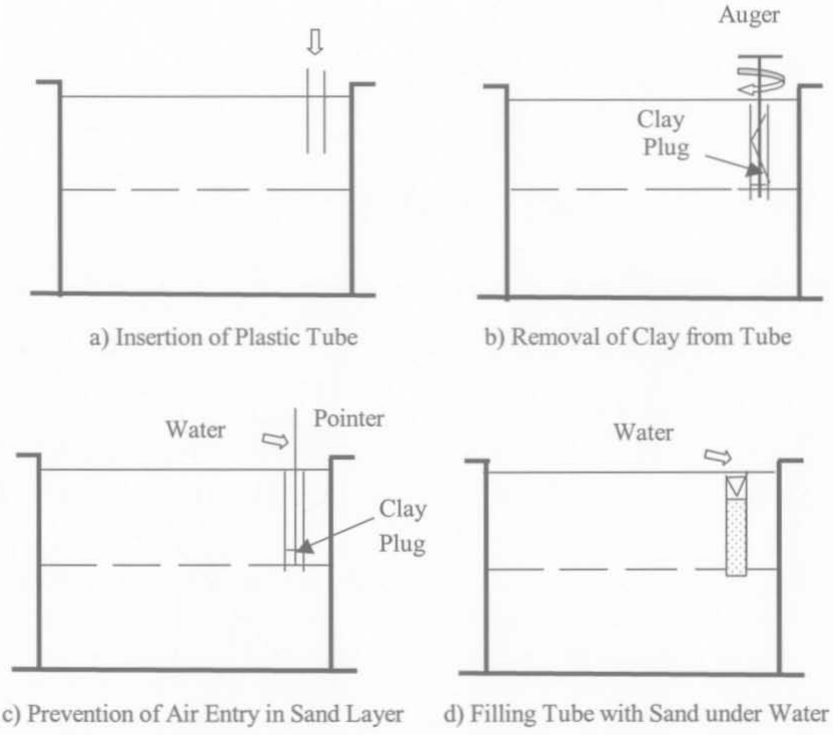

a) Insertion of Plastic Tube

b) Removal of Clay from Tube

c) Prevention of Air Entry in Sand Layer

d) Filling Tube with Sand under Water

Figure 3.7: Making of drainage path to sand drainage layer (Phillips, 1988)

If the testbed clay was overconsolidated in a stage during laboratory consolidation (i.e., Step 3), a constant effective vertical stress profile of 180 kPa along depth was applied to the testbed until 90% degree of consolidation was achieved (Figure 3.8). This testbed is called SOC clay in this study.

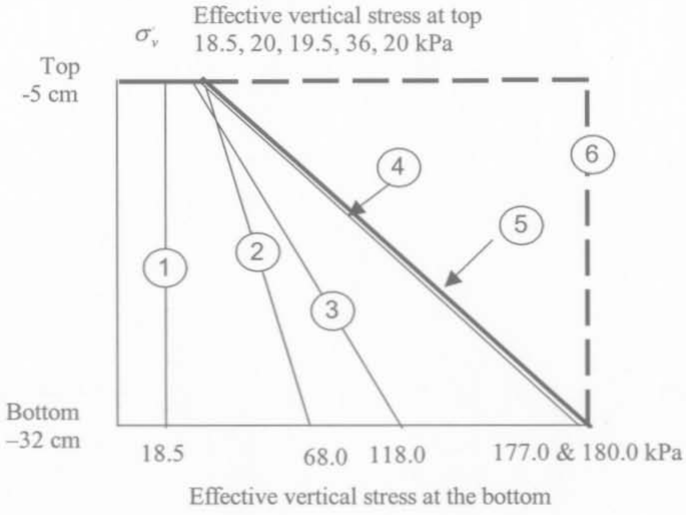

Figure 3.8: Effective vertical stress profile at each stage in SOC clay (SAT02)
(1-stage 1, 2-stage 2a, 3-stage 2b, 4-stage 2c, 5-design stress profile, 6-final stress profile)

3.3.2.4 Determination of C_v and λ

The consolidation coefficient of the clay, c_v, at different effective vertical stress can be determined using Taylor's method in laboratory consolidation. Figure 3.9 presents a typical vertical displacement against root of time ($\delta_v \sim \sqrt{t}$) curve when the clay was

subjected to an effective vertical stress of 20 kPa. As t_{90} can be obtained through laboratory consolidation tests, c_v can be calculated by

$$c_v = \frac{T_{90} H_s^{\ 2}}{t_{90}} \tag{3.2}$$

where T_{90} is non-dimensional time factor for 90% degree of consolidation and a theoretical value of 0.848 by assuming uniform u_0 with depth (Das, 1997) is used, and H_s is the thickness of the clay. The laboratory consolidation results of Test SAT06 are listed in Table 3.7.

Table 3.7: Laboratory consolidation results of Test SAT06 sample

Stage ID	$\sigma'_{v,ave}$ (kPa)	H_s (mm)		ΔH (mm)	t_{90} (second)	e	$\ln p'$	c_v (mm^2/s)
		Initial	Final					
1	20	450.0	361.5	88.5	513200	2.08	2.72	0.084
2a	45	361.5	337.0	24.5	163300	1.87	3.53	0.170
2b	70	337.0	326.5	10.5	88400	1.78	3.97	0.272
2c	100	326.5	314.5	12.0	80400	1.68	4.33	0.281

Note: p' is the mean effective stress

The c_v values in Table 3.7 are consistent with the results in the literature for speswhite kaolin clay as shown on Figure 3.10.

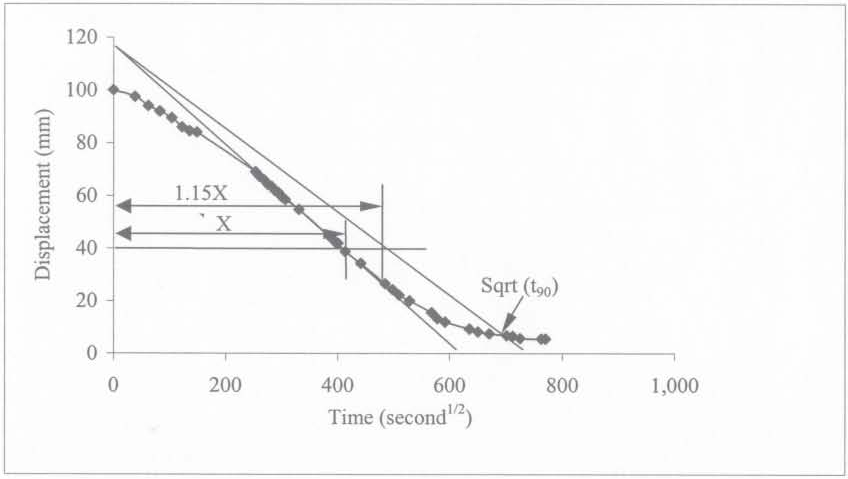

Figure 3.9: A typical curve of $\delta_v \sim \sqrt{t}$ and the determination method of t_{90}

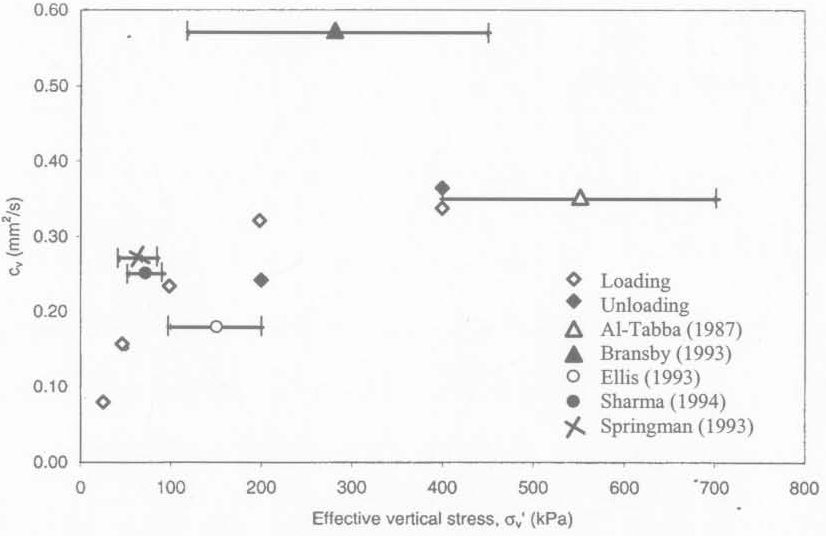

Figure 3.10: Relationship of c_v with effective vertical stress

Previous research showed that there is a linear relationship between void ratio e and $\ln(\sigma_v')$ for normally consolidated clay. For normally consolidated conditions, this relationship can be expressed by (Phillips, 1998)

$$e = 1.465 + 0.25\ln(\frac{184}{\sigma_v'}) \tag{3.3}$$

where σ_v' is the effective vertical stress. As

$$p' = \frac{\sigma_v' + 2\sigma_h'}{3} \tag{3.4}$$

where p' is the mean effective stress, $\sigma_h' = k_0\sigma_v'$ is the effective horizontal stress, k_0 is the coefficient of earth pressure at rest and is equal to 0.64. Then Eq. 3.3 can be written as

$$e = 2.695 - 0.25\ln p' \tag{3.5}$$

The coefficient of virgin compressibility, λ, can be obtained from the $e - \ln p'$ curve using

$$\lambda = \frac{de}{d(\ln p')} \tag{3.6}$$

Figure 3.11 presents all laboratory consolidation results on e and $\ln p'$. The value of λ calculated from those results changed from 0.245 to 0.273, and the average was 0.26. The intercept, e_0, ranged from 2.65 to 2.81, with an average of 2.78.

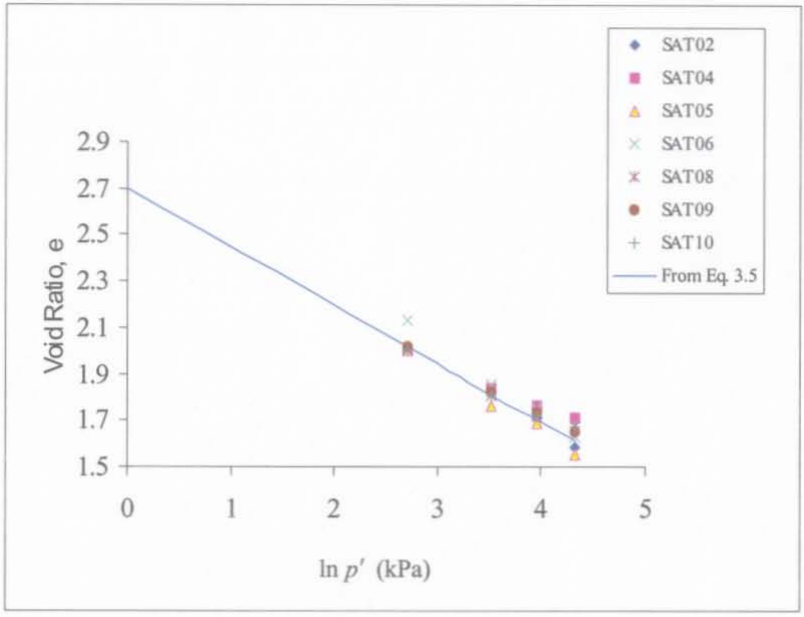

Figure 3.11 Relationship between e and $\ln p'$

3.3.2.5 Fall Cone Tests

In order to check the undrained shear strength profile of the testbed with the design s_u profile, three small samples were normally consolidated from clay slurry with water content of 120% to at least 90% degree of consolidation under the effective vertical stresses of 30, 60 and 110 kPa, to represent the effective vertical stresses of the soils at approximately 5 m, 10 m and 18 m depth in prototype, respectively. Fall cone tests were carried out for both undisturbed and completely remolded soils.

A fall cone with a weight of 100 grams and an angle of 30° was used. The test results are shown on Figure 3.12 with the best-fit line and the design undrained shear strength

profile (s_u = 1.14 kPa/m depth). The best-fit line of the test results is in agreement with the design s_u profile. The degree of sensitivity of the clay, defined here as the ratio of the undrained shear strength in undisturbed state to that in completely remolded state, was 1.6, 2.1, and 3.0 at the top, the middle, and the bottom test positions, respectively.

3.3.2.6 Mini Vane Shear Tests

A Pilcon Vane mini vane shear test apparatus was also used to determine the undrained shear strength and the sensitivity of the clay. This apparatus had two vanes: one with 19 mm diameter by 28 mm height for materials with shear strength 0 to 120 kPa, and the other one with 33 mm diameter by 49 mm height for material with shear strength 0 to 28 kPa. The Pilcon vane was pushed into the soil and then rotated until the soil failed. The undrained shear strength can be read at the top of the calibrated dial.

The same soils used for fall cone tests were also used for vane shear tests. The undrained shear strength of both undistributed and completely remolded soils was measured. The test results are presented on Figure 3.12 with the best-fit line and the design s_u profile (s_u = 1.14 kPa/m depth). The best-fit line of the test results from mudline to the position of 90 kPa effective vertical stress is under but very close to the design s_u profile. Below this position, the best-fit line is above and is also very close to the design profile. The degree of sensitivity of the clay by mini vane shear tests was 1.5, 2.0, and 2.8 at the top, the middle, and the bottom test positions, respectively.

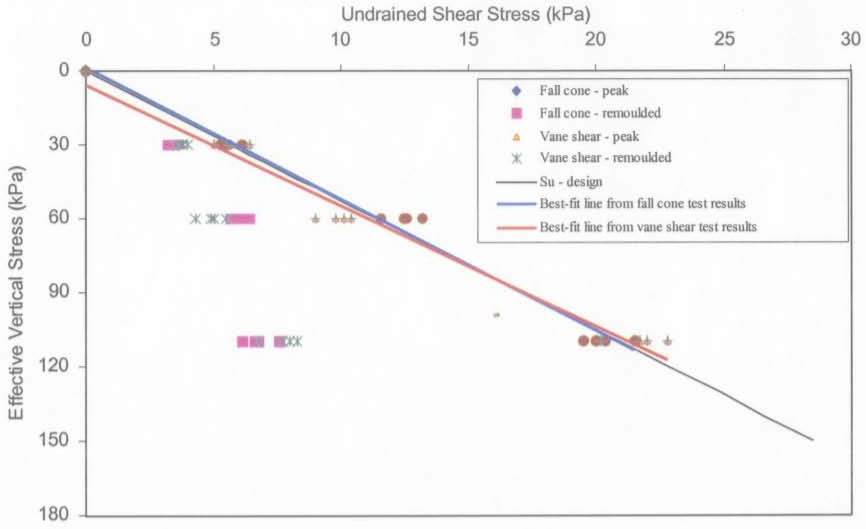

Figure 3.12 Undrained shear strength from laboratory tests

The best-fit lines on Figure 3.12 were obtained from the laboratory fall cone and vane shear test results using regression method. It can be seen from Figure 3.12 that, for a given elevation below mudline (clay surface), the maximum difference of s_u values is less than 15%. This error range is reasonable and acceptable in geotechnical engineering.

3.3.2.7 Permeability Tests

Falling-head method was used to measure the coefficient of permeability of testbeds. The equation applicable to this test can be derived (Bowles, 1992)

$$k_v = \frac{aL}{At} \ln \frac{h_1}{h_2} \tag{3.7}$$

where a is cross-sectional area of the standpipe, A is cross-sectional area of soil sample, h_1 is hydraulic head across sample at beginning of test ($t=0$), and h_2 is hydraulic head across sample at end of test ($t=t_{test}$).

Three tests were carried out in the soil laboratory of Faculty of Engineering, Memorial University of Newfoundland. The test results are presented in Table 3.8. The average value of k_v was 2.2×10^{-7} cm/s. Al-Tabbaa and Muir Wood (1987) measured the relationship between permeability (k_v) and void ratio (e) as

$$k_v = 0.53e^{3.16} x10^{-7} cm/s \qquad (3.8)$$

The predicted values of k_v using Eq. 3.8 are also presented in Table 3.8, and they are on the same order with the measured results.

Table 3.8 Permeability of speswhite kaolin clay

Test ID	σ'_v (kPa)	WC (%)	e*	k_v (cm/s)	k_v (cm/s) from Eq. 3.8
Test 1	30	66.4	1.93	2.5×10^{-7}	4.23×10^{-7}
Test 2	60	63.7	1.73	2.3×10^{-7}	3.00×10^{-7}
Test 3	110	56.1	1.56	1.8×10^{-7}	2.16×10^{-7}

* derived values based on G, r_{sat} and WC.

3.4 Centrifuge Facility and Test Equipment

3.4.1 Centrifuge Facility

C-CORE's centrifuge (Phillips et al., 1994) is located on the campus of Memorial University of Newfoundland. This facility is a two-story building enclosing a main bay

for model preparation, soil testing and radiography laboratories, mechanical and electrical workshops, a coldroom, data processing areas, offices, and the control room for the centrifuge itself. An Acutronic 680-2 centrifuge made in France is housed in a bunker-like structure adjacent to the S. J. Carew building. The facility was funded by industry and government. It opened on June 30, 1993.

The centrifuge has the ability to carry masses up to 2.2 tones to an inertial acceleration equivalent to 100 times gravity (100g) or 650 kg to 200 times gravity (200g). The maximum rotational speed is 189 r.p.m. A swinging platform is located at one end of the centrifuge arm and serves to carry the test package. The maximum payload size is 1.4 m long by 1.1 m wide and from 1.2 m to 2.0 m high. The other end of the arm holds a counter-weight of 22,000 kg. The activities inside the package and the centrifuge operation are visually monitored with television cameras mounted on the package and the wall of the chamber. The centrifuge is equipped with six rotary joints which permits fluids to flow through the central axis of the machine to the platform. Hence, water feed to the model can be conducted during centrifuge consolidation and testing. Electrical signals from transducers are acquired and recorded by a data acquisition system (through the electrical slip rings) located above the centrifuge and relayed to the centrifuge control room in the main building. Figure 3.13 shows C-CORE's centrifuge.

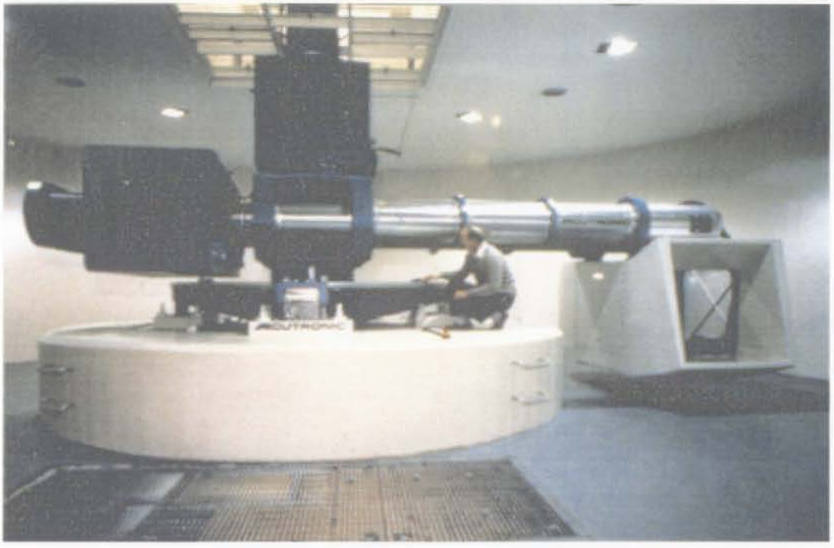

Figure 3.13: C-CORE's geotechnical centrifuge

3.4.2 Test Set-up

The test head works comprise of four main parts which are mounted on the steel strongbox: a horizontal drive, a caisson assembly, a cone penetration test (CPT) drive, and a suction device. Those parts are shown on Figures 3.14 and 3.15.

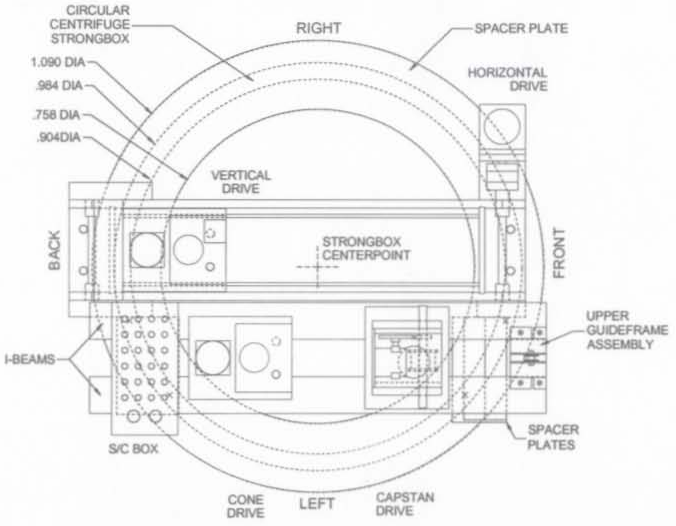

Figure 3.14: Schematics of centrifuge test set-up

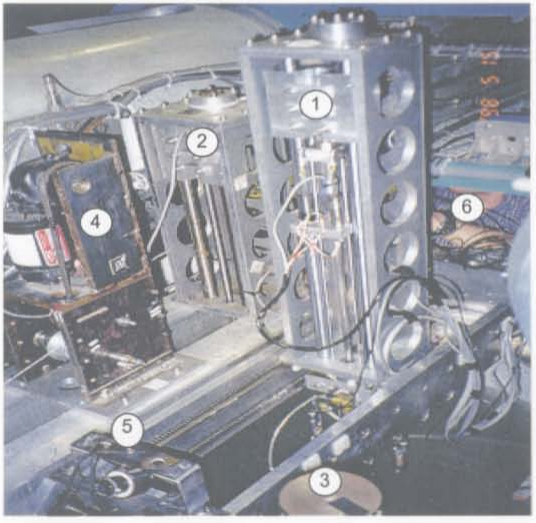

Figure 3.15: Overview of caisson assembly, CPT drive, horizontal drive, and the location of overflow for suction device (1-caisson assembly, 2-CPT actuator, 3-horizontal drive, 4-overflow actuator, 5-camera, and 6-person for scale)

The horizontal device driven by an actuator was used to relocate the suction caisson assembly horizontally so that a series of caisson tests can be carried out in succession without stopping the centrifuge in the same soil sample. This device was first placed at the center of the strongbox for test #1. It moved the caisson assembly back 210 mm to the location of test #2 after test #1 was finished. Finally the caisson assembly was moved 420 mm to the front to carry out test #3.

The caisson assembly, depicted on Figure 3.16, consists of the model caisson, a rod, two load cells (one for backup), a linear variable differential transformer (LVDT), and a vertical actuator driven by a stepper motor with 10 kN capacity. The LVDT and the controller for the vertical stepper motor were used to monitor and control the vertical displacement of the model caisson during both installation and pullout. Two high quality load cells, with the capacity of 3.5 kN and 2.5 kN were used to measure the vertical load in the caisson rod. The vertical actuator was used to lower and raise the caisson during the installation and extraction processes. The cable used to hold the caisson was kept slack during suction penetration phase using the LVDT feedback.

The CPT drive is a mini cone penetrometer connected to an actuator. The penetrometer has a 60° cone with a surface area of 1 cm^2. A load cell built into the cone rod measured tip resistance during penetration. This system was mounted on two aluminum I-beams spanning the circular strongbox.

The suction device consists of two three-way valves driven by two actuators and an overflow with a capstan actuator. These valves allow the drainage valve at the bottom of

strongbox to be opened during centrifuge consolidation and closed during caisson tests (see Figure 3.17). They were also used to control the drainage conditions during self-weight penetration, suction penetration and the vertical pullout tests.

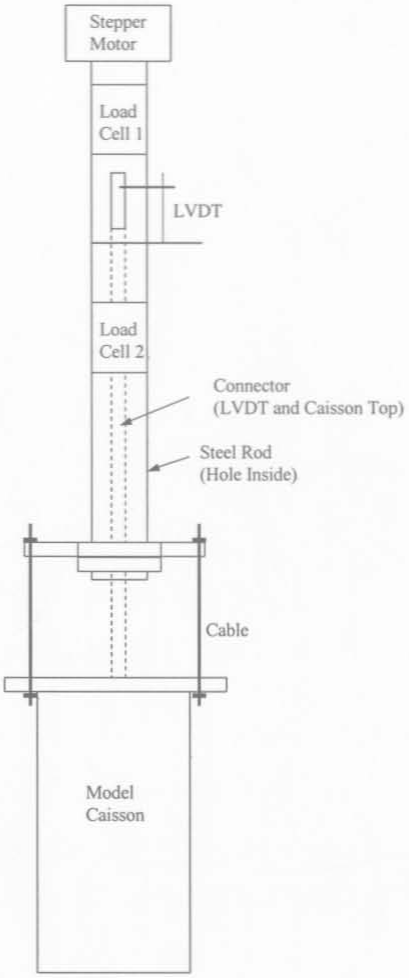

Figure 3.16: Suction anchor system

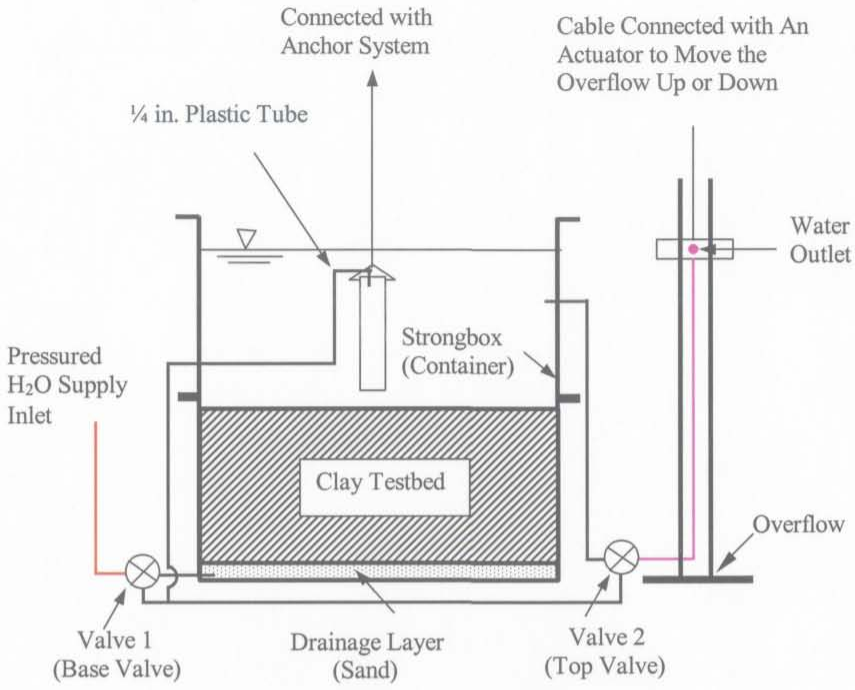

Figure 3.17: Plumbing diagram

3.4.3 Other Equipment and Instrumentation

A 5HP Bowers horizontal paste mixer was used as a clay mixer to prepare the clay samples. This mixer, using plough-type mixing blades, has a capacity of 200 liters and is capable of mixing at blade speeds ranging from 13 to 60 rpm. The mixer was designed to accept a vacuum, and 60 to 70 kPa of vacuum was applied during mixing.

A total of nine Druck PDCR81 miniature pore pressure transducers (PPTs) were used in each test. Six PPTs were embedded in the clay to measure the pore pressures. Their

readings were used to evaluate the consolidation process of the soil. One PPT was placed near the testbed surface in order to monitor the water depth above the surface and two PPTs were mounted on the inside and the outside of the caisson top surface to measure the pressure differential. The positions of these PPTs are presented on Figures 3.18 and 3.19.

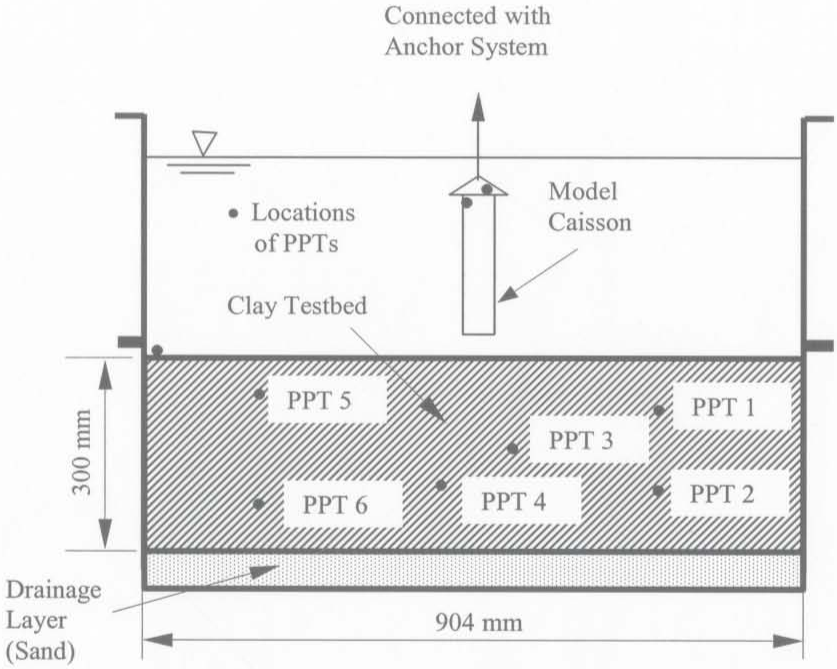

Figure 3.18: PPTs' positions during testing (front view)

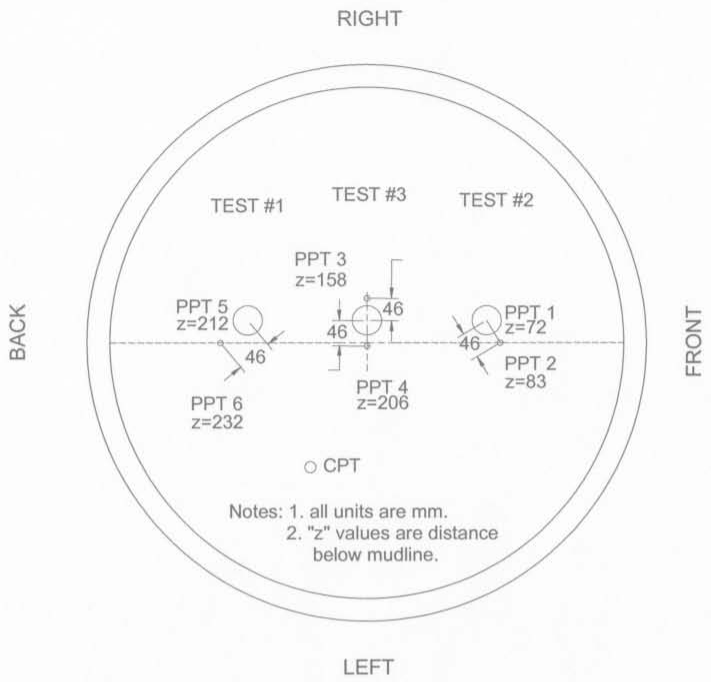

Figure 3.19: PPTs' positions during testing (top view)

3.5 Centrifuge Test Procedure

3.5.1 General

1. An in-flight cone penetration test (CPT) was used to measure the undrained shear strength profile of the clay testbed after the testbed was consolidated to 90% under its own self-weight at 100 g in the centrifuge. The penetration velocity was 3 mm/second.

2. Suction caissons were installed in-flight by both self-weight and active suction. The total design penetration depth was approximately 180 mm, including 100 mm to 130 mm self-weight penetration and 50 mm to 80 mm suction penetration.

3. The time interval between the end of the caisson's installation and the beginning of the pullout test was different for each test. The caisson pullout test was conducted after one of the pre-determined time periods: 1, 5, 10, 30, 120 and 150 minutes.

4. In order to investigate the effect of the EPPs to the pullout capacity of the caisson, the caisson top was closed right after the installation for Tests SAT01, SAT02 and SAT04. The EPPs inside the caisson were not released. For Tests SAT05, SAT06, SAT08, SAT09 and SAT10, the caisson top was opened after the caisson's installation, and the EPPs were released. The caisson top was closed before the beginning of the pullout test for these tests except Test SAT10.

5. The caisson pullout test was performed at a constant pullout velocity of 10 mm/second. In general, the pullout test was conducted in two stages. First, the caisson was pulled out at least 25 mm with its top closed in order to preserve the passive suction. When the maximum pullout capacity was reached, the caisson's top was opened to release the passive suction and the caisson was pulled back into the water column as a friction pile.

3.5.2 Centrifuge Consolidation

After the consolidation of the testbed in the laboratory was completed, a 70 mm thick clay slurry of 120% water content was placed on the top of the consolidated clay testbed, and about 560 mm water was added on the top of the slurry. The instrumented test package was transferred to the centrifuge. Both valves (Figure 3.17) were opened to the caisson after all plastic tubes and the caisson were filled with water. The centrifuge was accelerated in stages to 131 rpm (100g). At every stage, the speed was held constant for 5 to 10 minutes to allow all instruments readings to be checked. At the top speed of 131 rpm (100g), the testbed was consolidated to 90% degree of consolidation under its own self-weight. The progress of the consolidation process in the centrifuge was monitored from the six pore pressure transducers (PPTs) embedded in the clay testbed.

3.5.3 CPT Test

After 90% degree of consolidation was achieved, the undrained shear strength profile of the clay testbed was measured using an in-flight cone penetration test (CPT) device, with a 3 mm/second penetration velocity. The total penetration depth was approximately 250 mm. The cone position and tip resistance were collected and recorded at a rate of 50 Hz.

3.5.4 Self-weight Penetration

The caisson was held inside the water column above the clay surface by the caisson assembly system during the centrifuge consolidation and the CPT test in the centrifuge. In order to avoid soft clay blocking the plumbing during suction penetration, a deaired geotextile filter was attached on the inside top of the caisson. After the completion of the CPT sounding, Valve 1 (Figure 3.17) was closed and the caisson was opened to the surface water through Valve 2 (opening to the caisson), so that the water inside the caisson could flow out during self-weight penetration. The penetration rate of a caisson during self-weight penetration depends on the soil conditions, caisson weight and the velocity of the vertical actuator. In this study, the maximum penetration rate of the caisson under its self-weight was limited to 3 mm/second by the vertical actuator. This maximum penetration rate was selected based on the practical examples. In order to reduce the magnitude of the EPPs generated inside the caisson which compressed the soil plug, the caisson rod was moved down in 10 mm increments. There was a few seconds pause of each increment, so that EPPs could dissipate. The load cell recorded the change in the caisson weight due to the mobilization of the soil resistance, and its reading was also used to monitor the load transferring from the drive to the soil. The vertical movement was monitored by a LVDT and the stepper motor drive. The self-weight penetration was completed when the pressure inside the caisson had dissipated and the penetration resistance of the caisson was greater than its self-weight.

3.5.5 Suction Penetration

Following the completion of self-weight penetration, Valve 2 (Figure 3.17) was opened to the overflow, and the overflow line connected to the top of the caisson was lowered to generate a pressure differential between inside and outside of the caisson (i.e., active suction). At the same time, the vertical drive was lowered and the wires connecting the caisson with the stepper motor were kept slack using the LVDT feedback so that the caisson could continually penetrate into the soil. The suction penetration was completed when the caisson reached the design depth. The total design penetration depth was approximately 180 mm.

3.5.6 Pullout Test

In order to investigate the setup development and the EPPs, different time intervals between the end of the caisson's installation and the beginning of the pullout test were designed. The caisson pullout test, which was performed at a constant pullout velocity of 10 mm/second, was conducted after one of the six pre-determined time intervals: 1, 5 10, 30, 120 and 150 minutes. In general, the pullout test was carried out in two steps. The caisson was first pulled out at least 25 mm with its top closed in order to permit generation of passive suction (Valves 1 and 2 on Figure 17 were closed before testing). The maximum pullout capacity was reached within 25 mm displacement. Then, the caisson's top was opened to release the passive suction and the caisson was extracted back into the water column.

3.5.7 Test Completion

After the caisson was extracted back into the water column, the load cell reading was compared with its value before the installation of the caisson to check if the soil plug was out from the caisson. When the soil plug was still inside the caisson, Valve 2 (Figure 17) was opened to water supply and pressured water was applied to the inside top of the caisson through the plastic tube. Valve 2 was closed after the soil plug was washed out. The caisson assembly was moved to another location and the procedure described in section 3.5.4 to 3.5.6 repeated.

The centrifuge was spun down to a stop after all tests were completed. The test package was disassembled and the test data were analyzed.

3.6 In-flight Cone Penetration Tests (CPT)

3.6.1 General

In order to determine the undrained shear strength profile of the clay testbed and check with the design profile s_u = 1.14 kPa/m depth, an in-flight cone penetration test (CPT) was carried out. CPT testing was not carried out in Test SAT04. A tip resistance profile from the mudline to approximately 250 mm depth was obtained. Generally, the undrained shear strength can be determined from the measured cone tip resistance using the empirical relationship (Lunne et al, 1991)

$$s_u = (q_c - \sigma_{v0}) / N_k \qquad (3.9)$$

where s_u is the undrained shear strength, q_c is the cone tip resistance, σ_{v0} is the *in-situ* total vertical stress, and N_k is an empirical cone factor. In this study, the contribution to the cone tip resistance (q_c) from water column above mudline has been subtracted (see Figure 3.20). Therefore, the contribution to the *in-situ* total vertical stress from water column above mudline (u_{0m}) should also be subtracted, and Eq. 3.9 can be rewritten as

$$s_u = (q_c - (\sigma_{v0} - u_{0m}))/N_k \tag{3.10}$$

Previous research (Lunne and Kleven, 1981) showed that the cone factor, N_k, depended on type of cone penetrometer, rate of cone penetration, clay type and OCR. The relationship of N_k with OCR in clay was established through centrifuge tests. It was found that (Bolton et al., 1993), N_k was between 2.2 to 4.8 for normally consolidated clay; while for overconsolidated clay, N_k increased from 6.5 to 10 with OCR from 2.5 to 10 and then kept relatively constant after. Moreover, different N_k was used to analyze centrifuge modeling results for clay: 9 by Renzi et al. (1991), 6 to 9 by Fuglsang and Steensen-Bach (1991), 14 by Bezuijen and Hjortnaes-Pedersen (1992), and 10.7 by Clukey and Phillips (2002).

When CPT tests are used to determine the undrained shear strength profiles for the normally consolidated clay testbeds in this study, according to the above discussion, a reasonable value of N_k may range from 6 to 11.

3.6.2 CPT Tests in NC Clay

A typical in-flight cone penetration test (CPT) result of NC clay is shown on Figure 3.20. The total vertical stress and effective vertical stress increase linearly with depth. Generally, the cone tip resistance also increased linearly with depth. There were two small increases in the measured tip resistance. The first increase occurred at the slurry clay/clay interface (Lift #3/Lift #2) about 48 mm below the surface. The second increase occurred at the interface between clay/middle drainage sand/clay (Lift #2/sand/Lift #1) about 160 mm below the surface. This increase is due to the "local vicinity" of the interface as a clay hole was left in the drainage layer at the interface layer (Lift #2/sand/Lift #1) so that the cone penetrometer can go through during CPT testing.

The value of N_k can be derived through back-calculation using the test results of cone tip resistance, empirical Eqs. 3.1 and 3.10, as

$$N_k = \frac{q_c - (\sigma_{v0} - u_{0m})}{\alpha \sigma'_v (OCR)^{\beta}} \tag{3.11}$$

where q_c and σ_{v0} are cone tip resistance and total in-situ vertical stress from CPT tests, u_{0m} is the water pressure on the seafloor (mudline or clay surface), $\alpha = 0.19$ and $\beta = 0.59$ are empirical factors, OCR is the overconsolidated ratio and equals to 1 for NC clay, and $\sigma'_v = 6$ kPa/m depth is the effective vertical stress. The back-calculated values of N_k from CPT tests for all NC clay testbeds varied from 8.7 to 12.4, with an average value of 9.5. Those N_k values are in reasonable agreement with the N_k values, available in literature,

for NC clay mentioned in Section 3.6.1. Figure 3.21 presents the design s_u profile defined by Eq. 3.1 for the NC clay testbeds.

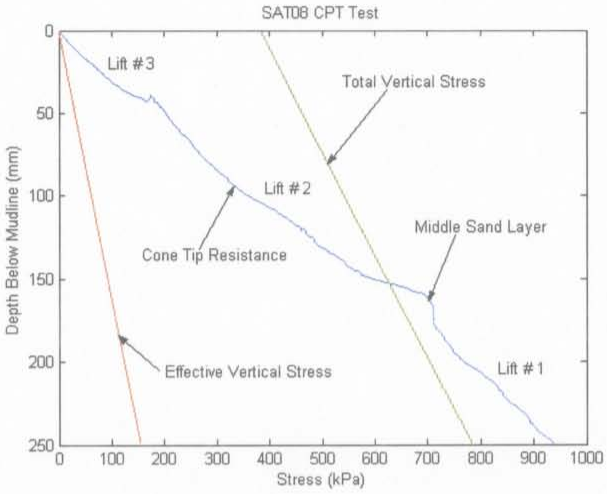

Figure 3.20: Vertical effective stress and cone tip resistance profiles

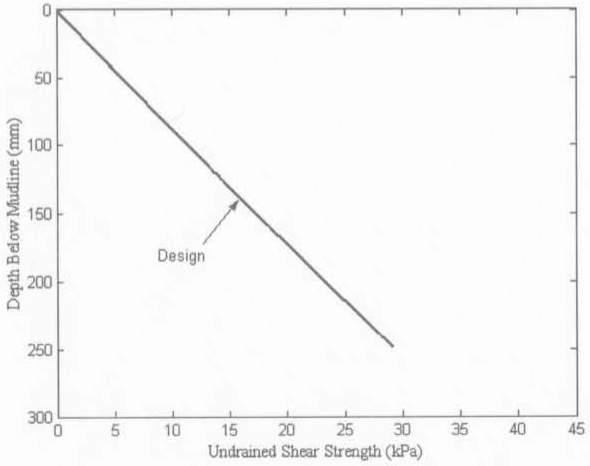

Figure 3.21: Design undrained shear strength profile of NC clay testbeds

3.6.3 CPT Tests in SOC Clay

Cone penetration tests (CPT) were also conducted in slightly overconsolidated clay (SOC) testbeds using the same cone penetrometer and penetration velocity as for NC clay. Eq. 3.11 and CPT test data were used to back-calculate the values of N_k. The values of N_k varied from 10.8 to 15.7, with an average value of 12. Figure 3.22 presents the design s_u profile for all SOC clay testbeds.

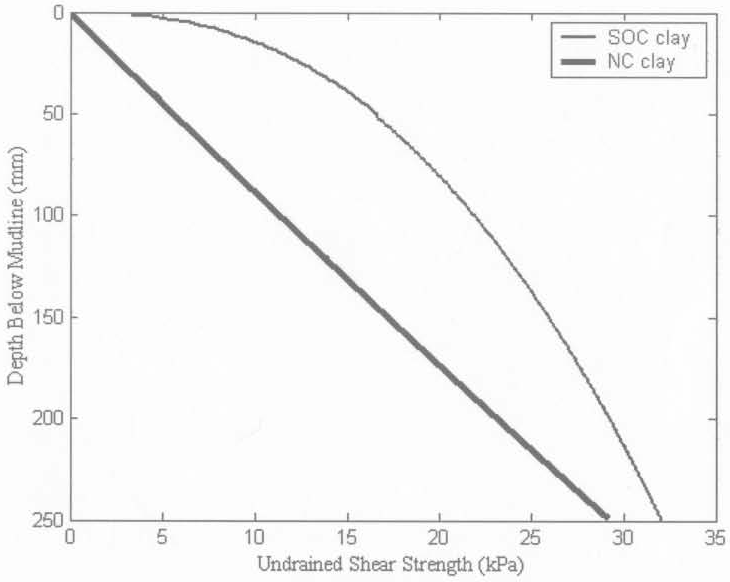

Figure 3.22: Design undrained shear strength profile of SOC clay testbeds

Chapter 4
Analyses of Centrifuge Test Results

4.1 Introduction

A total of eight centrifuge tests were carried out in this study, including 16 caisson tests shown in Table 4.1. These tests focused on penetration resistance, distribution of EPPs induced by installation of suction caissons and their dissipation, failure mechanism, setup development, F_{pu}-d behavior, and EPPs in the soil during pullout of a suction caisson.

The testbeds of Tests SAT06, SAT08, SAT09 and SAT10 were normally consolidated (NC), and their design undrained shear strength profile is presented in Figure 3.21. The testbeds of Tests SAT01, SAT02 and SAT05 were slightly overconsolidated (SOC), and Figure 3.22 shows their design undrained shear strength profile. The testbed of Test SAT04 was slightly underconsolidated (SUC), and no CPT test was carried out.

Table 4.1: Suction caisson centrifuge tests carried out in this study

Centrifuge Test ID		Caisson Used	Clay Test-bed	Penetration Depth (mm)			Waiting Time (minutes)	Pullout Testing		Remark
				By Self-weight	By Suction	Total		Total Pullout Force (kN)	Passive Suction (kN)	
SAT01	SAT01-1	SC #1	SOC	80	71	151	10.6	0.581	0.269	
SAT02	SAT02-1	SC #1	SOC	80	39	119	1.8	0.545	0.298	
SAT04	SAT04-1	SC #1	SUC	136.1	28.9	165	7.8	0.619	0.406	
	SAT04-2	SC #1		133.3	21.7	155	29.6	0.592	0.369	
	SAT04-3	SC #1		135.3	26.7	162	121.2	0.756	0.373	
SAT05	SAT05-1	SC #1	SOC	42	40	82	32.7	0.454	0.329	
SAT06	SAT06-1	SC #1	NC	145.0	39	184	9.3	0.624	0.343	
	SAT06-2	SC #1		141.2	34.8	176	30.0	0.656	0.358	
	SAT06-3	SC #1		157.2	19.8	177	125.0	0.651	0.324	
SAT08	SAT08-1	SC #1	NC	111.8	56.2	168	10.2	0.656	0.378	
	SAT08-2	SC #1		128.8	31.2	160	31.6	0.656	0.356	
	SAT08-3	SC #1		129.8	30.2	160	150.0	0.696	0.328	
SAT09	SAT09-1	SC #2	NC	150.0	30.0	180	-	-	-	No pullout test
SAT10	SAT10-1	SC #3	NC	174	10	174	4.4	0.269	-	Lid open during pullout
	SAT10-2	SC #3		161	0	161	7.6	0.251	-	
	SAT10-3	SC #3		151	0	151	11	0.242	-	

Note: 1. NC – normally consolidated clay, the clay was consolidated under $\sigma'_v = 6$ kPa/m depth effective vertical stress profile;
2. SOC – slightly overconsolidated clay;
3. SUC – slightly underconsolidated clay.

4.2 Penetration Resistance

4.2.1 Penetration Resistance in NC Clay

Figure 4.1, the penetration resistance against the penetration depth, presents the centrifuge test results of Test SAT06 conducted in this study. Model caisson SC #1 was installed in normally consolidated (NC) clay. The outside diameter and the wall thickness of the caisson were 51.7 mm and 0.65 mm, respectively, with a ratio of diameter to wall thickness (D/Δ) slightly over 79. The penetration depth was in range 176 mm to 185 mm including a self-weight penetration of approximately 140 mm, yielding a ratio of H/D (embedment to diameter) of about 3.5.

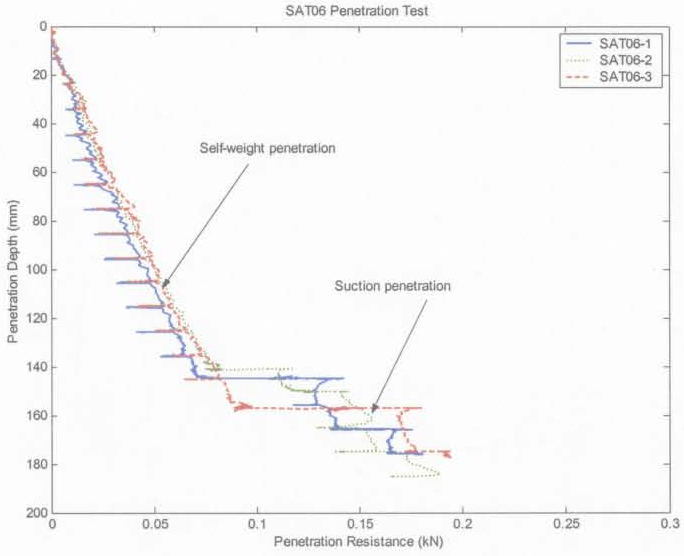

Figure 4.1: Penetration resistance against depth (SAT06, H/D ≅ 3.5)

Figure 4.1 shows that the penetration resistance increased with depth during both self-weight and active suction penetration. Also, a noticeable increase in the soil penetration resistance occurred when the suction was used to aid caisson penetration at a depth of about 140 to 150 mm. It is thought that this penetration resistance increase can be attributed to one or more of the following reasons:

1. The active suction applied after completion of self-weight penetration might have caused a different "soil flow" pattern. For example, less than 50% of the soil displaced by the caisson wall enters the caisson during self-weight penetration while more than 50% enters the caisson during suction penetration, Renzi et al. (1991), NGI (1999) and Andersen and Jostad (2002). This results in an increase in the penetration resistance from the end of self-weight penetration to the beginning of suction penetration.

2. The dissipation of excess pore pressures (EPPs) occurring in the soil outside the caisson during the time interval between the completion of self-weight penetration and the beginning of suction application resulted in an increase in the undrained shear strength of the soil at the caisson wall and, consequently, the friction resistance along the penetrated section of the caisson (setup effect). In this study, the time interval between the completion of self-weight penetration and the beginning of suction application ranged from 1 to 5 minutes. According to the analyses in Section 4.3.2, approximate 25% EPPs in the soil were dissipated during this time. That is to say, the effective stress in the soil was increased compared with that in the soil at the moment of the completion of self-weight penetration. The increase of the effective stress in the soil outside the caisson lead to an increase of the outside wall skin friction.

3. There is a thixotropy effect for remolded natural clays, which causes an increase in the undrained shear strength with time even though there are no changes in volume or effective stress, resulting in an increase of wall skin friction. Previous study (NGI, 1999) indicated that speswhite kaolin clay does not have much thixotropy. Consequently, the higher penetration resistance observed during the suction penetration is believed to be due to the effect of the active suction on the soil inside the caisson and the setup that occurred in the soil outside the caisson during the time period from the completion of self-weight penetration to the beginning of suction application.

4. The 5 mm fine sand layer in the middle of the testbed, shown in Figure 3.3, may make a contribution to the increase of penetration resistance in this local area. Even though no sand was placed in a 2-D (D - caisson diameter) area around the caisson test locations (see Figure 3.4), the undrained shear strength of the local clay may increase due to the "local vicinity" of the clay/sand/clay interface, resulting a local increase of penetration resistance.

Figure 4.2 presents the penetration test results of Test SAT08. Similar to Test SAT06, the testbed was a NC clay and model caisson SC #1 was used. Therefore, the same characteristics in the penetration resistance versus depth curve as those of Test SAT06 were observed.

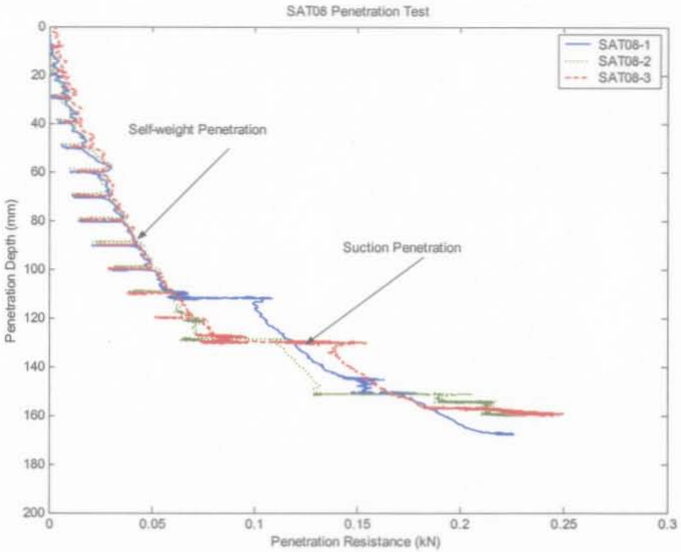

Figure 4.2: Penetration resistance against depth (SAT08, H/D ≅ 3.2)

The penetration resistance can be interpreted in a manner similar to that used for vertically loaded pile in clay. Using limit equilibrium theory, the vertical resistance of an open end caisson (R_{pe}) may be determined as the sum of the friction resistance generated along the caisson's wall areas (R_{sf}) and the end-bearing resistance (R_{tip}) generated along the base of the wall (the annular area of the caisson wall)

$$R_{pe} = R_{sf} + R_{tip} \tag{4.1}$$

The end-bearing resistance (R_{tip}) of the annular base area of the steel is determined using the following equation

$$R_{tip} = (N_c s_u + \gamma' h) A_{tip} \tag{4.2}$$

where s_u is the undrained shear strength of the soil at the tip, N_c is a bearing capacity factor (N_c is a function of penetration depth, its value is in range 5 to 9), γ' is the buoyant unit weight of soil, h is the penetration depth, and A_{tip} is the annular base area of the caisson.

The wall skin friction is often determined by the following equation

$$R_{sf} = \alpha_{pe} \bar{s}_u A_s \tag{4.3}$$

where α_{pe} is an empirical constant (penetration friction coefficient), $\bar{s}_u$ is the average undrained shear strength of the soil along the skirt over the penetration depth, A_s is the total interior and exterior wall skin areas of the caisson over which shearing resistance is generated.

Self-weight penetration phase:

Considering the centrifuge test set-up in this study, the soil resistance during self-weight penetration is evaluated as follows

$$LCR = W_c - R_{tip} - R_{sf} \tag{4.4}$$

where LCR is the load cell reading and W_c is the submerged weight of the caisson. Prior to the caisson installation, the load cell reading (LCR) is equivalent to the submerged weight of the caisson. As the caisson penetrates the clay testbed, the load recorded by the load cell transducer decreases due to the development of the friction and the end-bearing resistance until it reaches zero when the total mobilized resistance becomes equal to the submerged weight of the caisson in soil.

Using Eqs. 4.2, 4.3 and 4.4, the average friction coefficient developed along the caisson's wall over the penetration depth during the caisson's self-weight penetration α_{pe} is estimated as follows

$$\alpha_{pe} = [W_c - LCR - (N_c s_u + \gamma' h) A_{tip}] / [\bar{s}_u A_s] \tag{4.5}$$

Suction penetration phase:

The soil resistance during suction penetration is evaluated using the following procedure ($LCR = 0$ if the cable was kept slack during suction penetration test)

$$LCR = W_c - R_{tip} - R_{sf} + F_{asu} \tag{4.6}$$

where F_{asu} is the applied suction force, and equals to the force acting over the cross-section of the caisson top caused by the difference between the pressure inside the caisson (p_i) and the pressure outside the caisson (p_o) (these pressures are measured by the pore pressure transducers mounted inside and outside the caisson's top surface)

$$F_{asu} = (p_o - p_i) A_{sp} \tag{4.7}$$

where A_{sp} is the internal cross section area of the caisson. Combining Eqs. 4.2, 4.3, 4.6 and 4.7, the average friction coefficient α_{pe} developed along the caisson's wall over the penetration depth during suction penetration is estimated by

$$\alpha_{pe} = [W_c + F_{asu} - LCR - (N_c s_u + \gamma' h) A_{tip}] / [\bar{s}_u A_s] \tag{4.8}$$

The values of the average friction coefficient of Test SAT06 developed along the caisson's wall during self-weight and suction penetrations, estimated using Eqs. 4.5 and 4.8, are presented in Figure 4.3.

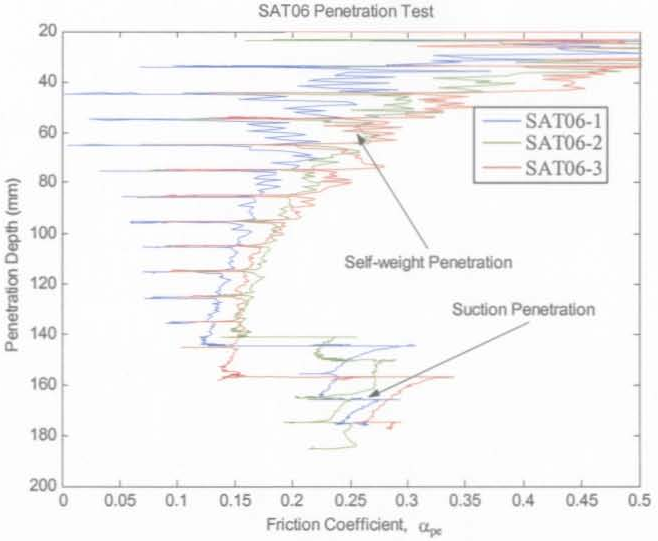

Figure 4.3: Friction coefficient against depth (SAT06, H/D ≅ 3.5)

The value of the friction coefficient α_{pe} at any penetration depth in Figure 4.3 represents the average α_{pe} value applicable to the entire caisson penetration above that depth. For example, a α_{pe} value of 0.4 at 50 mm penetration indicates that the friction resistance along the caisson's side areas at 50 mm depth is equivalent to 0.4 times the average soil undrained shear strength over the top 50 mm soil profile.

Figure 4.3 indicates that the value of the average friction coefficient α_{pe} during caisson's self-weight penetration decreased from about 0.6 at the surface to about 0.15 at 150 mm. This reduction indicates that the rate of soil resistance increase with depth is lower as the caisson penetration progressed due to the decrease of the rate of the effective stress increase in the soil with depth. As mentioned above, the effective stress in the soil

influences the penetration resistance. Two factors may make the rate of the effective stress increase lower with depth: first, the excess pore pressures (EPPs) in the clay induced by installation of the caisson increased with depth; second, for the top 40 mm (about half radius of the plastic zone) the dissipation of the EPPs was very fast due to the significant contribution of the vertical dissipation, the relative large permeability of the soil and short drainage distance. In the area below (below 40 mm from the mudline), the dissipation time of the EPPs increased with depth because the dissipation of the EPPs mainly depended on the horizontal dissipation. The drainage distance is longer due to the radius increase of the plastic zone and the permeability is smaller due to the decrease of void ratio (e) compared with the 40 mm soil on the top surface. Therefore, the friction coefficient α_{pe} decreased with depth.

Figure 4.3 clearly shows that a sudden increase in the soil resistance occurred when the active suction was applied. The value of the average friction coefficient α_{pe} increased from 0.15 at end of the self-weight penetration (140 or 160 mm below mudline) to about 0.35 when suction was applied. This increase was due to both the application of active suction which results in a different "soil flow" pattern, and the setup increase during the time interval from the end of self-weight penetration to the beginning of suction penetration (1 to 5 minutes) which may lead to about 25% EPPs dissipation and an increase in the effective stress in the soil as mentioned above. The increase in the penetration resistance associated with the suction application was also observed by others (Renzi et al., 1991). During suction penetration, the value of the average friction coefficient α_{pe} decreased from 0.35 at 140 or 160 mm (beginning of the suction

penetration) to about 0.27 over the penetration depth. As the EPPs in the soil outside the caisson increased again with the penetration depth during suction penetration, the effective stress in the soil outside the caisson decreased after the caisson started to penetrate. Therefore, the penetration resistance again decreased with depth. Similar findings regarding the behavior of the average friction coefficient α_{pe} was observed during the other tests in this study.

Figure 4.4 presents the results of Test SAT08, the friction coefficient α_{pe} against penetration depth. Even though Tests SAT06 and SAT08 were carried out in similar testbeds, caisson geometries and penetration velocity, the results of those tests were slightly different due to the difference of the applied active suction, including its magnitude and duration.

Figure 4.5 presents the centrifuge test result of Test SAT09. Model caisson SC #2 was installed in normally consolidated (NC) clay. The outside diameter and the wall thickness of this caisson were 103.4 mm and 1.60 mm, with a ratio of diameter to wall thickness (D/Δ) of about 65. The penetration depth was 190 mm including a self-weight penetration of approximate 170 mm, yielding an H/D ratio (embedment/diameter) of about 1.8.

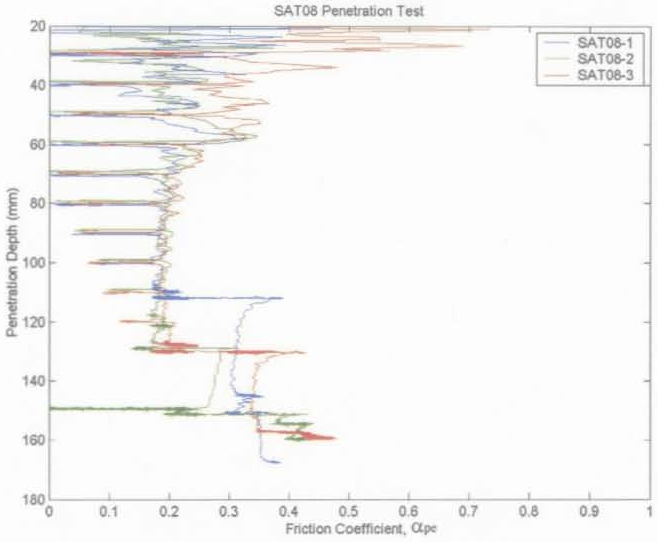

Figure 4.4: Friction coefficient against depth (SAT08, H/D ≅ 3.2)

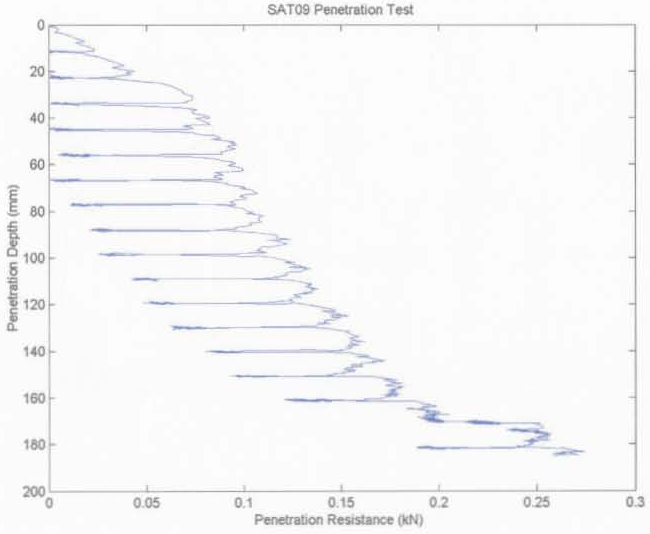

Figure 4.5: Penetration resistance against depth (SAT09, H/D ≅1.8)

Figure 4.6 presents the result of Test SAT09, the friction coefficient α_{pe} against penetration depth. The value of the average friction coefficient α_{pe} during caisson's self-weight penetration decreased from about 0.7 at the clay surface to about 0.07 at 170 mm. This coefficient increased from 0.07 to 0.1 from the end of self-weight penetration to the beginning of suction penetration, and a value of 0.1 maintained until the 20 mm suction penetration was completed. Compared with the results of Tests SAT06 and SAT08, the friction coefficient is almost the same in the top 60 mm below mudline as the rate of the effective stress increase in the soil is almost the same due to the vertical dissipation of the EPPs. The EPPs generated in the soil at the self-weight penetration depth are larger than those of Tests SAT06 and SAT08 due to the deeper penetration depth and more disturbance to the soil by the thicker wall of the caisson, resulting in a smaller relative effective stress increase in the soil, hence, the friction coefficient at the end of self-weight penetration (170 mm) is smaller than that of Tests SAT06 and SAT08. Also, the change in friction coefficient is found to be smaller than that in Tests SAT06 and SAT08 from the end of self-weight penetration to the beginning of suction penetration. Two reasons may result in that the rate of the effective stress increase in the soil was smaller than that of Tests SAT06 and SAT08: (1) the active suction applied inside the caisson was about 25 kPa which is less than the 55 to 60 kPa applied for Tests SAT06 and SAT08, and (2) the time interval from the end of self-weight penetration to the beginning of suction penetration was about 2 minutes which is shorter than 3 to 5 minutes in Tests SAT06 and SAT08.

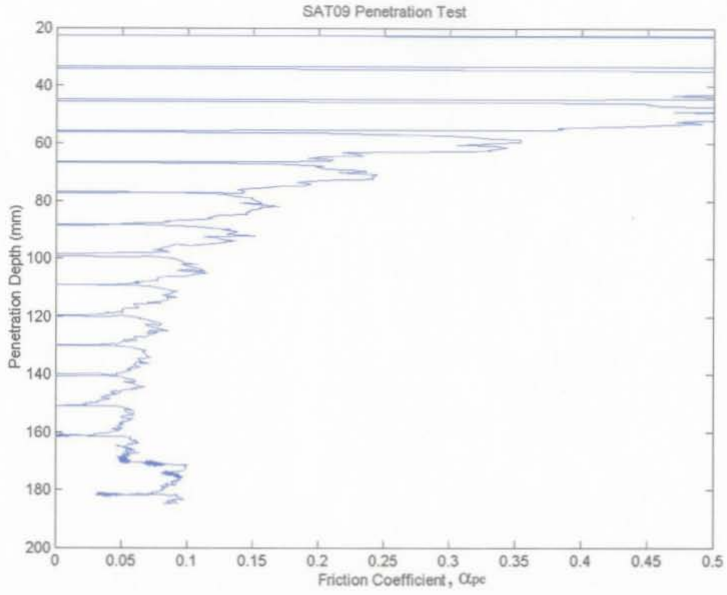

Figure 4.6: Friction coefficient against depth (SAT09, H/D ≅ 1.8)

Figure 4.7, presents the centrifuge test results of Test SAT10. Model caisson SC #3 was installed in normally consolidated (NC) clay. The outside diameter and the wall thickness of this model caisson were 28.7 mm and 1.0 mm, respectively, with a ratio of diameter to wall thickness (D/Δ) of about 29. The penetration depth ranged from 151 mm to 174 mm, yielding a ratio of embedment to diameter (H/D) of about 5.3 to 6.1.

It can be seen from figure 4.7 that the slope of penetration resistance had an increase at the penetration depth of about 110 mm below mudline. This indicates that a penetration depth of 110 mm (approximately 5D) may be the critical depth for model caisson SC #3. When the penetration depth is less than this depth, the failure of soil is

local shear failure (cut-in) mechanism, and the penetration resistance comes from external skin friction, internal skin friction and tip (annular wall) resistance. When the penetration depth is larger than this depth, the failure of soil changes into a confined general shear failure mechanism as defined in Section 5.4.1 of this thesis.

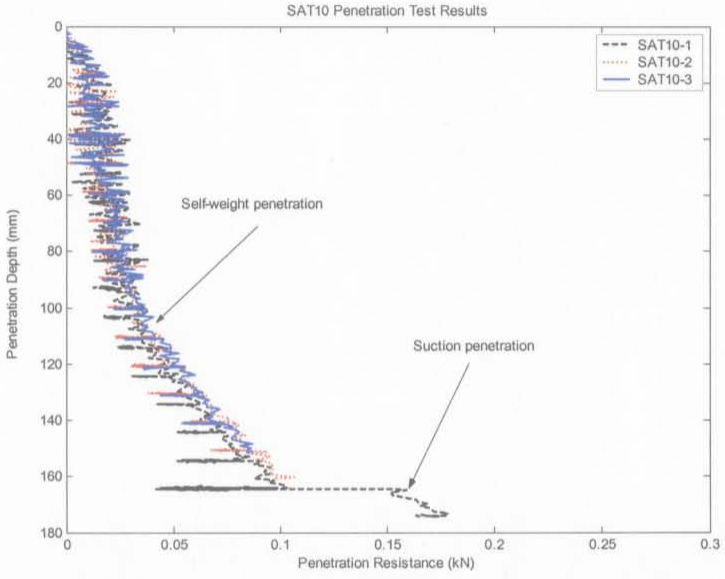

Figure 4.7: Penetration resistance against depth (SAT10, H/D ≅ 5.5)

Figure 4.8 presents the test result of Test SAT10, the friction coefficient α_{pe} against penetration depth. The value of the average friction coefficient α_{pe} during caisson's self-weight penetration decreased from about 0.7 at the clay surface to about 0.2 at 110 mm below, and then increased to 0.30 at 160 mm (this increase may be to the end bearing resistance which was taken as "internal skin friction" in calculation of α_{pe}). The friction coefficient increased from 0.30 at the end of self-weight penetration to about 0.5 at the

beginning of suction penetration, and this value maintained to the completion of the 10 mm suction penetration.

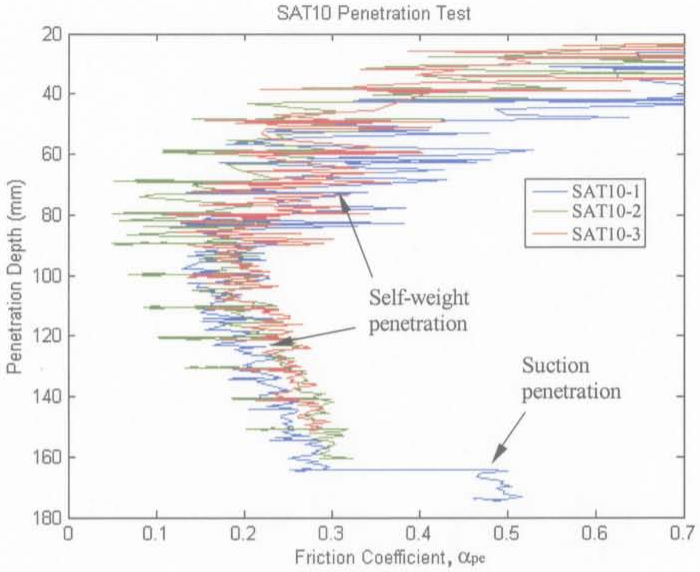

Figure 4.8: Friction coefficient against depth (SAT10, H/D ≅ 5.5)

Results of Tests SAT06, SAT08 and SAT09 indicate that, for caissons with D/Δ ratio (diameter to wall thickness) from 64 to 79 and H/D ratio (embedment to diameter) from 1.8 to 3.5, the penetration resistance can be predicted using a friction coefficient α_{pe} = 0.2 for self-weight penetration and α_{pe} = 0.3 for suction penetration (0.3 seems to be conservative for SAT09). Results of SAT10 indicate that, for caissons with a D/Δ ratio of about 28 and a H/D ratio of about 5.5, the penetration resistance can be calculated using α_{pe} = 0.3 for self-weight penetration and α_{pe} = 0.5 for suction penetration. It is noted that the shape of penetration resistance coefficient versus depth of Test SAT10 is

different from those of Tests SAT06, SAT08 and SAT09. As discussed above, this may be due to the caisson sensing to the presence of the 5 mm fine sand layer in the middle of the testbed in Test SAT10 (model caisson SC #3 was lighter than model caissons SC #1 and SC #2).

Based on the above test results, the following conclusions can be drawn:

1. The penetration friction coefficient α_{pe} depends on the effective stress in the soil which is affected by the EPPs induced by installation.

2. The active suction leads to an increase in the friction coefficient during the installation of suction caissons.

3. The setup that occurs during time interval from the end of self-weight penetration to the beginning of suction penetration increases the friction coefficient. Generally, the longer the time interval, the bigger the friction coefficient.

4. The friction coefficient is affected by the wall thickness. The larger the ratio of diameter to wall thickness (D/Δ), the smaller the friction coefficient.

5. For caissons with D/Δ ratio (diameter to wall thickness) from 64 to 79 and H/D ratio (embedment to diameter) from 1.8 to 3.5, the penetration resistance can be predicted using a friction coefficient α_{pe} = 0.2 for self-weight penetration and α_{pe} = 0.3 for suction penetration. For caissons with a D/Δ ratio of about 28 and a H/D ratio of

about 5.5, the penetration resistance can be calculated using α_{pe} = 0.3 for self-weight penetration and α_{pe} = 0.5 for suction penetration.

4.2.2 Penetration Resistance in SOC Clay

Model caisson SC #1 was used to investigate the penetration resistance in slightly overconsolidated (SOC) clays. Those tests included Tests SAT01, SAT02 and SAT05. The design undrained shear strength profile of the testbeds is shown in Figure 3.22. The average friction coefficient α_{pe} can also be calculated using Eq. 4.5 for self-weight penetration and Eq. 4.8 for suction penetration. Figures 4.9 and 4.10 respectively present the penetration resistance versus penetration depth curve and the friction coefficient versus penetration depth curve from centrifuge test results of Test SAT05.

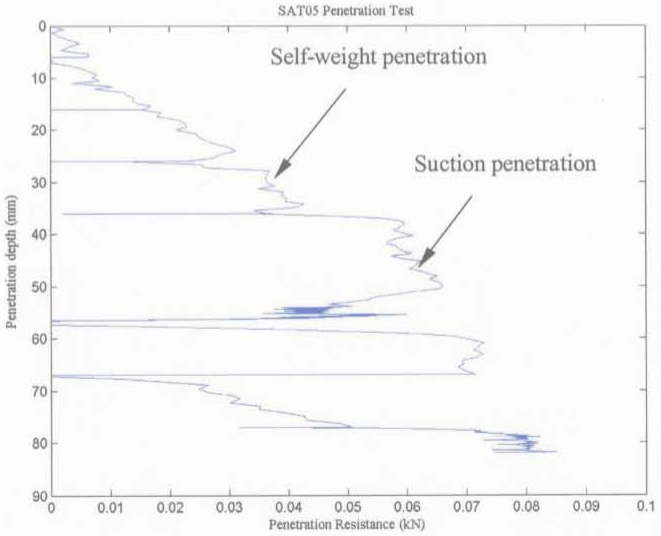

Figure 4.9: Penetration resistance against depth (SAT05, H/D ≅ 1.6)

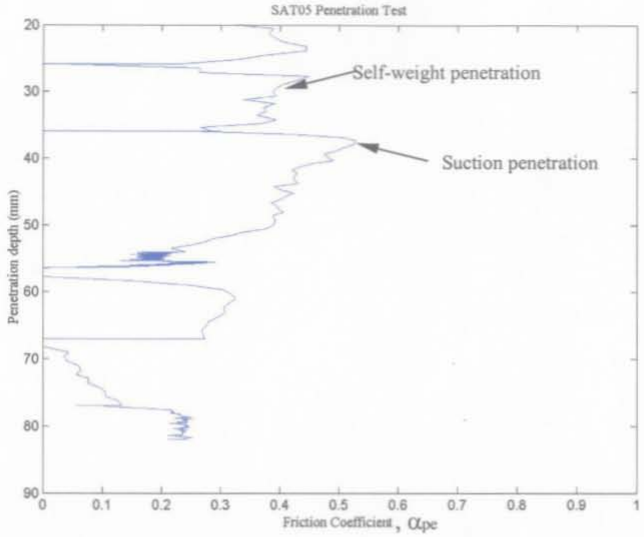

Figure 4.10: Friction coefficient against depth (SAT05, H/D ≅ 1.6)

The penetration resistance increased with penetration depth. The friction coefficient α_{pe} during self-weight penetration maintained about 0.4. This value increased to 0.53 when the active suction was applied. Then, it decreased with depth to about 0.25 at the completion of suction penetration. Compared with the test results in NC clay (i.e., Tests SAT06 and SAT08), the average friction coefficient α_{pe} is bigger in self-weight penetration and almost the same in suction penetration. However, they are less than the α_{pd} values shown in Figure 2.4, as α_{pd} values were observed some time after pile installation and the EPPs dissipated.

4.3 Distribution of EPPs and Their Dissipation

4.3.1 EPP Distribution

Excess pore pressures (EPPs) were induced in the clay by the installation of suction caissons. Six pore pressure transducers (PPTs), two for each caisson test location, were buried in clay outside the caisson, positioned 20 mm away from the wall and 72, 83, 158, 206, 212 and 232 mm below the mudline. The capacity of these PPTs ranged from 690 to 1724 kPa (100 to 250 psi). As observed in previous studies (Hjotnaes-Pedersen and Bezuijen, 1992), the highest excess pore pressure was recorded when the tip of the caisson reached the elevation at which the PPT was located.

Figure 4.11 presents the maximum changes recorded by the PPTs during caisson installation. The measured initial EPPs in the soil showed an increase with depth down to the elevation of the caisson's tip, followed by a rapid decrease down to a small value (i.e., little effect from caisson installation) at approximately half a caisson diameter below the tip. The excess pore pressures in the soil inside the caisson were not monitored due to the difficulty in installing PPTs inside the caisson.

The recorded distribution of the initial EPPs in the clay are compared with the predictions by cylindrical cavity expansion theory in Table 4.2 and Figure 4.11. In accordance with cylindrical cavity expansion theory, the EPPs are given by Eq. 2.5. The rigidity index ($I_r = G/s_u$) is generally between 130 to 230 for normally consolidated

speswhite kaolin clay (Hjortnaes-Pedersen and Bezuijen, 1992). A value of 150 is used in this study.

Table 4.2: Predicted and measured EPPs

h (mm)	u_{max} at $r=r_0$ from Eq. 2.5 (kPa)	u_{max} at $r=r_0+20$ mm (kPa)		
		From Eq. 2.5	Measured	
			SAT06	SAT08
72	16.5	7.2	8.2	6.0
83	19.2	8.3	10.2	12.2
158	36.4	15.7	16.1	15.2
206	-	-	3.4	3.0
212	-	-	2.7	2.7
232	-	-	2.2	1.5

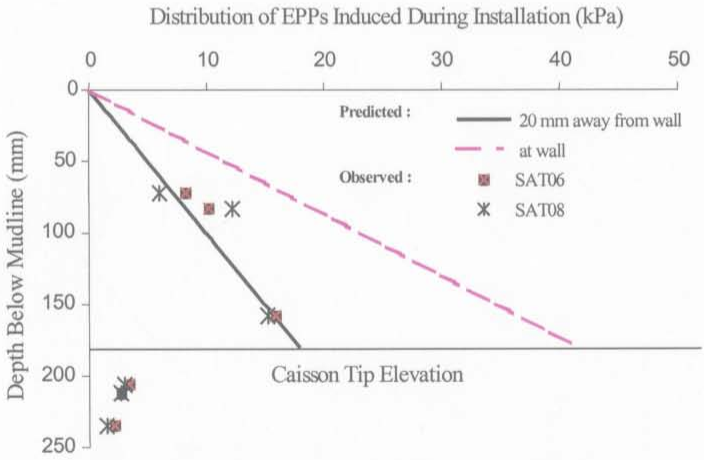

Figure 4.11: Predicted and measured EPP distributions

The measured initial EPPs in the soil outside the caisson at elevations above the caisson's tip were in reasonable agreement with the predictions using cylindrical cavity expansion theory.

4.3.2 EPP Dissipation

The pullout capacity of suction caissons is related to the EPPs. The dissipation of these EPPs was investigated in this study. Figure 4.12 presents the results of a typical centrifuge test, the change in excess pore water pressures during the installation phase (0 to about 500 second) and the consolidation phase from the end of installation to the beginning of the pullout test (about 500 to 8200 second). The EPPs increased during installation from 0 to about 500 second, and they decreased with time after the installation.

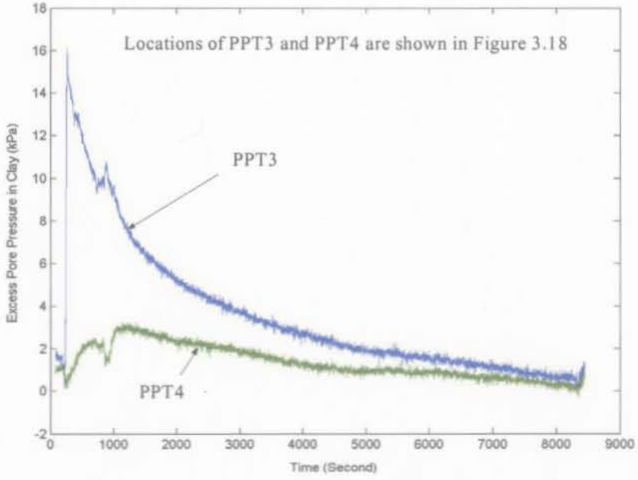

Figure 4.12: EPP's development and dissipation with time

Table 4.3 presents the local measurements (20 mm away from caisson wall) on the times of 25%, 50%, 75% and 90% EPP dissipation in the centrifuge tests.

Table 4.3: Local measurements of EPP dissipation

Degree of Consolidation U (%)	Measured Time (second)		Averaged Time (second)
	SAT06	SAT08	
25	220	285	253
50	821	526	673
75	2091	1588	1840
90	3820	4400	4110

Note: PPT was embedded 20 mm away from caisson wall and 158 mm below mudline.

Radial consolidation theory is used to predict the dissipation of the EPPs around a driven pile (Soderberg, 1962) from

$$\frac{\partial u}{\partial t} = c_h \left[\frac{\partial^2 u}{\partial r^2} + (\frac{1}{r})(\frac{\partial u}{\partial r}) \right] \tag{4.9}$$

where c_h is the two-dimensional coefficient of lateral consolidation, u is the excess pore pressure. A time factor T , as expressed by Eq. 4.10, is used to predict the EPP dissipation.

$$T = \frac{c_h t}{r_p^2} \tag{4.10}$$

where t is the time of EPP dissipation, r_p is the pile diameter, and c_h is the coefficient of lateral consolidation.

Radial consolidation theory was also used to predict the dissipation of the EPPs for suction caissons in clay (Hjotnaes-Pedersen and Bezuijen, 1992). However, it is difficult

to determine the drainage distance. Suction caissons act as cookie cutters (i.e., normally without the formation of soil plug), therefore, both the diameter and wall thickness should be considered in the estimation of drainage distance. In this study, using the annular base area of the caisson, an equivalent value of r_p in Eq. 4.10 is derived as

$$r_p = \frac{\sqrt{D_0^2 - D_i^2}}{2} \tag{4.11}$$

The outside diameter and wall thickness of model caisson SC #1 used for Tests SAT06 and SAT08 are 51.7 and 0.65 mm, and the derived value of r_p is 5.76 mm. Therefore, the dissipation of the EPPs in the soil can be described by Eq. 4.9, with an initial EPP distribution in form of Eq. 2.5, and boundary conditions as

$$u\big|_{r=R_p} = 0 \tag{4.12}$$

$$\left.\frac{\partial u}{\partial r}\right|_{r=r_p} = 0 \tag{4.13}$$

where R_p is the plastic zone radius.

The general solution of Eq. 4.9 with the initial EPP and boundary conditions described by Eqs. 2.5, 4.12, and 4.13 was discussed by Randolph and Wroth (1979), Zhu and Yin (2001) and Guo (2000). The solution procedure is briefly presented as follows:

Separation of the variables of Eq. 4.9 leads to

$$u = \sum_{m=1}^{\infty} A_m R_m(r) \exp(-\mu_m^2 \frac{c_h t}{r_1^2}) \tag{4.14}$$

where R_m in Eq. 4.14 can be expressed as a function of Bessel functions of the first kind (J_0, J_1) and of the second kind (Y_0, Y_1) as in Eq. 4.15.

$$R_m(r) = Y_0(N_1\mu_m)J_0(\mu_m\frac{r}{r_1}) - J_0(N_1\mu_m)Y_0(\mu_m\frac{r}{r_1}) \tag{4.15}$$

The quantity μ_m is the m-th positive root of Eq. 4.16

$$Y_0(N_1\mu_m)J_1(\mu_m) - J_0(N_1\mu_m)Y_1(\mu_m) = 0 \tag{4.16}$$

where $N_1 = \frac{R_p}{r_0}$ (4.17)

and $$A_m = \frac{2s_u\int_{r_0}^{R_p} r\ln(\frac{R_p}{r})R_m dr}{\int_{r_0}^{R_p} rR_m^2 dr} = \frac{4s_u R_m(r_0)}{\frac{4}{\pi^2} - \mu_m^2[R_m(r_0)]^2} \tag{4.18}$$

Letting $T_h = \frac{\mu_1^2 c_h t}{r_0^2}$ $C_m = \frac{A_m}{s_u}$ (4.19)

The normalized excess pore pressure (EPP) is

$$\frac{u}{s_u} = \sum_{m=1}^{\infty} C_m R_m(r)\exp\left[-\frac{\mu_m^2}{\mu_1^2}T_h\right] \tag{4.20}$$

The normalized EPP u/s_u in the plastic zone can be numerically solved for different N_1, r/r_0 and T_h and the eigenvalues.

The solutions of Eq. 4.9 under initial EPP and boundary conditions described by Eqs. 2.5, 4.12, and 4.13, using $T = \frac{r_0^2}{r_p^2 \mu_1^2} T_h$ (T is defined as Eq. 4.10), are presented in Figure 4.13. Here, x-axis is the distance from the local location to the caisson wall, and y-axis is the consolidation degree expressed as a ratio of the dissipated EPP at a point to the initial EPP at this point $(1-u(r,t)/u(r,0))$.

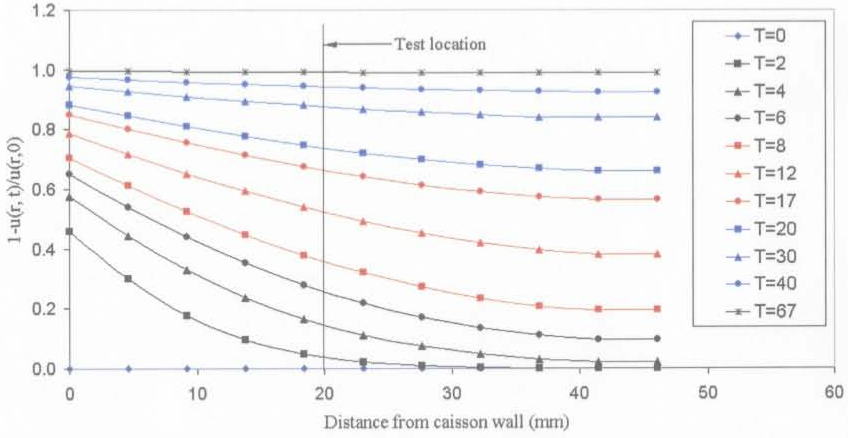

Figure 4.13: EPP dissipation results by radial consolidation theory

Generally, the local degree of consolidation at the location 20 mm away from caisson wall is less than that close to the caisson wall. This difference is about 0.3 to 0.4 for T values of 12 and less, 0.1 to 0.2 for T values between 15 to 22, and less then 0.07 for T values larger then 30. Therefore, the EPP dissipation rates from radial dissipation measured in this study (20 mm away from caisson wall) should be slower then the EPP dissipation rates near the caisson wall. That is using records at 20 mm away from caisson

wall may underestimate the dissipation rates of the EPPs near the caisson wall. However, the vertical consolidation at the top and the tip of the caisson in the above theoretical analyses is neglected. Suction caissons usually have an embedment ratio in the range from 1 to 7, which is much less than that of the piles. Hence, the difference of consolidation degree between the caisson wall and 20 mm away for practical cases should be less than that obtained from radial consolidation theory, as the vertical dissipation of the EPPs in the soils at the top and at the tip of the caisson should not be neglected.

Assuming c_h of the testbed clay is 0.21 mm^2/s (Al-Tabbaa and Muir Wood, 1991) and using Eq. 4.10, the measured values of time factor (T) from Tests SAT06 and SAT08 are presented in Figure 4.14, together with the predictions using radial consolidation theory. The theoretical time factor (T) values are larger than the test results for a given degree of consolidation. This difference is attributed to the vertical dissipation at the seafloor and caisson's tip in the model test. After installation of the caisson, 50, 80 and 90% EPPs dissipated at time factors (T) of about 4, 16 and 26, respectively. Even though those results are local measurements, as discussed above, it may be appropriate when they are used to estimate the EPP dissipation in suction caisson design.

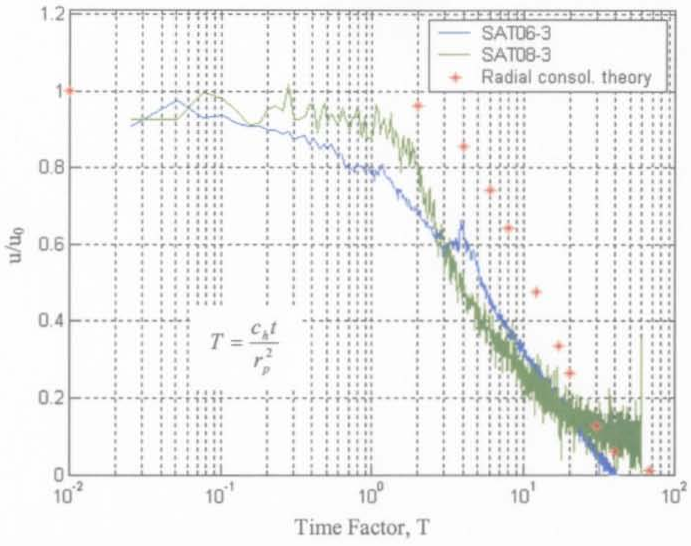

Figure 4.14: Measured local EPP dissipation and theoretical predictions

For driven piles of $D/\Delta \leq 50$ (D is the diameter and Δ is the wall thickness of the pile), an empirically determined hyperbolic consolidation-time equation was presented by Bogard and Matlock (1990) to estimate the degree of consolidation of porewater pressure at the pile surface, which closely fitted their field observed data at Harvey and Empire

$$U = t/t_{50}/(1.1 + t/t_{50}) \tag{4.21}$$

where U is the degree of consolidation, and t_{50} is the time at which the EPPs are reduced to half the initial maximum values.

Eq. 4.21 cannot be directly used to predict the dissipation of the EPPs for these centrifuge tests due to the fact that D/Δ is greater than 50. Two bounds of U can be achieved when the ratio of diameter to wall thickness of the caisson is adjusted to 48

(recommended maximum value to be used with Eq. 4.21) by assuming either its diameter or its wall thickness. When the wall thickness is kept constant and the diameter is adjusted to a value by $D/\Delta = 48$, Eq. 4.21 gives the upper bound U. When the diameter is kept constant and the wall thickness is adjusted to a value by $D/\Delta = 48$, Eq. 4.21 gives the lower bound U. Model caisson SC #1 had a 5.17 m diameter and 65 mm wall thickness at prototype scale. Using Eq. 4.21, the upper bound U is estimated using wall thickness of 65 mm and adjusting the diameter to 3.1 m (to keep the D/Δ ratio to 48), and a lower bound U is estimated using a diameter of 5.17 m and adjusting the wall thickness to 108 mm (to keep the D/Δ ratio to 48). Figure 4.15 presents the centrifuge test results and the predictions using Eq. 4.21 after adjusting either the diameter or the wall thickness of the caisson, as described above.

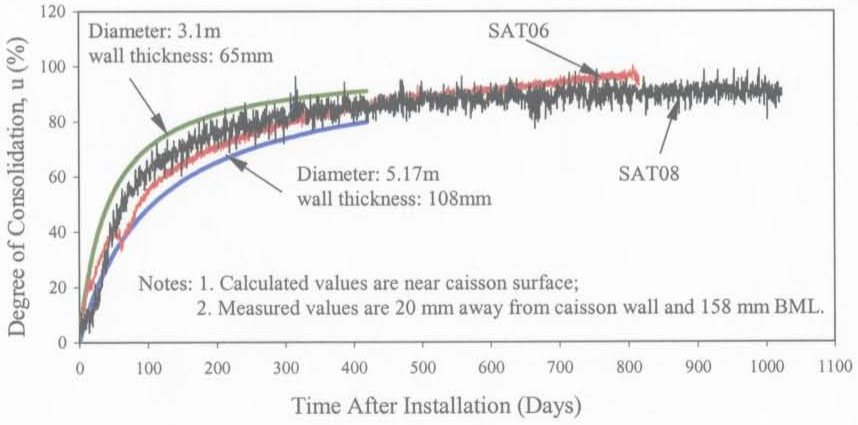

Figure 4.15: Comparison of EPP dissipation

As can be seen, the degree of consolidation values at any time, obtained from the centrifuge test results are bounded by the theoretical lower and upper bounds, indicating that modified Bogard and Matlock method can also be used to predict the dissipation of the EPPs in clay soils around the suction caissons.

The above analyses show that both radial consolidation theory and modified Bogard and Matlock method can be used to predict the consolidation time of the EPPs in the soil for suction caissons. When radial consolidation theory is used, an equivalent r_p can be calculated based on the annular base area of the caisson. When modified Bogard and Matlock method (Eq. 4.21) is used, adjustments should be made to the diameter or the wall thickness so as to keep the D/Δ ratio (diameter/wall thickness) a maximum value of 48.

4.4 Pullout Resistance Mobilization

It is very important for designers and operators of suction caissons to understand how the pullout resistance is mobilized with vertical displacement ($F_{pu} - d$). The $F_{pu} - d$ behavior of suction caissons is different from that of driven piles. It usually depends on the behavior of the soil, the passive suction in the soil inside the caisson and below the tip, and the pullout velocity.

Two kind tests were designed in this study (as shown in Figure 4.16) to investigate the $F_{pu} - d$ behavior of suction caissons. Type A is a suction caisson with its top closed

during pullout test, and model caisson SC #1 was used. Type B is an open topped pile, and model caisson SC #3 was used.

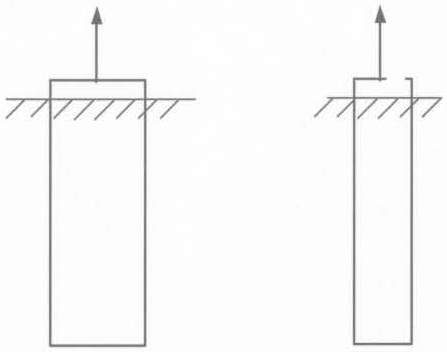

Figure 4.16: Test types used for investigating $F_{pu} - d$ behavior

Figure 4.17 presents a typical $F_{pu} - d$ curve of test type A. Both the total pullout force and suction force developed with the vertical displacement. A relative large pullout force could be mobilized in a small displacement. However, a vertical displacement of 4 to 10% diameter was required to achieve the ultimate pullout force (capacity) and the maximum suction. The suction force, measured using two PPTs mounted inside and outside the caisson top, was about 40 to 60% of the total pullout force. After its peak, the passive suction slowly decreased with increasing displacement until the caisson had a relative large vertical displacement (i.e., a half diameter).

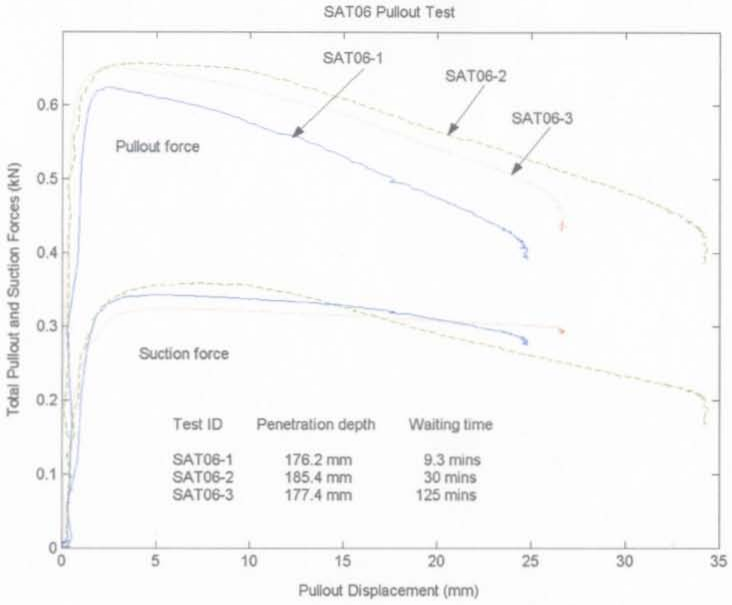

Figure 4.17: A typical $F_{pu} - d$ curve of suction caissons

Figure 4.18 presents a typical $F_{pu} - d$ curve of test type B. The pullout force was quickly mobilized with displacement. The pullout capacity arrived its maximum at a vertical displacement of approximate 1% diameter or less, and then decreased with further displacement.

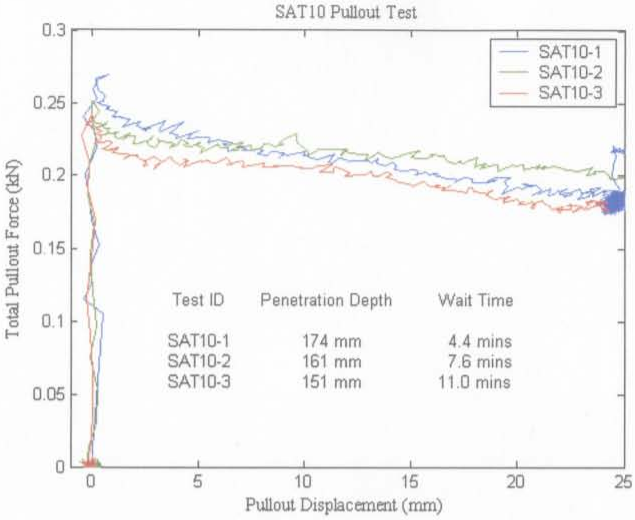

Figure 4.18: A typical $F_{pu} - d$ curve of top opened caissons

Figure 4.19 presents the centrifuge test results of Tests SAT06 (type A) and SAT10 (type B). Here, the pullout capacity is the sum of the external skin friction resistance and the reverse end bearing (*REB*) for Test SAT06 (type A), and the internal skin friction resistance (as discussed in Section 4.6.3, this resistance is limited to the buoyant weight of the soil plug) and the external skin friction resistance for Test SAT10 (type B). The normalized pullout capacity is defined as the ratio of pullout capacity to $(\bar{s}_u \times A_{se})$, where $\bar{s}_u$ is the average undrained shear strength of clay along the caisson/pile wall, and A_{se} is the external wall skin area of the caisson/pile. The normalized capacities obtained from Test SAT10 (type B) were only about 50 to 60% of those obtained from Test SAT06 (type A). The embedment ratio may have an effect on the normalized capacity. However, this effect could be very small because the

embedment ratios of those tests are between 2 to 7, a typical range for suction caisson design. Compared with the test results of Test SAT06 (type A), the normalized pullout capacities of Test SAT10 (type B) were small because no passive suction was generated and the internal skin friction is limited to the buoyant weight of the soil plug during the pullout test. Therefore, it is suggested that the caisson should be sealed after installation, so that the passive suction can be effectively mobilized.

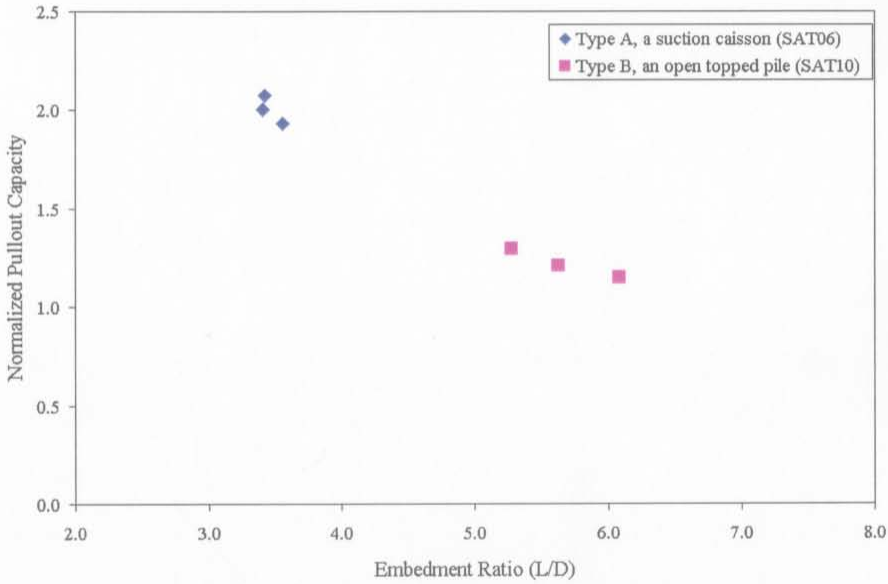

Figure 4.19: Test result comparison between Type A and Type B

It is usually considered that the REB can only be mobilized for a suction caisson under a relatively large loading rate. However, studies (Randolph and House, 2002) showed that a sealed top caisson had a larger pullout capacity than an open topped caisson/pile even under a very slow loading rate. Therefore, it is suggested that the

caisson should be sealed after installation, so that the passive suction can be effectively mobilized.

This comparison indicates that the $F_{pu} - d$ behavior of suction caissons is completely different from that of open topped caissons/piles. Suction caissons can generate a very large passive suction, which is one of the main components contributing to the capacity. However, a relative large displacement is required to mobilize the passive suction.

4.5 Failure Mechanism

Centrifuge tests indicated that a confined general shear (CGS) failure, defined in Section 5.4.1, is the most appropriate mechanism to describe the failure of a deeply embedded suction caisson in NC or SOC clay. At the beginning of the pullout of a caisson, the soil close to the caisson outside wall had a little upward movement due to the mobilization of friction between caisson-soil interface, until the shear force exceeded the maximum friction at a large vertical displacement then the caisson/soil slippage occurred. The failure occurred at the interface of the caisson wall and the outside soil. The passive suction in the soil inside the caisson and below its tip quickly developed with the pullout displacement. The recorded maximum passive suction force (defined as reverse end bearing *REB* in this study) inside the caisson top was larger than the sum of the plug weight and the calculated tension force of the soil at the tip of the caisson, which means that *REB* was mobilized during the pullout. From the analysis on the EPP changes in clay outside the caisson during pullout (see Section 4.7), it could be concluded that the

development of *REB* accompanied by a small upward movement of the adjacent soil outside the caisson and a "soil flow" pattern from the soil outside and away from the caisson to the inside of the caisson. Both the total force and passive suction started to drop off with the displacement after their peaks. For most cases, as shown in Figure 4.20, the soil plug was always found to come out off from the caisson after test. These features indicate that a confined general shear (CGS) failure is the most appropriate failure mechanism. This failure mechanism was confirmed by the finite element analyses conducted in this study (see section 5.4.1).

Figure 4.20: Evidence of plug falling out from the caisson

Based on the confined general shear (CGS) failure mechanism, the pullout capacity of suction caissons can be derived through limit equilibrium analysis. Figure 4.21 indicates the forces applying on both the caisson and the soil plug during pullout.

For the caisson, the pullout capacity can be written as

$$F_{pu} = F_{psu} + F_{ef} + F_{if} + W_c \tag{4.22}$$

where F_{pu} is the pullout capacity, F_{psu} is the suction force applied on the inside top of the caisson, F_{ef} and F_{if} are the external and internal wall skin frictions, W_c is the buoyant weight of the caisson.

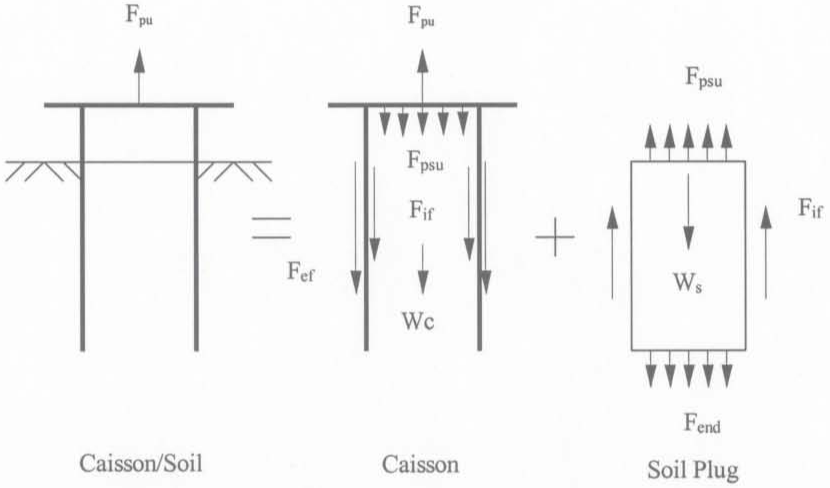

Figure 4.21: Failure mechanism of suction caissons in clay

If the resultant effect of the buoyant weight of the soil plug, the internal wall skin friction and the tension and the suction of the soil at the caisson tip is assumed as the reverse end bearing (*REB*), Eq. 4.22 can be rewritten as

$$F_{pu} = F_{ef} + REB + W_c \tag{4.23}$$

where *REB* is the passive suction force acting on the caisson, and can be calculated by

$$REB = A_{sp}(p_i - p_o) \tag{4.24}$$

where A_{sp} is the internal cross section area of the caisson, p_i and p_o are the readings of the two PPTs mounted on the outside and inside caisson top (p_i - p_o is the passive suction).

In this study, a reverse end bearing factor N_E was used to describe the *REB*, as

$$N_E = \frac{REB}{s_u A_{sp}} \tag{4.25}$$

where s_u is the undrained shear strength of the soil at the caisson tip.

The external wall friction, F_{ef} during pullout can be described by a friction coefficient (α_{pu}) governed by

$$F_{ef} = \alpha_{pu} \bar{s}_u A_{se} \tag{4.26}$$

where α_{pu} is friction coefficient during pullout of a caisson, $\bar{s}_u$ is the average undrained shear strength of the outside soil along the wall skin (skirt), A_{se} is the external wall skin area of the caisson over which shearing resistance is generated.

Both the friction coefficient and the reverse end bearing factor measured from the centrifuge tests will be discussed in Section 4.6.

4.6 Reverse End Bearing Factor and Setup Development

In the centrifuge tests, the pullout force was measured by a load cell, and the passive suction was monitored by two pore pressure transducers (PPTs) mounted inside and outside the top of the caisson. Using the confined general shear failure mechanism

described in Sections 4.5 and 5.41 and the centrifuge test data, the friction coefficient and the reverse end bearing factor during pullout of suction caissons can be obtained. The setup curve was determined through the analysis of the friction coefficient increase with time. The passive suction is first discussed in this section because it is assumed to equal the reverse end bearing in this failure mechanism.

4.6.1 Passive Suction

The passive suction is defined as the pressure differential of the inside and the outside caisson top. During the centrifuge tests of this study, the passive suction was directly measured by two PPTs mounted on the inside and the outside caisson top surfaces. Figure 4.22 presents the passive suction test results of Test SAT06. The passive suction increased very fast at the beginning of pullout, and peaked after a vertical displacement of 4 to 10% diameter. This suction slightly dropped off with displacement after its peak until the caisson had a relative large vertical displacement (i.e., a half diameter). The recorded maximum passive suction was in the range from 160 to 180 kPa when the caisson was installed in NC clay and the penetration depth was approximately between 170 and 185 mm.

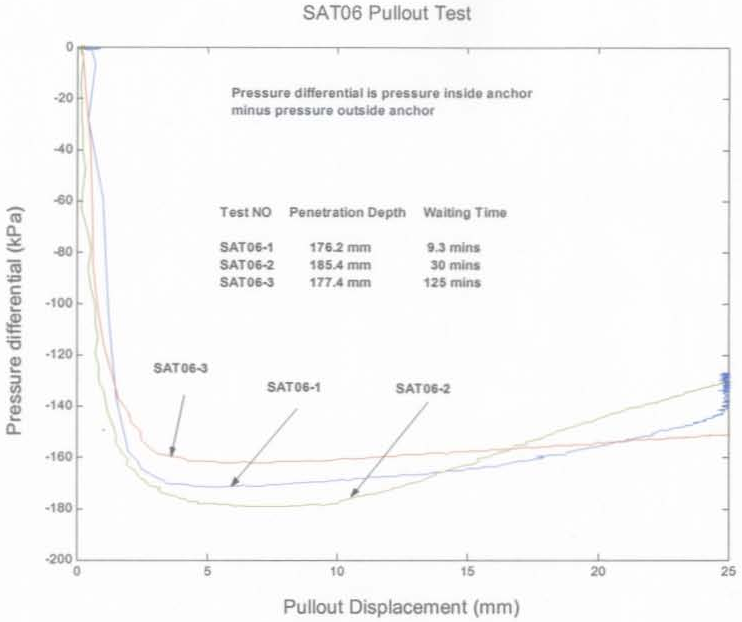

Figure 4.22: Suction development during pullout test

4.6.2 Reverse End Bearing Factor

Figure 4.17 presents the pullout test results of Test SAT06. The passive suction was monitored by the two PPTs mounted on the inside and the outside top of the caisson, and the reverse end bearing factor N_E was calculated by Eq. 4.25.

The reverse end bearing factors measured from centrifuge tests are presented in Table 4.4. The reverse end bearing factor N_E varied from 6.5 to 10.8, and the average is 8.7.

Table 4.4: Reverse end bearing factors from centrifuge tests

Test ID	Penetration Depth (mm)	Passive Suction Force (kN)	N_E	Wait Time (minutes)
SAT04-1	165	0.406	10.8	7.8
SAT04-2	155	0.369	10.5	29.6
SAT04-3	162	0.373	10.1	121.2
SAT06-1	176	0.343	7.0	9.3
SAT06-2	184	0.358	7.2	30.0
SAT06-3	177	0.324	6.5	125.0
SAT08-1	168	0.378	9.3	10.2
SAT08-2	160	0.356	8.6	31.6
SAT08-3	160	0.328	7.9	150.0

The test results in Table 4.4 indicate that the N_E value slightly decreased with the length of wait time in each test (such as SAT04 or SAT08). This slight decrease might be due to the decrease of the effective stress in the soil inside the caisson and around its tip. Generally, the effective stress in the soil inside the caisson suddenly increases when active suction (negative EPPs) is applied during installation. The effective stress in the soil inside the caisson decreases with time after installation due to the seepage gradient (the top of the caisson was opened). The longer the wait time is, the more the effective stress decreases. However, the EPPs (negative values) in the soil inside the caisson and below its tip develop very fast with the pullout displacement, the effective stress in the soil can rebound in a very short time. Therefore, the reduction of the *REB* due to the decrease of the effective stress in the soil inside the caisson and below its tip is very small. Moreover, the EPPs generated in the soil outside caisson are positive and the

effective stress in the soil decreases during installation. As the EPPs dissipate, the effective stress in the soil outside caisson increases with the wait time after installation, leading to an increase of the external wall skin friction. Usually, the increase in external skin friction is much bigger than the decrease in the *REB*, resulting in a general increase in the total pullout capacity.

The reverse end bearing factor N_E is affected by a number of factors, such as soil properties, caisson geometries, loading types (static or cyclic) and loading rate. As N_E is calculated using both the test data and the undrained shear strength of the soil at the tip s_u, its value is also influenced by the undrained shear strength of the soil. Therefore, the value of N_E can be different when different methods are used in the determination of s_u. As mentioned in Section 2.2.6, N_E was found to range from 4.7 to 11.3 by Fuglsang and Steensen-Back (1991), from 1.5 to 4.5 by Das et al. (1994), from 3.5 to 7.5 by Datta and Kumar (1996), and from 2 to 5 by Rao at al. (1997). Randolph and House (2002) used physical model tests to investigate the behavior of suction caissons. They found that the reverse end bearing factors ranged from 14.6 for short term monotonic loading, and down to 9.1 for sustained loading. Clukey and Phillips (2002) reported a value of 9.4. The N_E values found in this study (from 6.5 to 10.8) are close to the upper bound results of Steensen-Bach (1992) and lower bound results of Randolph and House (2002). The average value of N_E (8.7) is between 7 and 9, which is the customarily assumed range for offshore design. The comparison between the measured N_E of this study and the literature results is presented in Figure 4.23.

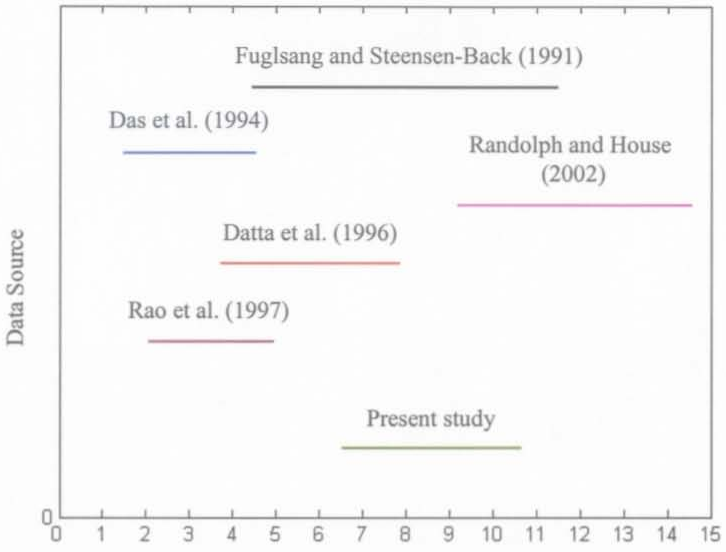

Figure 4.23: Comparison of reverse end bearing factor

4.6.3 Friction Coefficient and Setup Development

The external wall skin friction makes a significant contribution to the pullout capacity of a suction caisson. As discussed in Section 4.5, the pullout capacity of suction caissons, the *REB* and the external wall skin friction can respectively be calculated by Eqs. 4.23, 4.24 and 4.26.

Combining Eq. 4.23 and Eq. 4.26, the friction coefficient α_{pu} can be expressed as

$$\alpha_{pu} = \frac{F_{pu} - REB - W_c}{\bar{s}_u A_{se}} \tag{4.27}$$

Figure 4.17 presents a typical pullout test result. The buoyant weight of the caisson was determined before the test started. Therefore, the friction coefficient can be calculated by Eq. 4.27 using the test data, and Table 4.5 and Figure 4.24 present the centrifuge test results carried out in this study.

Table 4.5: Friction coefficients from the centrifuge tests

Test ID	Penetration Depth (mm)	Total Capacity (kN)	*REB* (kN)	Wall Friction (kN)	α_{pu}	Wait Time (minutes)
SAT04-1	165	0.619	0.406	0.163	0.65	7.8
SAT04-2	155	0.592	0.369	0.173	0.78	29.6
SAT04-3	162	0.756	0.373	0.333	1.37	121.2
SAT06-1	176	0.624	0.343	0.231	0.66	9.3
SAT06-2	182	0.656	0.358	0.248	0.78	30.0
SAT06-3	177	0.651	0.324	0.277	0.86	125.0
SAT08-1	168	0.656	0.378	0.188	0.66	10.2
SAT08-2	160	0.656	0.356	0.210	0.83	31.6
SAT08-3	160	0.696	0.328	0.278	1.10	153.0

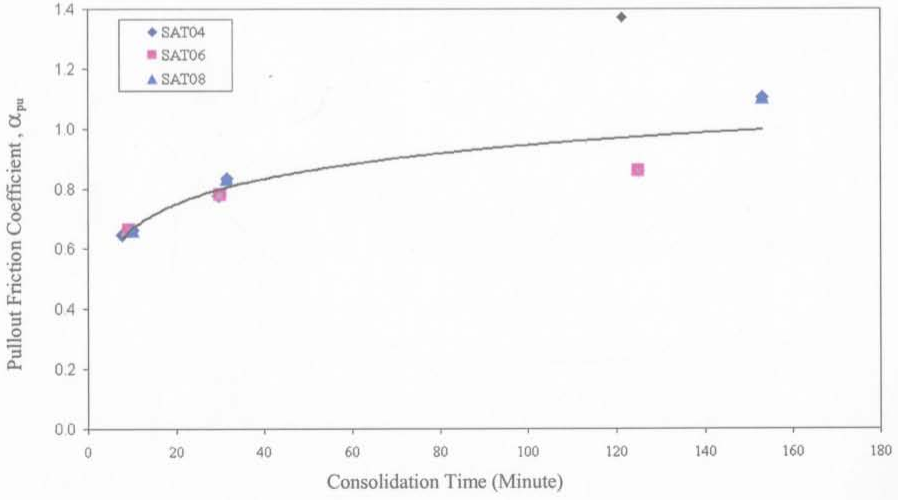

Figure 4.24: Wall skin friction development of suction caissons

The measured friction coefficient α_{pu} during pullout test changed with the time interval from the end of the installation to the beginning of the pullout test. The friction coefficient α_{pu} during the pullout test is larger than the friction coefficient α_{pe} during installation. During installation, the EPPs were generated in the clay. The effective stress in the soil decreased with the generation of the EPPs, leading to a reduction in the wall skin friction resistance. The EPPs induced during installation dissipated with time. From Section 4.3.2, about 50, 75 and 95% of initial EPPs were dissipated when the caisson was installed in the clay for 10, 30 and 120 minutes, respectively. The dissipation of the EPPs caused an increase of the effective stress in the soil, resulting in an increase in the external wall skin friction. Generally, the longer the wait time after installation of the caisson, the larger the friction coefficient during pullout of the caisson.

Based on the confined general shear failure mechanism discussed in Sections 4.5 and 5.4.1, the development of pullout capacity depends in part on the development of the external wall skin friction. The increase of the wall skin friction with time is due to the regain of shear strength of the outside soil along the caisson's wall after installation, and is defined as setup.

The pullout friction coefficient was measured in this study and the setup development can be determined through analyzing the test results of the friction coefficient. Using the test results presented in Table 4.5 and Figure 4.24, a setup curve was developed and presented in Figure 4.25. In this curve, a time factor T, defined by Eq. 4.10 was used to describe the consolidation of the clay. From the test results, 60 to 75% friction resistance

could be mobilized at a time factor T = 3.5. The caisson can achieve 75 to 85 % friction resistance at T = 11.4, and at least 95% wall skin friction could be developed when $T \geq 46$.

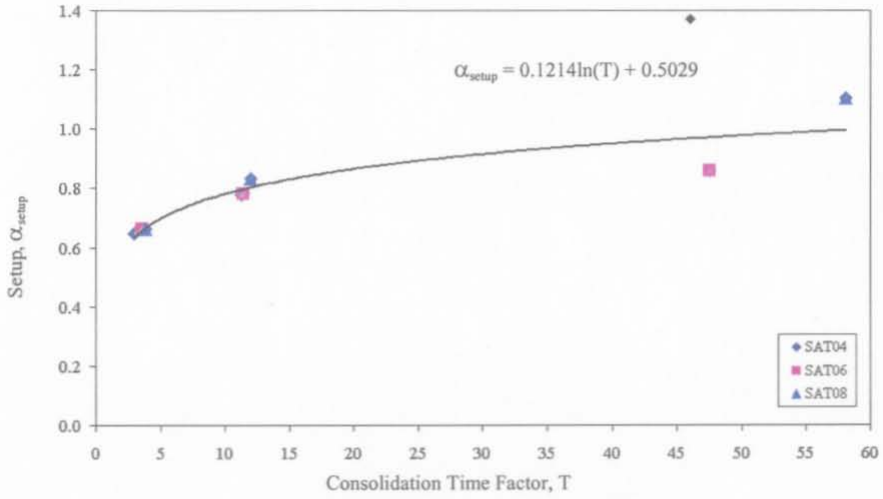

Figure 4.25: Setup development with time

Based on the centrifuge test data, the following regression equation can be used to describe the setup development with time

$$\alpha_{setup} = 0.1214 \ln(T) + 0.5029 \tag{4.28}$$

where T is the time factor defined by Eq. 4.10.

According to the centrifuge test results, the time factor T for developing 90% setup is 16.3 (i.e., 16 months in prototype), which is smaller than the corresponding time factor T based on the results presented by Hjotnaes-Pedersen and Bezuijen (1992) and Renzi et al. (1991).

Test SAT10 was carried out to investigate the behavior of open topped caissons/piles in NC clay. The test results are presented on Figures 4.18 and 4.19 and Table 4.6.

Table 4.6: Friction coefficients from Test SAT10

Test ID	Penetration Depth (mm)	Total Capacity (kN)	Soil Plug Weight (kN)	Wall Friction (kN)	α_{pu}	Wait Time (minutes)
SAT10-1	174	0.269	0.061	0.118	0.77	4.4
SAT10-2	161	0.251	0.056	0.105	0.79	7.6
SAT10-3	151	0.242	0.052	0.100	0.85	11.0

For open topped caissons/piles, the internal skin friction resistance is limited to the buoyant weight of the soil plug during pullout test. The measured external friction coefficient varied from 0.77 to 0.85 with the time factor T from 1.5 to 4.2 (i.e., 4.4 to 11 minutes in centrifuge) after installation. Compared with the results of Tests SAT06 and SAT08 (suction caissons), the external skin friction develops fast with time factor T as the model caisson size was smaller. However, the development of the internal friction is limited to the buoyant weight of its soil plug, and no passive suction could be mobilized during pullout test. Therefore, the total pullout capacity of an open topped caisson/pile is smaller than that of a suction caisson (see Figure 4.19 in Section 4.4).

4.7 EPP Distribution during Pullout Test

Figure 4.26 presents the measured distribution of the excess pore pressures (EPPs) in the soil during the pullout test from the six embedded pore pressure transducers (PPTs),

at three caisson test locations indicated on Figures 3.18 and 3.19. These PPTs were embedded in clay 20 mm away from the caisson's outside wall. Their embedment depths below the mudline were 72 mm for PPT 1, 83 mm for PPT 2, 158 mm for PPT 3, 206 mm for PPT 4, 212 mm for PPT 5 and 232 mm for PPT 6.

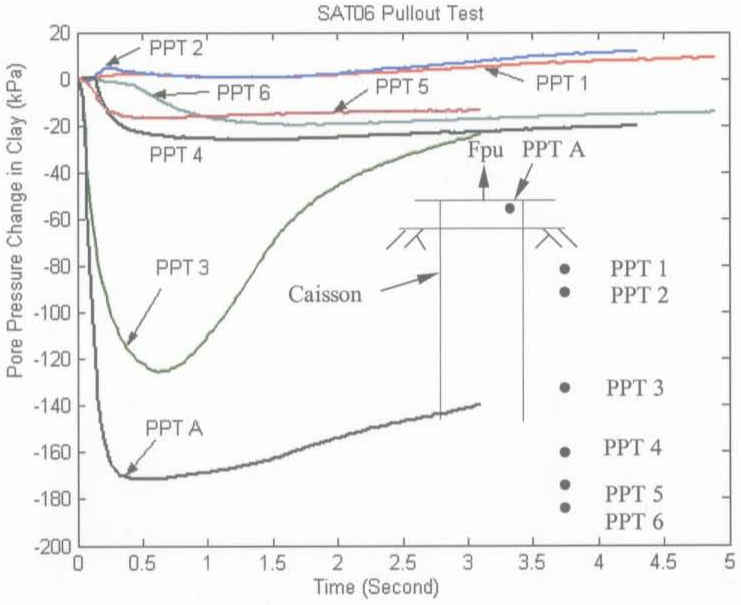

Figure 4.26: Distribution and development of the EPPs during pullout test

The EPP, also called the pore pressure change, is defined as the change in the pore pressure transducer's reading during the pullout test. The EPP (change of pore pressure) increased from a very small value (almost 0) at the top surface to about 130 kPa suction at 158 mm depth, then decreased to 30, 18 and 15 kPa at 206, 212, 232 mm below mudline, respectively. The maximum EPP (change of the pore pressure) in the soil

outside the caisson occurred around the caisson's tip. The EPP increased slowly with depth from mudline to the caisson, and then decreased with depth to about zero a few diameters below the caisson's tip. This clearly indicates the development of the reverse end bearing in the soil around the caisson's tip.

Figure 4.26 indicates that the EPPs measured by PPT 1 and PPT 2 had a slight increase (positive values). This increase of EPPs might be due to the elevation changes of the PPTs by the downward movement of the around soil during pullout test. The EPPs measured by PPT 4, PPT 5 and PPT 6 were negative values, and indicated the soil around those PPTs had an upward movement. Therefore, it could be concluded that the development of *REB* was accompanied by downward movement of adjacent soil outside the caisson and upward movement of the soil below its tip.

When uplift loading is applied on the caisson, the caisson starts to move upward (or it has an upward moving tendency). The saturated soil around the caisson provides a resistance to stop the caisson's movement. As the top of the caisson is sealed and its wall is impermeable, the relative movement (tendency) between the caisson and the around soil generates negative excess pore pressures in the soil which is called passive suction. Also, the soil plug has an uplift movement (tendency) due to both the passive suction inside the caisson and the internal friction and the soil below the caisson's tip resists this movement, leading to the generation of the negative excess pore pressures (passive suction) in the soil below the caisson's tip. The passive suction in the soil below the

caisson's tip decreases with depth due to the increase of seepage in the soil from all directions and the decrease of the shear strains of the soil.

The maximum EPPs inside the caisson top (defined as passive suction in this study) during pullout test were between 160 kPa to 180 kPa (see Figure 4.22). The generated EPPs in the soil decreased along the path from the plug top (PPT A in Figure 4.26) to its bottom (tip of the caisson), then to the location of PPT3, and further to the outside soil far away from the caisson tip. This clearly indicates that a high seepage gradient was developed, resulting in the occurrence of piping inside the caisson.

As the caisson was pulled out at a velocity of 10 mm/second in the centrifuge tests, Figure 4.26 also indicates that the excess pore pressures in the soil outside the caisson developed very fast with the pullout displacement. The maximum change of the EPPs were mobilized when the caisson was pulled out a displacement of about 4 to 10% diameter (approximately 2 to 6 mm).

4.8 Summary

Centrifuge tests were carried out to investigate the behavior of suction caissons in NC and SOC clay. The following conclusions can be drawn from the test results:

1. The penetration resistance of suction caissons increased with depth during both self-weight and suction penetration. It depends on the soil properties and the effective stress in the soil which is influenced by the excess pore pressures induced during installation of the caisson. The application of active suction from the end of self-weight

penetration changes the "soil flow" pattern, resulting in a sudden increase in penetration resistance. As the effective stress in the soil outside caisson increases during the time due to the dissipation of the EPPs generated during self-weight penetration, leading to an increase in the external skin friction, a part of the penetration resistance. Therefore, the delay from the end of self-weight penetration to the beginning of suction penetration should be minimized, so that the penetration resistance can be reduced.

2. The friction coefficient is affected by the wall thickness. The larger the ratio of diameter to wall thickness (D/Δ), the smaller the friction coefficient.

3. For caissons with D/Δ ratio (diameter to wall thickness) from 64 to 79 and H/D ratio (embedment to diameter) from 1.8 to 3.5, the penetration resistance can be predicted by using a friction coefficient α_{pe} = 0.2 for self-weight penetration and α_{pe} = 0.3 for suction penetration. For caissons with a D/Δ ratio of about 28 and a H/D ratio of about 5.5, the penetration resistance can be calculated using α_{pe} = 0.3 for self-weight penetration and α_{pe} = 0.5 for suction penetration.

4. The excess pore pressures (EPPs) generated in the soil during the installation of a suction caisson increased with depth from mudline to the maximum penetration depth (i.e., the tip of the caisson). Then, the EPPs quickly decreased to a small value (almost zero) in the soil at half diameter below the caisson's tip.

5. Cylindrical cavity expansion theory expressed by Eq. 2.5 (originally developed for driven piles) can be used to estimate the distribution of the initial EPPs in the soil induced by installation of suction caissons.

6. Centrifuge tests showed that, after installation of the caisson, 50, 80 and 90% EPPs dissipated at time factors (T) of about 4, 16 and 26, respectively. Even though those results are local measurements, as discussed in Section 4.3.2, it may be appropriate when they are used to estimate the EPP dissipation in suction caisson design.

7. Radial consolidation theory can be used to predict the dissipation of the EPPs in the soil induced by installation of a suction caisson. The theoretical time factor (T) values are larger than the test results for a given degree of consolidation. This difference is attributed to the vertical dissipation at the seafloor and caisson's tip in the model test.

8. Modified Bogard and Matlock method (initially derived for driven piles) can also be used to predict the dissipation of the EPPs in clayey soils for suction caissons, provided adjustments are made to the diameter or the wall thickness of the caisson, so as to keep the ratio of diameter to wall thickness (D/Δ) to a maximum value of 48.

9. Centrifuge tests indicated that, for a suction caisson under an undrained loading condition (fast loading rate), a confined shear failure mechanism was the most appropriate one to describe the failure of suction caissons in NC and SOC clay. The passive suction developed quickly with the pullout displacement. A displacement of approximately 4 to 10% diameter was required to mobilize both the maximum passive suction and the maximum pullout capacity. The passive suction force was in range between 40 and 60% of the pullout capacity.

10. The effective stress in the soil outside the caisson increased with the dissipation of EPPs, resulting in that the friction resistance increases with time.

11. The reverse end bearing factor varied from 6.5 to 10.8, with an average of 8.7. The average value is between 7 to 9, which is the customarily assumed range for offshore design.

12. The setup, used to describe the development of external wall skin friction, increased with time after installation of the caisson. 60 to 75%, 75 to 85 % and at least 95% setup could be developed for time factors (T) of 3.5, 11.4 and 46, respectively. The setup development with time can be predicted using Eq. 4.28.

13. The pullout capacity for an open topped caisson-pile was smaller than that of a suction caisson. The failure mechanism of a suction caisson partially depends on the loading rate for a given caisson and soil conditions. Usually, general shear failure (i.e., mobilization of REB) occurs when the loading rate is fast. Local shear failure (i.e., mobilization of internal skin friction) occurs when the loading rate is slow. However, based on this study and Randolph and House's studies (2002), it is suggested that the caisson should be sealed after installation, so that a large passive suction can be effectively mobilized under a large loading rate, and a small passive suction which is still larger than the internal skin friction can be generated under a very small loading rate.

Chapter 5
Finite Element Analysis

5.1 Introduction

Finite element analysis (FEA), also called finite element method, is a technique for solutions of mathematical problems governed by systems of partial differential equations (Templeton, 2002). It can produce close approximate solutions to problems with highly complex geometries, material behaviors and boundaries which would result in highly complex fieldwise variations in the solution variables. The method can be simply described as: (1) the solution space is subdivided into many finite elements so that the variations in the solution variables can be well approximated within each element by interpolation functions; and (2) all of the governing equations are then solved on all of the elements through the nodes, and the elemental solutions are assembled into solution for the whole range, subject to compatibility and continuity requirements. This method has been used to solve various geotechnical problems since 1970s (Desai and Christian, 1977), including settlement and consolidation of soil, embankments and excavations, slope stability analysis and earth retaining structures, hydrology and foundations. In recent years, finite element analyses have been used to investigate the behavior of suction caissons for offshore industry, including performing parametric studies (Zdravkovic et al., 1998 and 2001, and Deng and Charter, 2002), and checking the results of other calculation methods (Randolph and House, 2002), centrifuge test results (Clukey and Morrison, 1993) and the design of suction caissons (NGI, 1999).

Several commercial FEA software programs are available to study various types of problems both static and dynamic analyses for geotechnical engineers. ABAQUS, a general purpose finite element code developed by Hibbitt, Karlsson & Sorenson, Inc. (1998), in Pawtucket, Rhode Island, is one of those programs and was used to analyze the behavior of suction caissons in this study. It supplies an extensive library of elements which can model virtually any geometry: solid (continuum) elements, rigid elements, beam elements, infinite elements, membrane elements, elbow elements, shell elements, interface elements, hydrostatic fluid elements and other more special elements. ABAQUS also contains a wide range of material models that can simulate the behavior of most typical engineering materials including elasticity, plasticity, and thermal properties, hydrostatic and pore fluid flow properties, mass diffusion and other properties. Therefore, a most complicated problem can be easily simulated by combining various option blocks. The following features were used in this study: (1) soil behavior by Modified Cam-Clay model, (2) coupled field equation capabilities for two phase media, and (3) contact analysis capabilities for simulating the caisson-soil interface. Moreover, ABAQUS/Post, an interactive and graphical postprocessor, provides a wide range of options to interpret the results.

The main purpose of the FEA work in this study was to introduce a method for numerical simulation of passive suction. One single FEA model was developed, according to the conditions of centrifuge test SAT06, i.e., caisson geometries, soil parameters, loading and boundary conditions. Two FEA runs were submitted. Run 1 was used to check the capability of the numerical model to correctly simulate the caisson-soil

interaction. In this first run, the measured passive suction was applied as input data. In Run 2, the passive suction was generated by the finite element model. The FEA results from Run 2 were only compared with the results of centrifuge test SAT06 because other tests had different embedment depths from the FEA model. A study on the effect of mesh size and dimensions of the discretized field may improve the FEA results, but this aspect was not addressed here. The size of analysis domain was selected to correspond to the experimental conditions.

5.2 Finite Element Analysis Model

5.2.1 Finite Element Mesh and Boundaries

Centrifuge test SAT06 was modeled using the finite element analysis. Model caisson SC #1 was simulated at the prototype scale. This model caisson had a 51.7 mm outside diameter and 0.65 mm wall thickness, and 0.491 N (50 grams) buoyant weight. The penetration depth was approximately 184 mm.

In order to select the most appropriate element type for simulating soil material in a similar transient boundary value problem, a study was performed at C-CORE in the pipe-soil interaction analysis (C-CORE, 1999 and Popescu et al., 2002). Both the 4-noded bilinear element and the 8-noded biquadratic element were tested, and finally the 8-noded biquadratic element with reduced integration and bilinear pore pressure, CAX8RP, was selected as the best finite element type for simulating the behavior of two-phase materials in a 2D problem. In this study, both soil mass and caisson material were modeled using 8-

node biquadratic displacement, bilinear pore pressure and reduced integration elements (CAX8RP).

An axisymmetric assumption was used in this study. The mesh consisted of 1228 nodes, 573 CAX8RP elements for the soil material, and 39 CAX8RP elements for the caisson.

The FEA was performed at the prototype scale and the FEA results presented in this thesis are expressed as model scale. The finite element mesh and boundary conditions are shown in Figure 5.1. The side boundaries of the FEA mesh were assumed to be frictionless surfaces constrained from moving in the horizontal direction. The bottom was fixed in both vertical and horizontal directions. Symmetry conditions were imposed at caisson axis.

The caisson's top was sealed and a very low permeability (i.e., $1.0\text{x}10^{-14}$ mm/second) was assumed for its walls. The initial hydrostatic water pressure (condition) in the soil was zero on the mudline and increased at $p = r_w z$ depth, where r_w is the unit weight of water and z is the depth below mudline; The hydrostatic water pressure on the mudline (seafloor) outside the caisson maintained zero, and the two sides and the bottom of the mesh were assumed to be impermeable during the finite element analysis.

The caisson and the clay were completely submerged in the equivalent of over 50 meter water depth in the centrifuge test. In practice, the water depth varies from ~10 meters to about 1500 meters. However, the difference in water depth does not affect the

effective stress response of the suction caisson-saturated soil system under these loading conditions. Therefore, the water column above the mudline was not simulated in FEA.

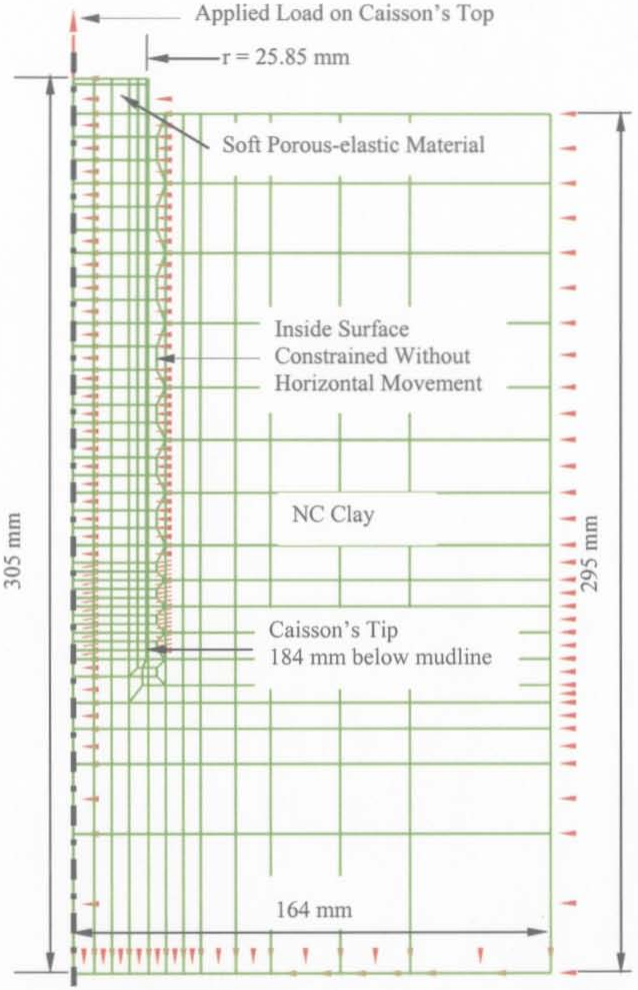

Figure 5.1: FEA mesh and its boundary conditions (model scale)

In practice suction caissons are usually subjected to cyclic loading condition. However, a monotonic (static) load was applied on the caisson top in the FEA of this study due to:

1. The FEA model was developed according to centrifuge test SAT06. The same loading condition as this test was used.

2. Various tests (Larsen, 1989, Clukey and Morrison, 1993, and Randolph and House, 2002) verified that the pullout capacity of a suction caisson under cyclic loading was about 60 to 85% of its capacity under monotonic (static) loading. Therefore, it is very important to understand the behavior of suction caissons under a monotonic (static) loading condition.

5.2.2 Constitutive Model for Soil Material

In this study, the behavior of suction caissons in normally consolidated clay was investigated. Therefore, an appropriate model for simulating the behavior of the normally consolidated clay should be selected. Many studies were carried out on clay constitutive models. The Modified Cam-Clay model was an appropriate model for simulating both partially saturated and fully saturated clays (Phillips, 1986, Vanapalli et al., 1996 and Popescu et al., 2002). This model was also widely used for FEA analyses to simulate the interaction of pipe-soil interface at C-CORE. Therefore, it was also selected to model the stress-strain behavior of the soil in this study. The soil was assumed fully saturated with the flow of the pore fluid through its voids governed by Darcy's law.

The Modified Cam-Clay model implemented in ABAQUS/Standard uses a yield surface shown in figure 5.2 and figure 5.3 (Hibbitt, Karlsson & Sorensen, Inc., 1998). It can be expressed as (Hibbitt, Karlsson & Sorensen, Inc., 1998)

$$\frac{1}{\beta_1^2}(\frac{p'}{a_0}-1)^2+(\frac{t_m}{Ma_0})^2-1=0 \tag{5.1}$$

where:

$p'=-\frac{1}{3}trace\sigma$ is the mean effective stress;

$t_m=\frac{q}{2}[1+\frac{1}{K}-(1-\frac{1}{K})(\frac{r}{q})^3]$ is a measure of the deviatoric stress at failure;

$q=\sqrt{\frac{3}{2}S:S}$ is the Mises equivalent stress;

$r=(\frac{9}{2}S:S:S)^{\frac{1}{3}}$ is the third stress invariant, and S is the deviatoric stress tensor;

M is the critical state ratio defined as the ratio of the Mises equivalent stress, q, to the effective pressure, p', at critical state. The ratio M can be estimated using the stress values in triaxial compression tests, when the material is at the critical state;

β_1 is the wet cap parameter, which controls the shape of the yield surface on the wet side of the critical state;

a_0 is the initial overconsolidation parameter, which can be estimated using the $e-\ln p'$ plots along with the initial effective stress; and

K is the third stress invariant parameter, which introduces a smooth approximation of the Mohr-Coulomb surface.

Other parameters in the Modified Cam-Clay model in ABAQUS/Standard implementation include:

υ, Poisson ratio;

κ, logarithmic elastic bulk modulus; and

λ, logarithmic hardening modulus.

Parameters κ and λ can be estimated from the results of the hydrostatic compression test (slope of the rebound line) and from an oedometer test (slope of the virgin compression line) in an $e - \ln p'$ plot. Other parameters, such as the initial void ratio e_0, the initial effective stress σ'_{v0} and the coefficient of earth pressure at rest k_0, which correspond to the initial effective stress state, are also needed.

In practice, excess pore pressures are induced in the soils during caisson installation because some soil is displaced by caisson wall, resulting in a reduction in the effective stress of the soils around the caisson (i.e., soils in the area from caisson center line to a distance of plastic radius away). As the caisson was whished into the soil (i.e., the caisson was magically replaced the soil without any effect to the adjacent soils) in the FEA of this study, the reduction in effective stress of the soils around the caisson by installation was not taken into consideration. Hence, the FEA results (i.e., wall friction/capacity) may be slightly larger than the centrifuge test results, as shown on Figure 5.26.

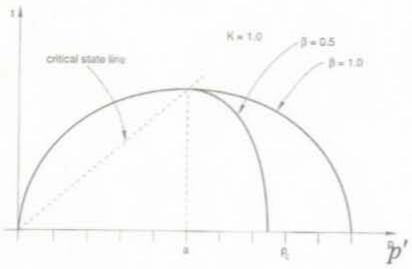

Figure 5.2: Modified Cam-Clay yield surfaces in the $p'-t$ plane

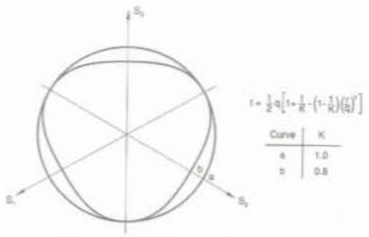

Figure 5.3: Modified Cam-Clay yield surface sections in the π-plane

The parameters used in the modified Cam-Clay model were estimated using the results of laboratory consolidation tests, direct shear tests, fall cone penetration and mini vane shear tests, as well as C-CORE's in-house data and other published data in the literature. A summary of the parameters used in the model is presented in Table 5.1.

Table 5.1: Soil parameters used for the Modified Cam-Clay model

Soil Parameter	Value Used
Poisson's ratio, ν	0.3
Logarithmic elastic bulk modulus, κ	0.01
Logarithmic hardening modulus, λ	0.26
Critical state ratio, M	0.9
Initial overconsolidation parameter*, a_0	4.56 kPa/m
Wet cap parameter, β	1.0
Third stress invariant parameter, K	1.0
Initial void ratio*, e_0	1.1~1.48
Permeability k	2.2×10^{-9} m/sec
Coefficient of earth pressure at rest, k_0	0.64
Unit submerged weight, γ'	6.0 kN /m^3
Friction coefficient at caisson-soil interface, α_f	0.25

* variable with depth;

In order to simulate the passive suction, as will be discussed in Section 5.2.4, the water inside the caisson top was replaced by a soft porous-elastic material through which the suction was applied at the top of the caisson. The parameters of this material (i.e., E and ν) were adjusted so that its bulk modulus was equal to that of water, i.e., B = 2000 MPa. A study on parameters of this soft porous-elastic material was performed. Two sets of E and ν were used: (1) E = 120 MPa, ν = 0.49, and (2) E = 12 MPa, ν = 0.499. In order to investigate the influence of the permeability of the soft porous-elastic material on the behavior of the caisson, three permeability coefficients (i.e., k = 8, 8 x 10^{-2}, and 8 x 10^{-5} m/s) were assumed for each set of E and ν. In all analyses, a buoyant unit weight $\gamma' = 6\ kN/m^3$ was used for this soft porous-elastic material.

Figure 5.4 (load versus displacement curve) and Figure 5.5 (passive suction versus displacement curve) present the FEA results, using E = 120 MPa and ν = 0.49, and k = 8, 8 x 10^{-2}, and 8 x 10^{-5} m/s, respectively. These figures show that the pullout behavior of a suction caisson (i.e., load versus displacement curve and passive suction versus displacement curve) did not change with the permeability of the soft porous-elastic material inside top of the caisson. In other words, the effect of the permeability on the generation of passive suction could be neglected. Similar conclusion was drawn for another series of FEA, using E = 12 MPa and v = 0.499, and k = 8, 8 x 10^{-2}, and 8 x 10^{-5} m/s, respectively.

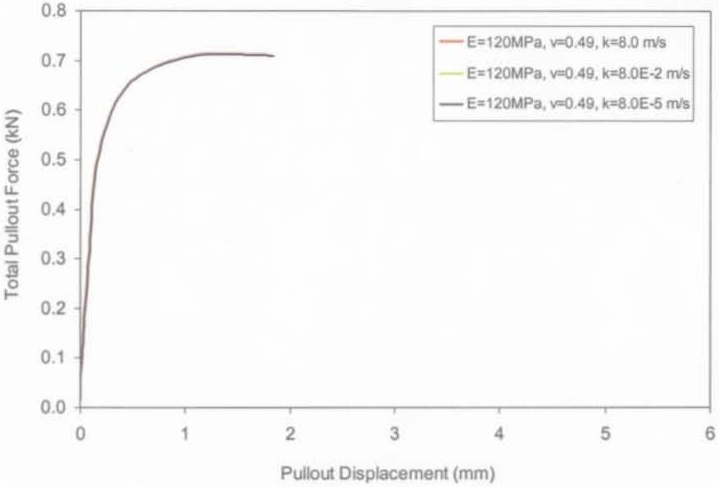

Figure 5.4: Load versus displacement curve (model scale)
soft porous-elastic material: E = 120 MPa, $\nu = 0.49$

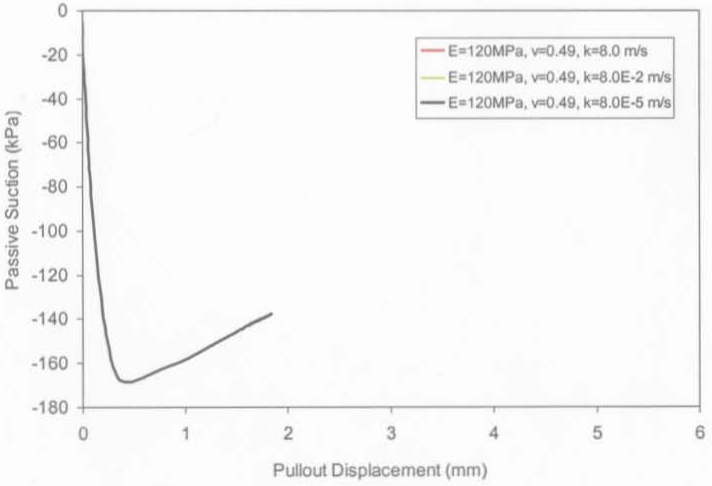

Figure 5.5: Passive suction versus displacement curve (model scale)
soft porous-elastic material: E = 120 MPa, $\nu = 0.49$

Figures 5.6 and 5.7 present the FEA results, using two sets of E and ν for the soft porous-elastic material: (1) E = 120 MPa, ν = 0.49 and k = 8 m/s, and (2) E = 12 MPa, ν = 0.499 and k = 8 m/s. Those figures show that the development of the total pullout force of a suction caisson with displacement was not influenced by the values of E and ν of the soft porous-elastic material on the inside caisson top, and the influence of E and ν on the development of passive suction was very small, providing a bulk modulus of 2000 MPa (same as that of water) can be derived using E and ν.

Based on the above study, following parameters were used for the soft porous-elastic material in the FEA: (1) Young's modulus E = 12.0 MPa, (2) Poisson's ratio ν = 0.499, (3) permeability coefficient k = 8.0 m/s, and (4) the buoyant unit weight $\gamma' = 6\ kN/m^3$.

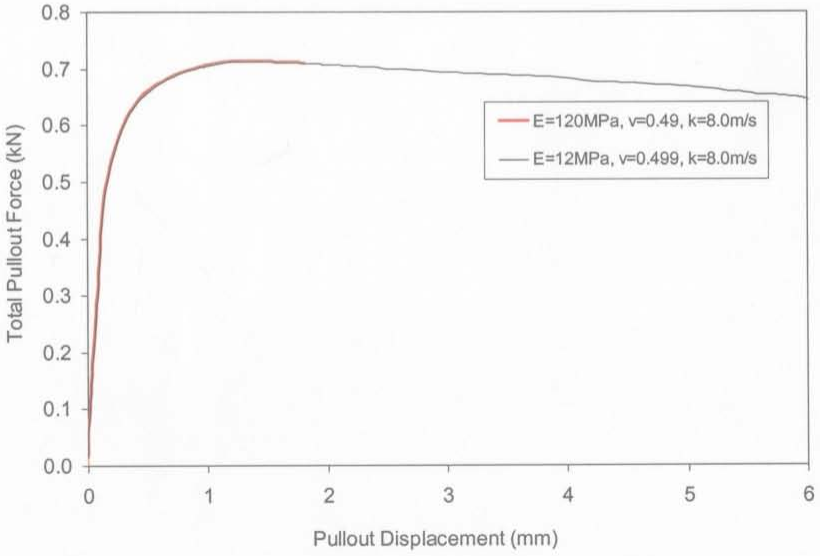

Figure 5.6: Comparison of Load vs. displacement curves (model scale)

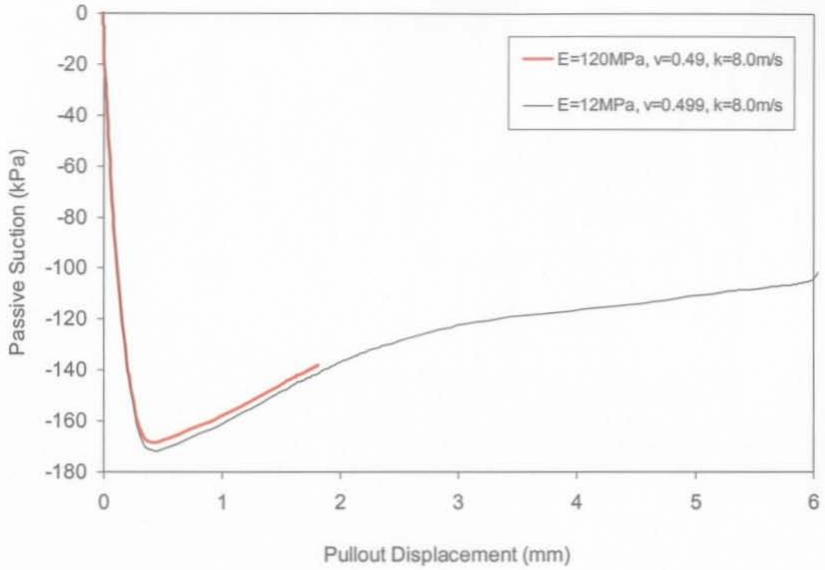

Figure 5.7: Comparison of passive suction vs. displacement curves (model scale)

5.2.3 Caisson-Soil Interaction

In order to effectively simulate the behavior of suction caissons in clay, the caisson-soil interaction was considered as a contact problem. Two approaches could be used in ABAQUS for specifying finite sliding interaction between deformable bodies: (1) the contact element approach, and (2) the contact surface approach. The contact element approach is used more frequently since it is applicable in more situations. In this study, however, the contact surface approach was used based on the modeling and computational efforts of a study conducted to identify the most appropriate technique for simulating pipe-soil interaction (C-CORE 1999 and 2001, and Popescu et al., 2002). In

the contact surface approach, ABAQUS automatically generates the appropriate contact elements.

Two pairs of surfaces were used to simulate the caisson-soil interaction: (1) the caisson wall surface and the soil surface in contact with the caisson, and (2) the soil surface inside the caisson with the soil surface outside the caisson. The first pair (Figure 5.8 (a)) simulated the caisson-soil interaction. The second pair (Figure 5.8 (b)) prevented inter-penetration of the soils outside and inside the caisson during and after the caisson retraction.

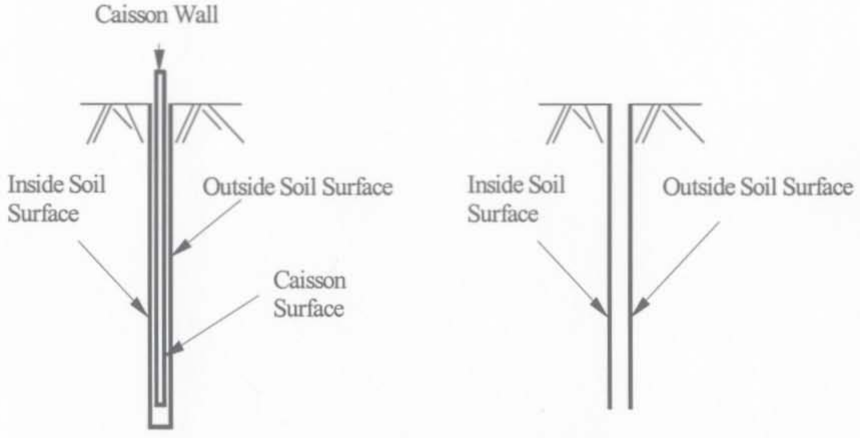

(a) Caisson-soil surfaces (b) Soil surfaces inside and outside caisson

Figure 5.8: Definition of contact surface pairs

In practice, suction caissons are generally classified into two main types based on the wall skin conditions: smooth-walled caissons (i.e., steel wall caissons) and rough-walled caissons (i.e., concrete caissons). The interaction between caisson wall of different skin

condition and soil can be well simulated using Coulomb friction contact in FEA. An appropriate value of friction coefficient, selected according to the caisson wall skin condition, can be used to correctly simulate the slippage between caisson wall and soil for smooth-walled caissons. The "ROUGH" option in ABAQUS software can be used to simulate the situation of no-slippage at caisson-soil interface for rough-walled caissons, and the failure occurs in the soil.

In this study, Coulomb friction contact was used. The shear stress between the surfaces in contact, i.e. unit wall skin friction (f_s), is limited by a value

$$\tau_{limit} = \alpha_f \sigma'_n \tag{5.2}$$

where α_f is an user-defined friction coefficient (in Table 5.1) and σ'_n is the effective normal contact pressure acting on the interfaces and equivalent to the horizontal stress σ'_h in the soil adjacent to the caisson. The caisson elements were assigned a non-zero very low permeability as a signal to the ABAQUS software that this effective pressure, and not the total normal pressure, governed the interface behavior. No apparent numerical instability resulted from this assignment.

The user-defined friction coefficient α_f was assigned as 0.25. This value was selected as follows:

Usually, the unit wall skin friction is calculated by

$$f_s = k_\tau s_u \tag{5.3}$$

where s_u is the undrained shear strength and k_τ is a stress transfer coefficient. According to the centrifuge test results (Cao et al. 2001, and 2002) and literature (API, 1993, NGI, 1999, and Andersen and Jostad, 2002), the average value of k_τ is about 0.85 (equivalent to α_{pu} in Table 4.5 of Section 4.6.3) with consideration of internal and external wall skin friction as well as the effect of self-weight and active suction penetration.

The undrained shear strength of clay, s_u can be estimated by

$$s_u = \alpha (OCR)^\beta \sigma'_v \tag{5.4}$$

where α and β are empirical coefficients equal to 0.19 and 0.59 respectively for speswhite kaolin clay, OCR is the overconsolidation ratio equal to 1 for normally consolidated clay, and σ'_v is the effective vertical stress.

Eq. 5.4 can be written as

$$s_u = \alpha (OCR)^\beta \frac{\sigma'_h}{k_0} \tag{5.5}$$

where σ'_h is the effective horizontal stress, and k_0 is the coefficient of earth pressure at rest for normally consolidated clay and is equal to 0.64.

Substituting Eq 5.5 into Eq. 5.3, then

$$f_s = \frac{k_\tau \alpha (OCR)^\beta}{k_0} \sigma'_h \tag{5.6}$$

Comparing Eq. 5.2 and Eq. 5.6, where τ_{limit} equals to f_s and σ'_n is equivalent to σ'_h, the friction coefficient, α_f, results:

$$\alpha_f = \frac{k_r \alpha (OCR)^{\beta}}{k_0} = 0.25 \tag{5.7}$$

Therefore, the friction coefficient at caisson-soil interface, $\alpha_f = 0.25$ was selected in the FEA.

5.2.4 Simulation of Passive Suction

One advantage of suction caissons is that passive suction is generated during uplift loading, resulting in an increase in the foundation pullout capacity. The passive suction contributes to the overall pullout capacity through developing a reverse end bearing resistance at the base of the caisson and also through increasing the effective stress in the soil both inside and outside the caisson, leading to higher skin friction along the caisson's wall. Consequently, the correct simulation of passive suction plays a key role in the successful modeling of the behavior of suction caissons in the numerical analyses.

In parallel with this research, Handayanu et al. (2000) tried to numerically simulate the pore water pressure change (passive suction) in the soil for suction caissons in clay during pullout, using ABAQUS software and a subroutine. Their FEA model was developed based on the same conditions of two laboratory tests performed by MIT and University of Texas (Austin). A maximum pore water pressure of about 50 kPa, in agreement with the test results, was obtained. Chicata (2000) also used FEA to simulate the pullout capacity of suction caissons, including generation of passive suction. His FEA models were developed based on the conditions of the laboratory tests done by University of Texas (Austin). The suction force (not suction pressure) from FEA was in agreement

with these test results. However, no details on the generation of passive suction were presented in his Ph. D. thesis.

The above two studies were conducted based on several laboratory tests. Usually, the maximum passive suctions from laboratory tests are much lower than these from centrifuge tests or from practical examples, and also, the passive suction versus displacement curves are different, due to the limitations of laboratory test. Therefore, the simulation of generation of passive suction is still a challenging problem.

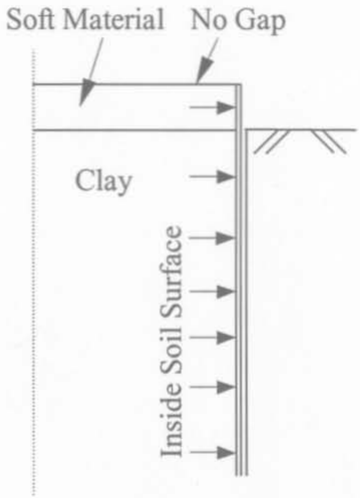

Figure 5.9: Simulation of passive suction

Passive suction may be simulated using the ABAQUS software when some aspects are taken into consideration. There are various elements that could be selected in ABAQUS. For example, when pore pressure elements are used, passive suction could be

simulated by the development of negative pore water pressures in a soft porous-elastic material subjected to tension strains. As shown in Figure 5.9, three aspects were considered in the simulation of passive suction in this study:

1. The water inside the caisson top was replaced by a soft porous-elastic material through which passive suction was applied at the top of the caisson. At the contact with soil, the soft porous-elastic material elements shared the same nodes with the soil.

2. Perfect contact between the soft porous-elastic material and the caisson cap was assumed. The top surface of the soft porous-elastic material did not have any relative movement with respect to the caisson cap during pullout.

3. Both the soft porous-elastic material and the soil inside the caisson at caisson-soil interface were constrained from horizontal movement, resulting in the elimination of cavity development between water, soil and the caisson's internal wall. Compared with using transient thin elements near caisson walls (i.e., hard contact between caisson and inside soil), both methods limit the soil mass on the internal wall from lateral movement. Moreover, this method can simulate the relative vertical movement between soil mass and internal wall of the caisson. As shown on Figure 5.23, the normal pressures on the inside wall surface along the caisson clearly indicates that the soil on the inside caisson skin is never in tensile. Therefore, the zero lateral displacement assigned in the FEA is appropriate.

Considering the dependence of passive suction to loading rate, the consolidation time and the loading time units in the FEA have been set based on the centrifuge data and

according to similitude laws. The passive suction measured in centrifuge tests was used to verify the FEA model (i.e., use of contact surface) and to compare with the FEA results. After the model was verified, the measured passive suction in the centrifuge test was not used.

5.3 Validation of Caisson-Soil Interaction

In order to validate the caisson-soil interaction, the caisson top was separated from the mudline by a gap. The soft porous-elastic elements replacing the water inside the caisson top described in the previous Section were not used in this first round of calculation. The passive suction measured during centrifuge test was applied on both the mudline nodes as negative pore pressures and the inside top surface of the caisson as downward pressures (Figure 5.10).

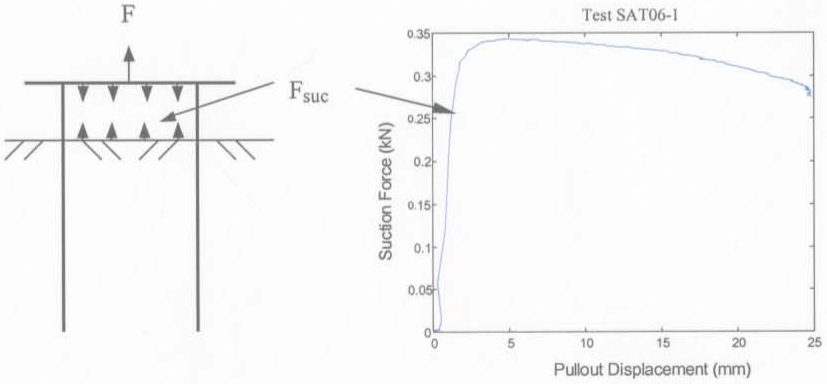

a) Approach applying passive suction in FEA

b) Centrifuge test result of passive suction against vertical displacement

Figure 5.10: Validation of caisson-soil interaction - I (model scale)

Figure 5.11 presents the comparison of the finite element analysis results with those measured in the centrifuge test. As can be seen, the total pullout forces obtained from the finite element analysis run are in close agreement with those measured in the centrifuge test (i.e., the difference is less than 10%). Consequently, it was concluded that the numerical model could adequately simulate the caisson-soil interaction measured in the centrifuge tests.

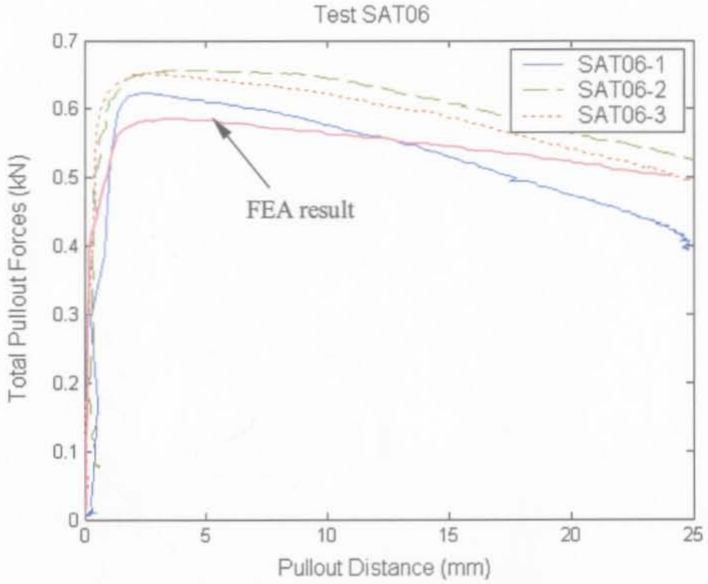

Figure 5.11: Validation of caisson-soil interaction - II (model scale)

A finite element analysis run was conducted following the validation of caisson-soil interaction to simulate the generation of passive suction as described in Section 5.4. The water inside the caisson top was simulated by a soft porous-elastic material.

5.4 FEA Results and Comparison

5.4.1 Failure Mode

A 25 mm vertical displacement at the model scale was applied on the top of the caisson in the finite element analysis. This vertical displacement is equivalent to 2.5 m at the prototype scale. To conveniently compare with the centrifuge test results, the FEA results were presented at the model scale.

Development of reverse end bearing (REB):

Figure 5.12 indicates that, below caisson tip, large plastic strains (i.e., 15% or more) occurred in the soil along a 45-degree line (curve) from the caisson wall to the caisson center line, resulting in a dead wedge. Figure 5.13 shows the curved failure zone at the caisson tip expanding (curving) upwards into the overlying clay and away from the caisson wall above the caisson tip. This failure mechanism is reminiscent of that for an axial loaded pile (Randolph and Houlsby, 1984) or a cone penetrometer (Eslami and Fellenius, 1997). There exists the concept of critical depth for piles under axial loading. When the embedment is less than this depth, the failure mechanism (Figure 5.14 (a)) associates with end resistance comes to the ground surface. When the embedment is larger than this depth, the failure mechanism (Figure 5.14 (b)) wraps back onto the pile in a local area around the tip (Randolph and Houlsby, 1984). Figure 5.14 (c) shows the failure of the cone penetrometer with deep embedment in friction soil (Eslami and

Fellenius, 1997). For suction caissons in clay under the conditions of present study, the observed failure mechanism from FEA is the reverse of that for a deeply embedded pile.

The general shear failure defined by Fuglsang and Steensen-Bach (1991) and Christensen et al. (1991) shown in Figure 2.1 (c) is appropriate for shallow embedment. The observed failure mechanism, Figure 5.14 (d) is appropriate for deep embedment and is defined as a confined general shear (CSG) failure mechanism in this study.

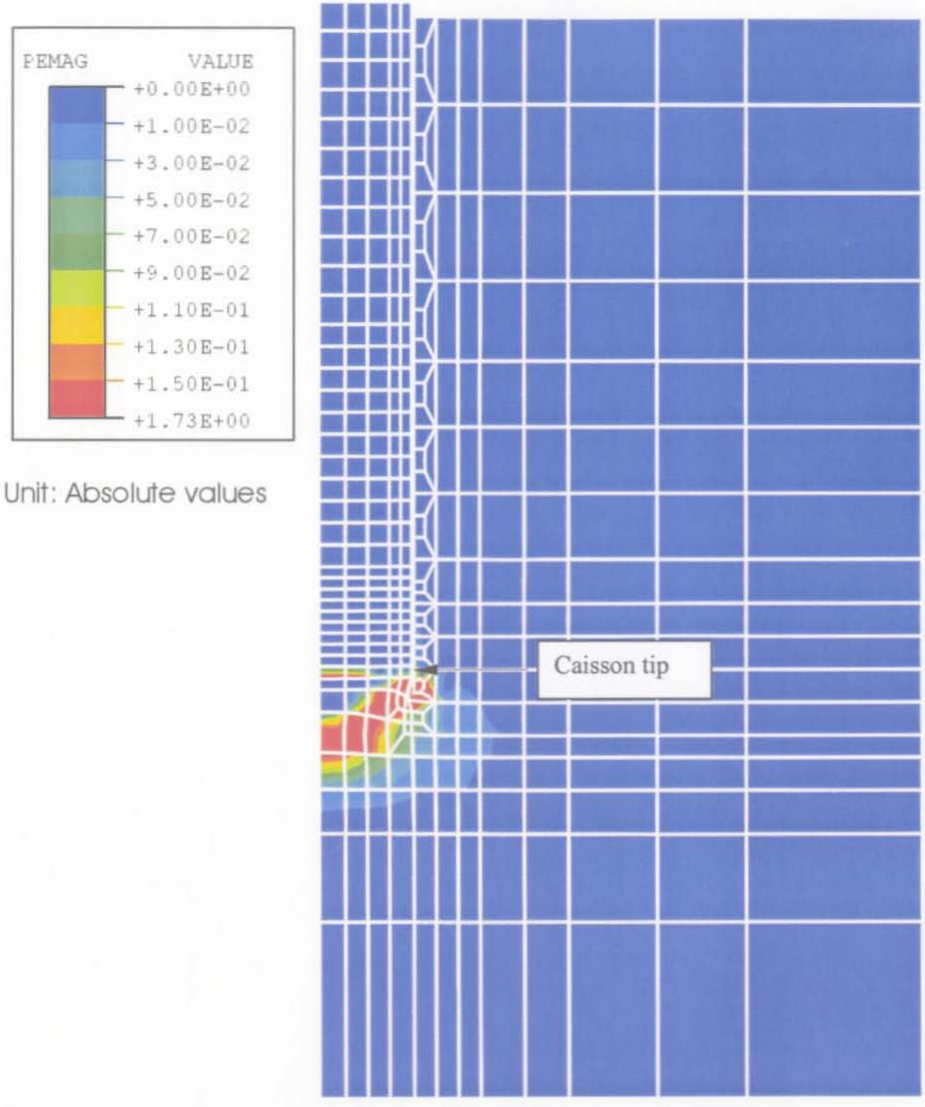

Figure 5.12: Plastic shear strain contours at 2.1 mm vertical displacement (model scale)

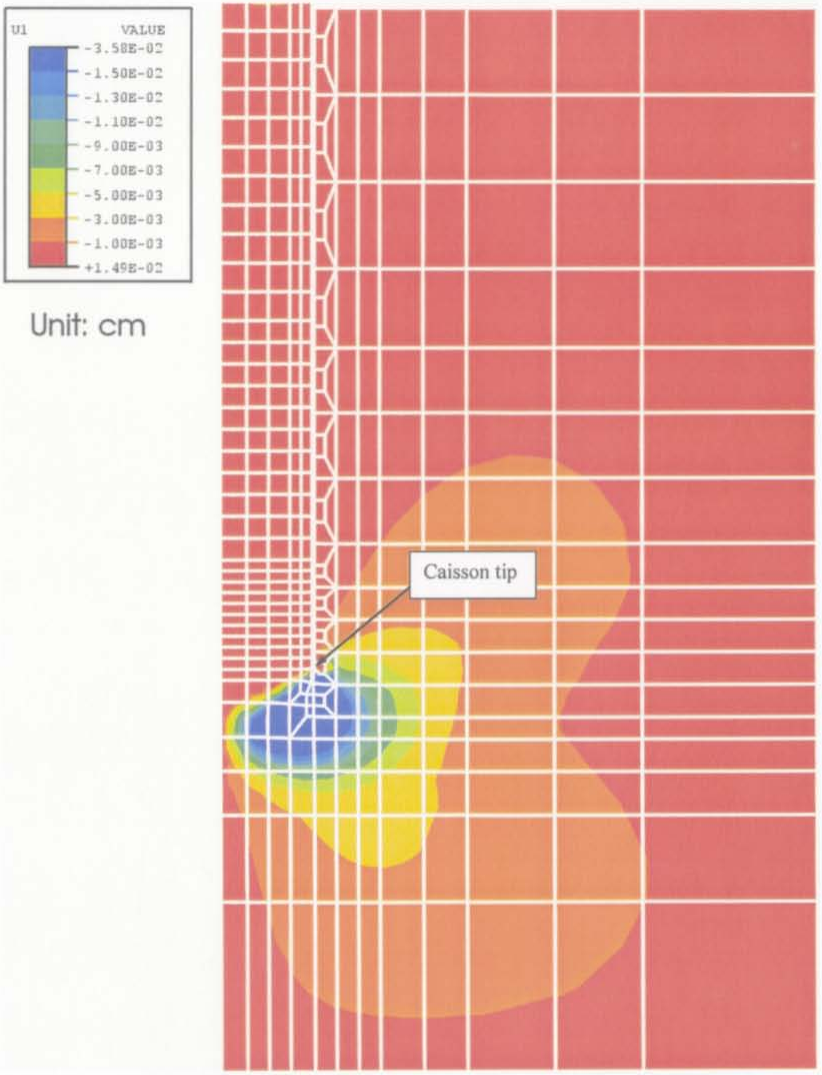

Figure 5.13: Lateral displacement contours at 2.1 mm vertical displacement (model scale)

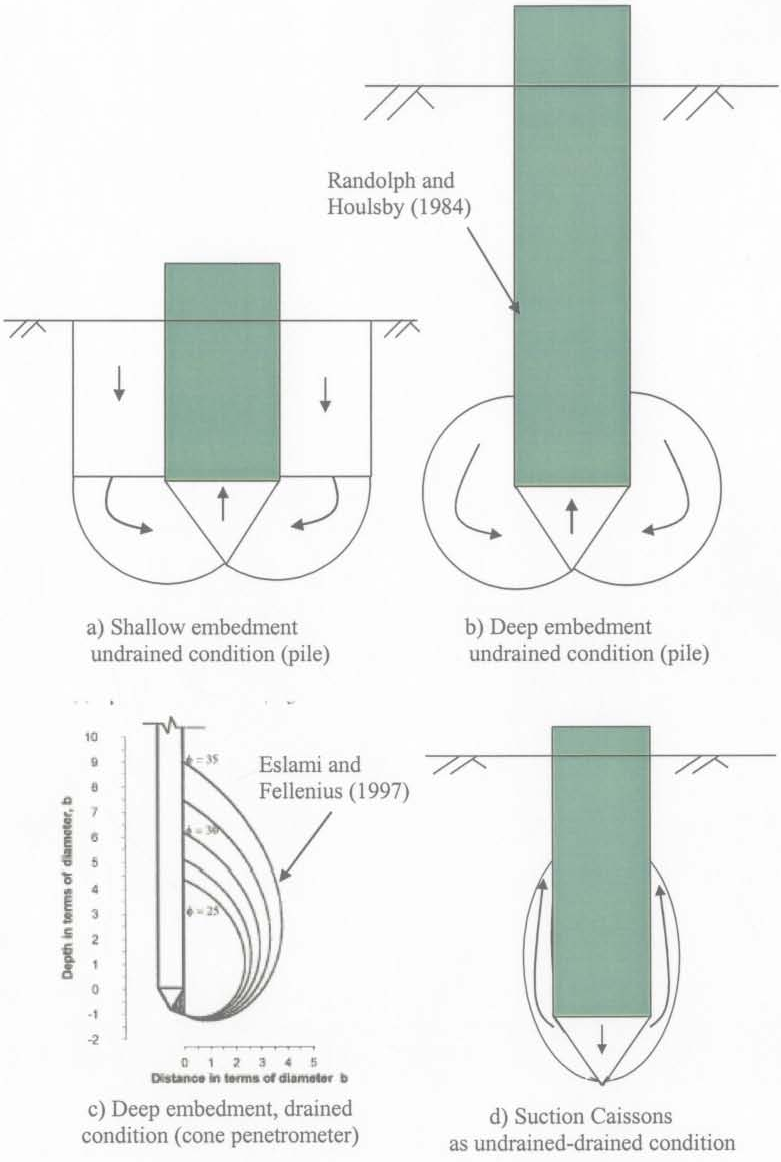

Figure 5.14: Observed general shear failure mechanisms under various conditions

Figure 5.15 presents the deformed mesh around the caisson's tip with the original one after a vertical displacement of 0.5 mm was applied. The soil both inside the caisson (points C and D in the figure) and below its tip (point E in the figure) had almost the same upward displacement as the caisson, and passive suction was developed to its maximum at this displacement (as shown in Figure 5.27). The soil outside the caisson at the caisson tip experienced very little upward movement (points A and B in the figure). There existed a relative movement between the caisson-soil surfaces (shearing). Figures 5.16 to 5.18 present the further failure progress of the soil around the caisson's tip. The upward movement of the soil inside the caisson and below its tip was proportional to the vertical pullout displacement of the caisson. The soil outside the caisson from mudline (as shown in Figure 5.20) to the tip of the caisson (shown in Figures 5.15 to 5.18) experienced very little movement (or a small downward movement), resulting in the development of a large relative displacement between the caisson wall and the outside soil (shearing). The failure progressively occurred at the interface of the caisson wall and the soil outside caisson. At the same time, the passive suction started to drop off with vertical displacement after its maximum at 0.5 mm displacement because the seepage gradient increased with the development of the EPPs at the tip of the caisson. As discussed above, a confined general shear failure mechanism is used to describe the observed failure for suction caissons in the present study.

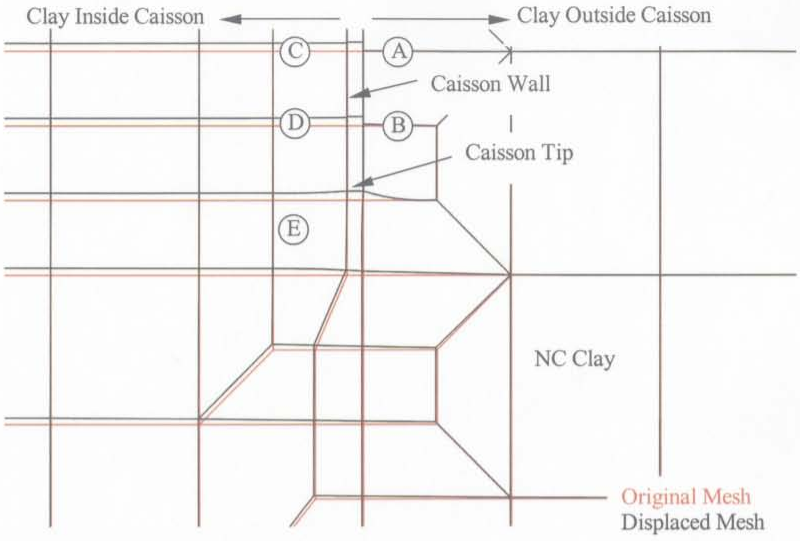

Figure 5.15: Deformed mesh at 0.5 mm vertical displacement (model scale)

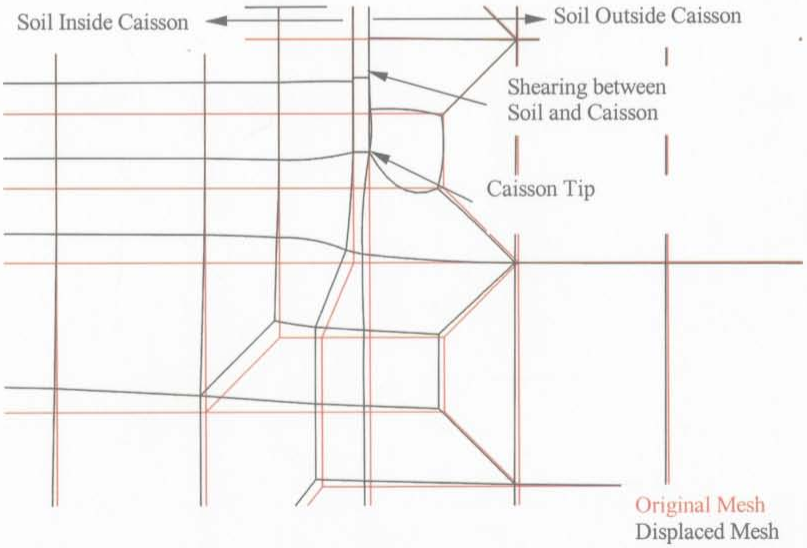

Figure 5.16: Deformed mesh at 1.57 mm vertical displacement (model scale)

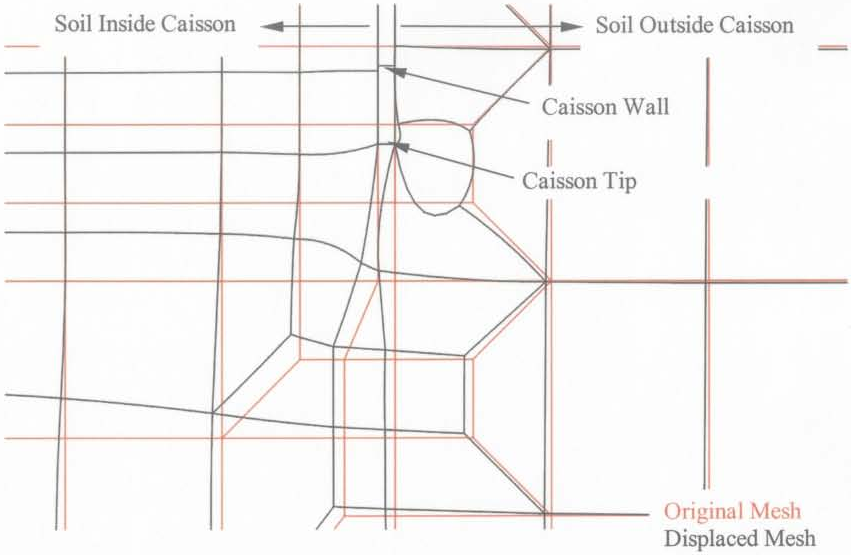

Figure 5.17: Deformed mesh at 2.38 mm vertical displacement (model scale)

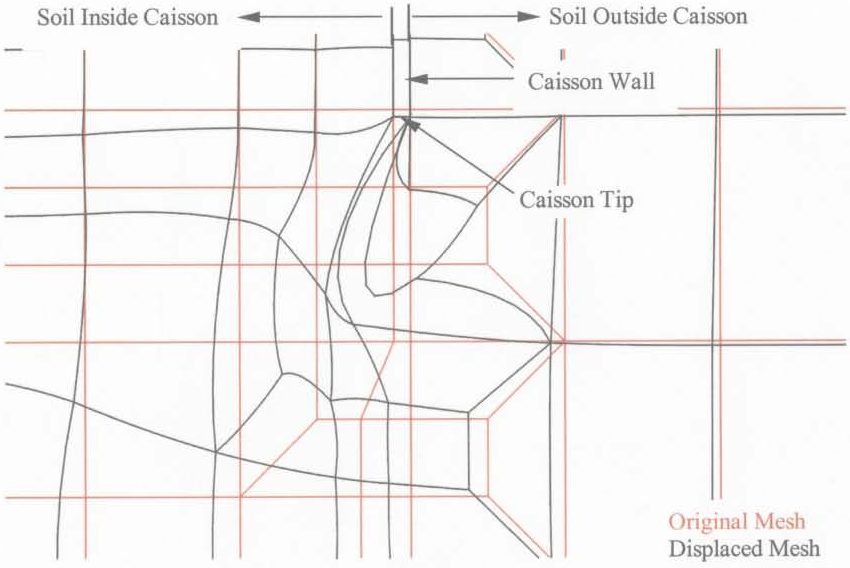

Figure 5.18: Deformed mesh at 5.84 mm vertical displacement (model scale)

As mentioned in Section 5.1, Run 1 was used to check the capability of the numerical model to correctly simulate the caisson-soil interaction. The same soil parameters as the testbed clay of centrifuge test SAT06, presented in Table 5.1, were used and the measured passive suction was applied as input data. Figure 5.11 of load vs. displacement curve from Run 1, together with the measured results of test SAT06, shows that the initial choice of inputs (i.e., soil parameters, mesh size and boundary conditions, etc.) was appropriate. Error analysis like parametric study is beyond the scope of this thesis. As shown on Figures 5.15 through 5.18, significant mesh distortions are to be expected with such large relative movements, but the numerical instabilities caused by these very localized excessive distortions do not seem to have affected the overall integrity of the analysis.

Development of external friction (caisson wall-soil interface behavior):

Figure 5.19 of vertical displacement in the soil clearly shows the relative movement between the caisson and the outside soil. The outside soil close to the caisson wall had an upward movement due to the mobilization of the friction on the caisson-soil interface, until the shear force exceeded the maximum friction at a large vertical displacement, and caisson-soil slippage occurred. Figure 5.20 shows that, at a relatively large displacement (i.e., 16.5 mm), the top of the soil plug had almost the same upward movement as the caisson, while the clay at outside the caisson wall experienced a small downward movement, and shear failure developed along the caisson at the interface of caisson wall and the outside soil. Soil around the caisson tip moved towards inside the caisson. The

arrows show the movement directions and their lengths indicate the magnitudes of the movement at points (nodes). The magnitude of the upward movement for the soil below the caisson decreased with the distance away from the caisson tip. This figure clearly indicates a "soil flow" from the soil outside and away from the caisson to the inside of the caisson during the pullout.

Figure 5.21 of normal pressure distribution on the external caisson wall indicates these pressures were almost the same as the initial values from the mudline (clay surface) to about 7 cm below, and then, the normal pressure increased with depth, to approximately 70 kPa over its initial value at the caisson tip (18.4 cm below mudline). The increase of the normal pressure on the external caisson wall with depth reasonably reflected the mobilization of the reverse end bearing on the surrounding soil, Figure 5.14 (d). Figure 5.22 presents the ratio of shear stress to normal pressure on the caisson-outside soil interface at 2.1 mm vertical displacement. This figure clearly shows that slippage occurred at the caisson-outside soil interface when the shear force at the interface exceeded its maximum friction, and the caisson-soil behavior was correctly modeled by the caisson-soil interface.

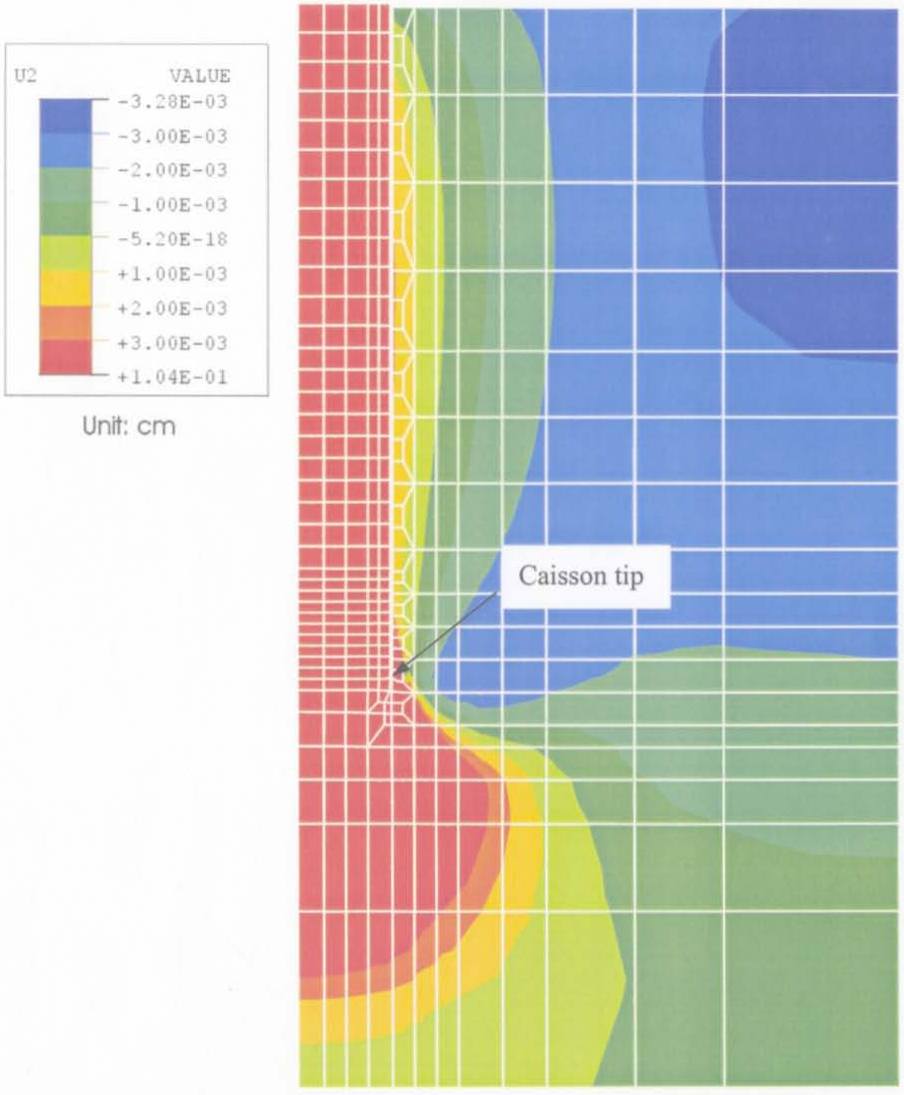

Figure 5.19: Vertical displacement contours at maximum value of 1.04 mm (model scale)

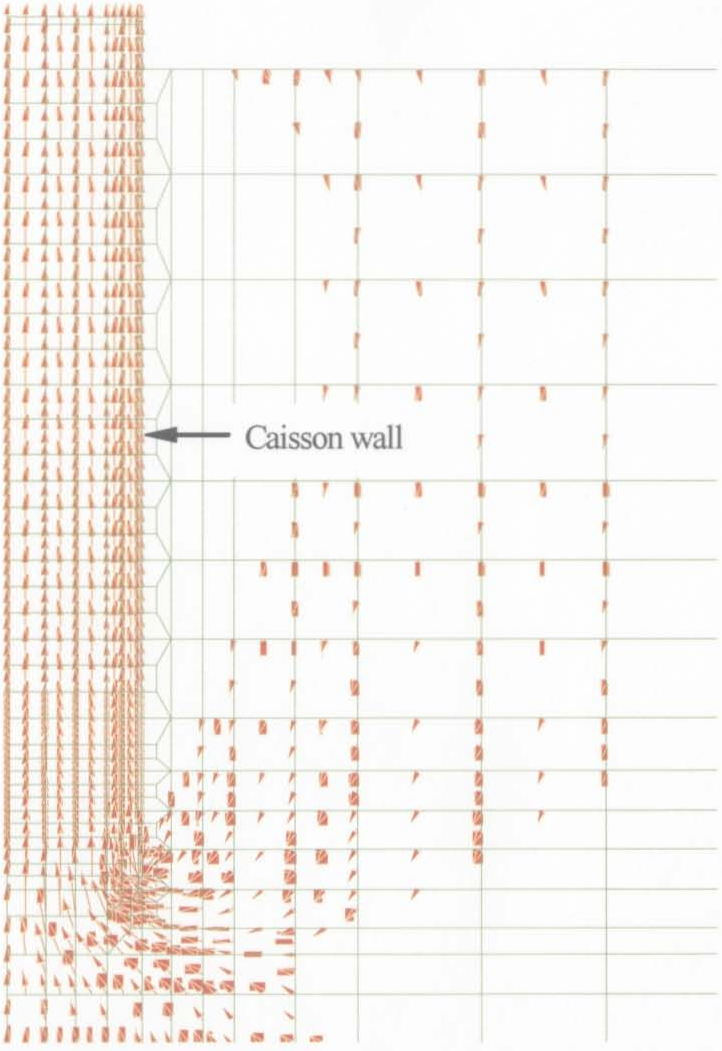

Figure 5.20: Displacement vectors after 16.2 mm vertical displacement (model scale)

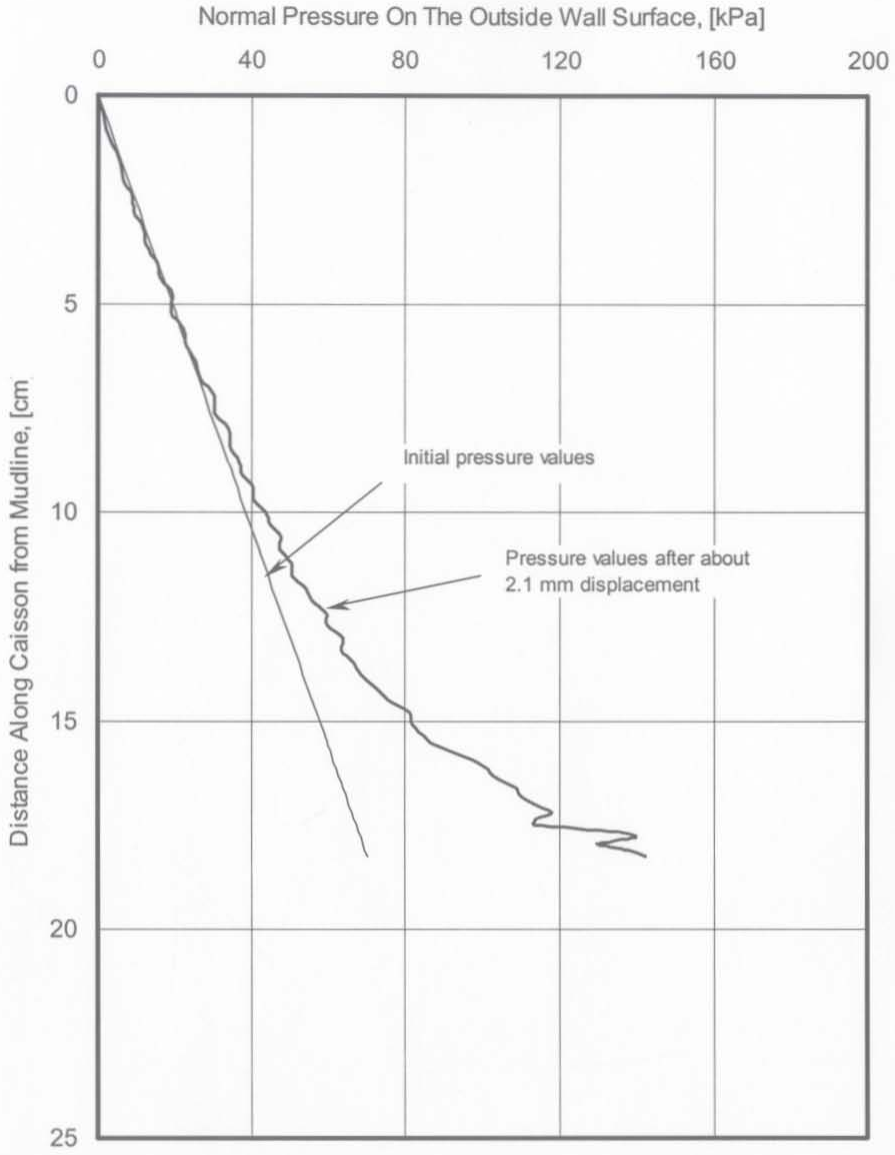

Figure 5.21: Normal pressure on the outside wall surface at 2.1mm vertical displacement (model scale)

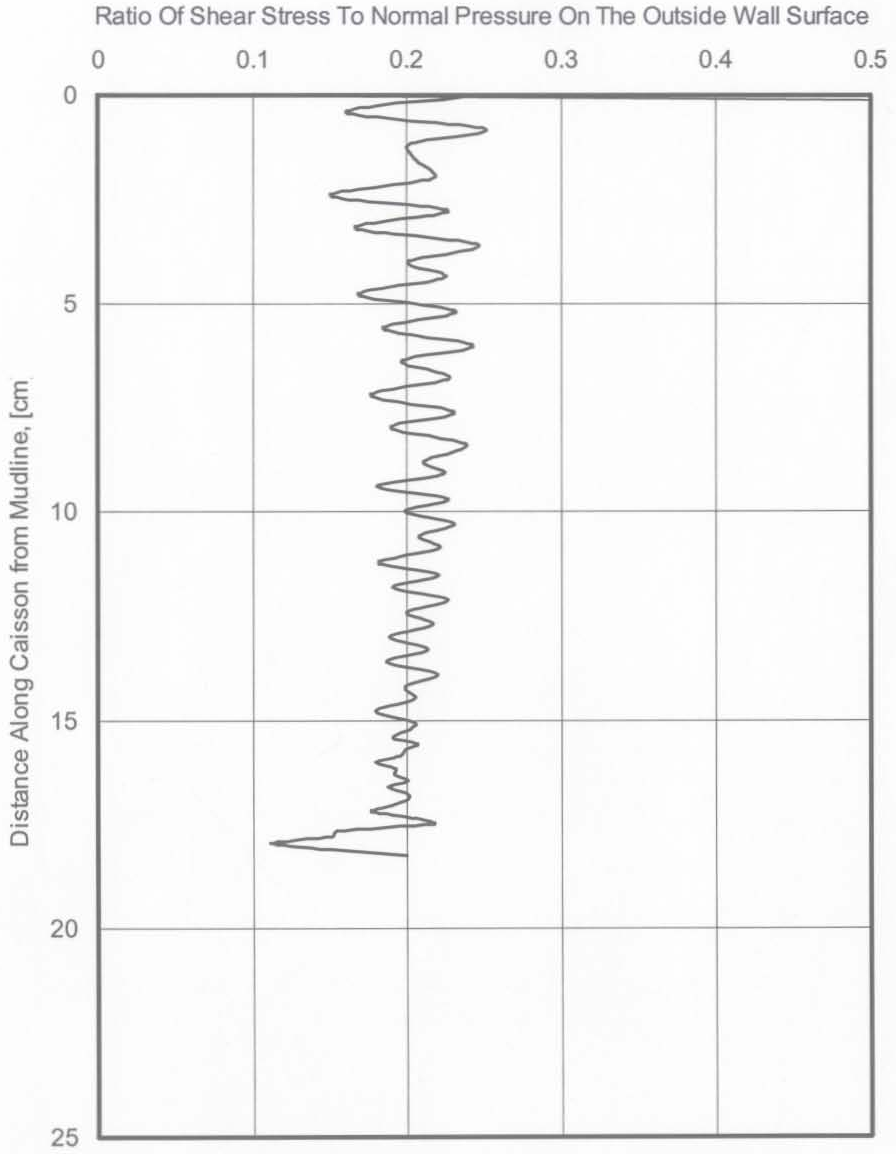

Figure 5.22: Ratio of shear stress to normal pressure on the outside wall surface at 2.1 mm vertical displacement (model scale)

Figure 5.23 of normal pressure distribution on the internal caisson wall indicates these pressures were almost the same as the initial values from the mudline (clay surface) to about 12 cm below, and then, the normal pressure increased with depth, to approximately 45 kPa under its initial value at the caisson tip (18.4 cm below mudline). This figure clearly indicates that the soil near the internal caisson skin is never in tension. Figure 5.24 of shear stress on the inside caisson wall along the caisson at 2.1 mm vertical displacement shows that the mobilized shear stress on the caisson-inside soil surface from mudline to about 9 cm was very small and essentially negligible, and then, the shear stress increased with depth, to approximately 17 kPa.

As indicated on Figure 5.25, no (or essentially negligible) slippage occurred between the inside soil and the caisson wall from mudline (clay surface) to about 17 cm depth, due to that the generated passive suction in turn provided an uplift load on the soil plug. This resulted in that the shear force was less than the maximum friction on the caisson-soil interface (Figure 5.24). A slip occurred between internal wall and the soil inside caisson from the caisson bottom to about 1.5 cm above the caisson tip because the uplift load on the soil provided by the generated passive suction in this part was small compared to that on the plug top, due to the shorter drainage distance, and the shear force was larger than the maximum friction on the caisson-soil interface (Figure 5.24).

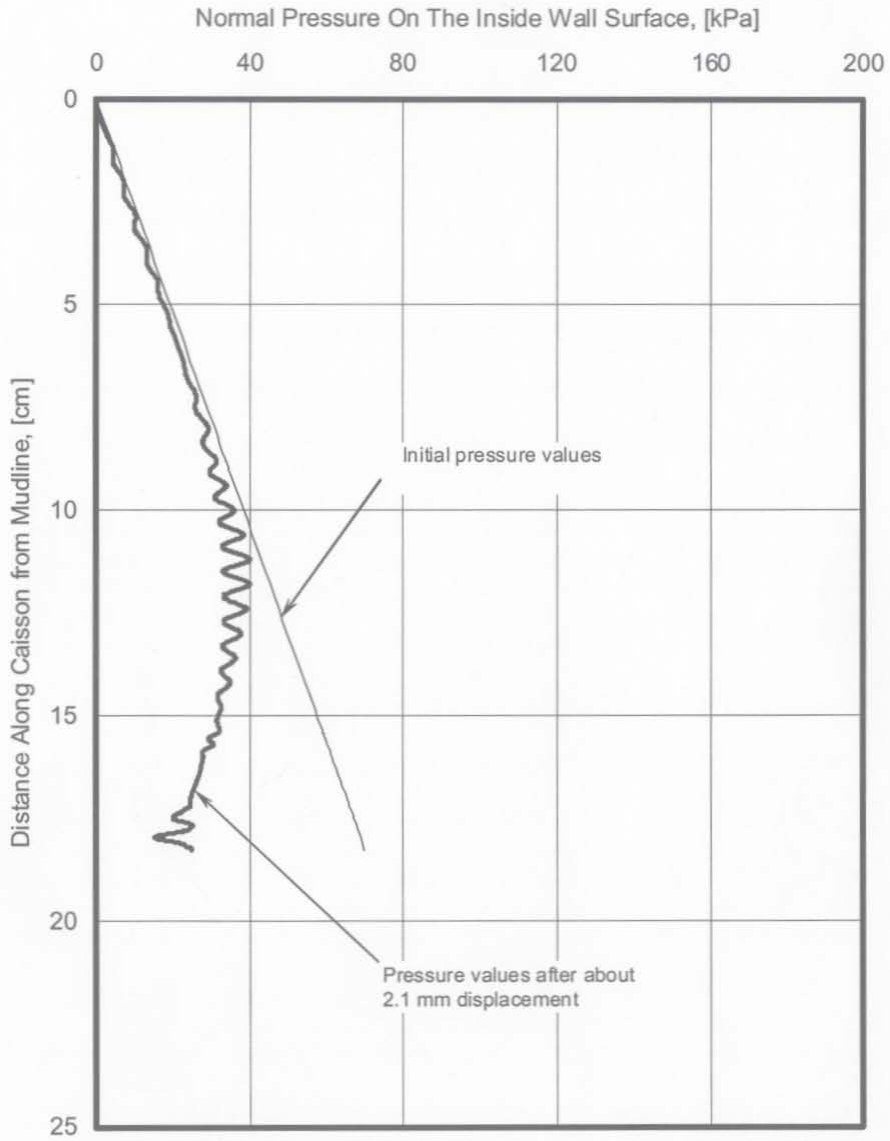

Figure 5.23: Normal pressure on the inside wall surface at 2.1mm vertical displacement (model scale)

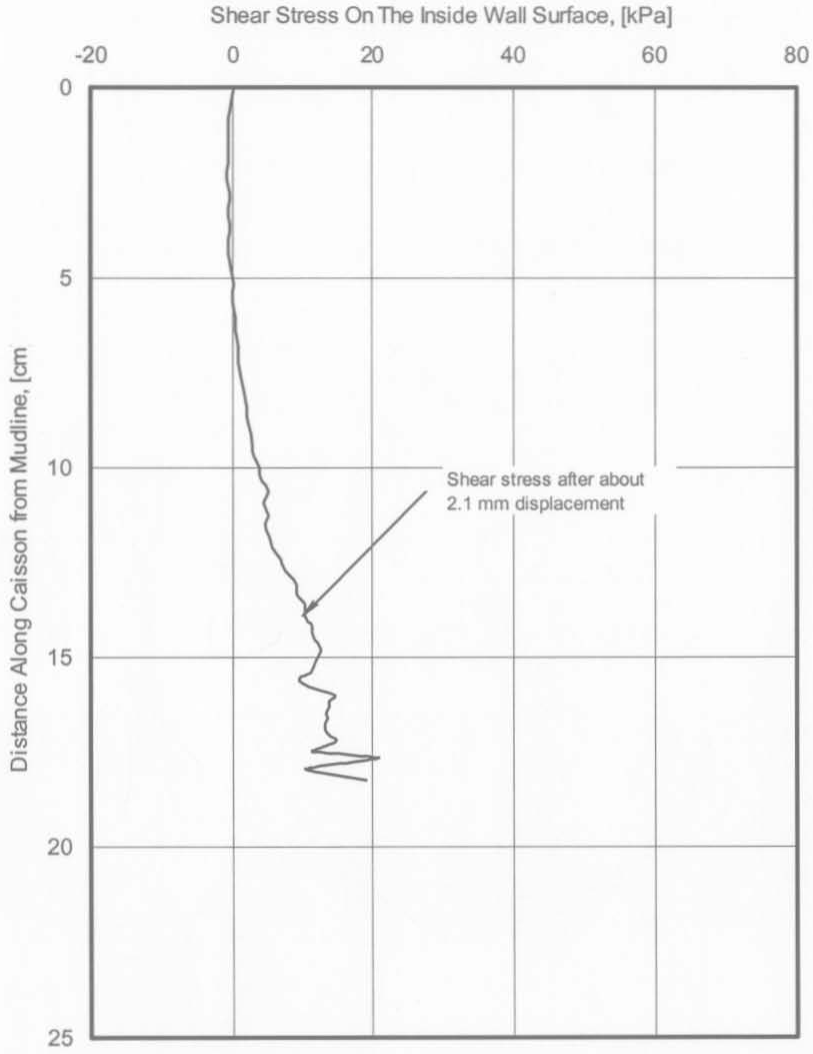

Figure 5.24: Shear stress on the inside wall surface at 2.1mm vertical displacement (model scale)

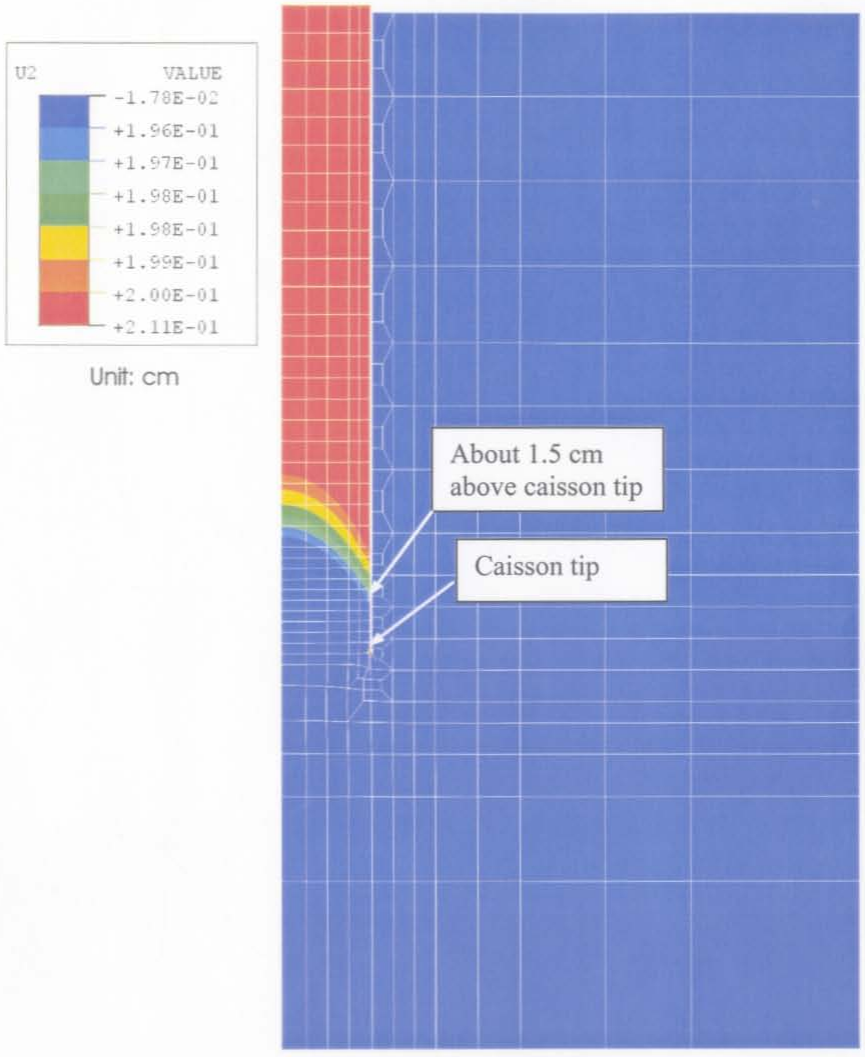

Figure 5.25: Vertical displacement contours at maximum value of 2.1mm (model scale)

5.4.2 Pullout Resistance Mobilization

Figure 5.26 presents a comparison between the total pullout force obtained from the finite element analysis and those measured in the centrifuge test. The experimental curves showed a general monotonic increase with some fluctuations to 0.5 kN and then flattening out due to the resolution of displacement measurements in centrifuge test (at 100 g). Generally, the finite element analysis results indicated that the pullout force developed very rapidly as the caisson's vertical displacement increased. The peak pullout force value was reached after a vertical displacement equivalent to about 2% of the caisson diameter. The agreement between the total pullout force versus pullout displacement curve obtained from the finite element analysis and that measured in the centrifuge test is very encouraging.

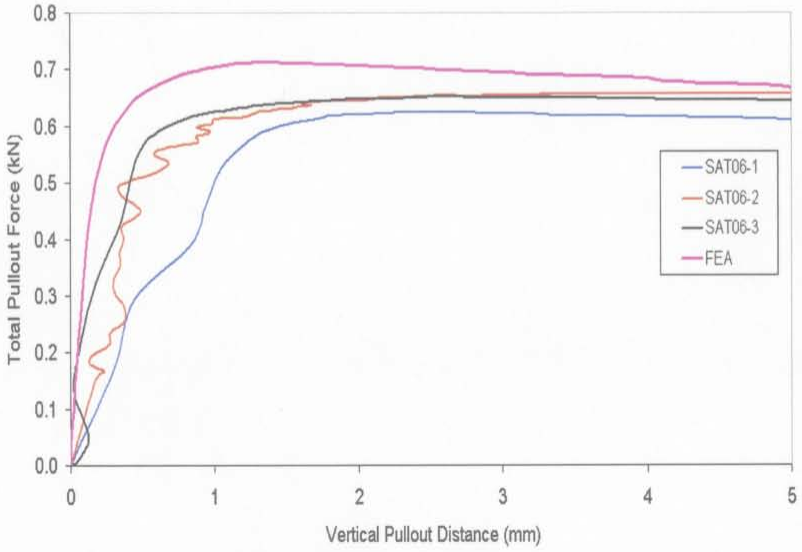

Figure 5.26: Comparison of total pullout force development (model scale)

When the passive suctions were generated by the finite element model (ABAQUS software), the pullout capacity of a suction caisson was about 10 to 15% larger than the measured capacities, Figure 5.26. However, when the measured passive suctions were used in the FEA as input data, the pullout capacity was about 10% less than the measured capacities, Figure 5.11. As the intent of this FEA study was to numerically simulate the generation of passive suction, the same conditions as centrifuge test SAT06 (i.e., caisson geometries, soil parameters and loading) were used. No parameter study or calibration was performed to fit the capacity curves. Therefore, one should exercise caution when using this method for modeling passive suction for practical projects. However, this difference is mainly attributable to the calculated rapid mobilization of the passive suction compared to that measured as described in Section 5.4.3.

5.4.3 Mobilization of Passive Suction

Figure 5.27 presents a comparison between the passive suction development observed in the finite element analysis and that measured in the centrifuge test. The finite element analysis results indicated a faster development of passive suction compared to that measured in the centrifuge test. Also, the passive suction obtained from the finite element analysis started to drop off after it reached the peak. The peak/maximum passive suction measured in the centrifuge test, on the other hand, remained constant to a relatively large vertical displacement.

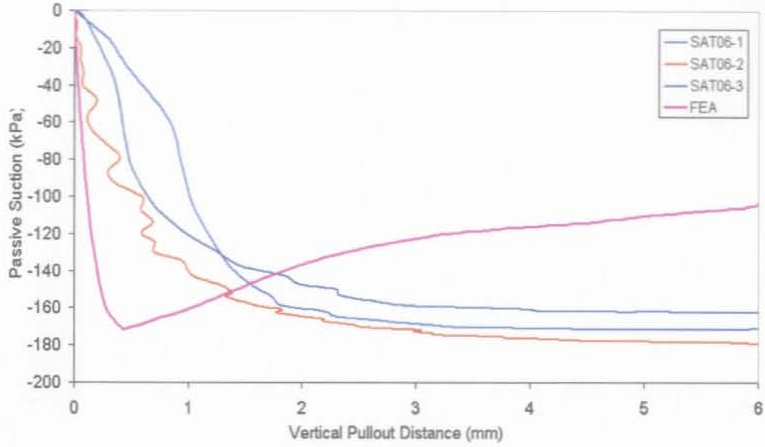

Figure 5.27: Comparison of passive suction development (model scale)

The passive suction development measured in the centrifuge test is different from that predicted by the finite element analysis due to the limitations of the numerical model. These limitations include the simulation of the discontinuous materials using a continuum medium and the behavior of the Cam-Clay model in extension (i.e., subyield behavior of soil mass and soil permeability). Moreover, the FEA was performed using the soil properties of the clay testbeds to compare with the centrifuge test results, not to fit the centrifuge test curves. However, it can be concluded that passive suction may be reasonably simulated using finite element analysis.

5.4.4 Excess Pore Pressure (EPP) Development in Soil

The pullout of the caisson develops excess pore pressures in the soil. These excess pore pressures influence the effective stress in the soil, which affects the development of the pullout capacity.

Figure 5.28 presents the distribution and the development of the excess pore pressures in the soil along the caisson's inside wall and below its tip in the finite element analysis. The excess pore pressures in the soil decreased with depth from 168 kPa at 25 mm below mudline to 20 kPa at about one diameter below the caisson's tip (232 mm below mudline). The maximum excess pore pressures in the soil at various elevations were developed at a vertical displacement of about 1% caisson's diameter. They started to drop off after the peak to approximate 80% at the vertical displacement of 5% diameter, and the remaining EPPs were maintained to a relatively large vertical displacement.

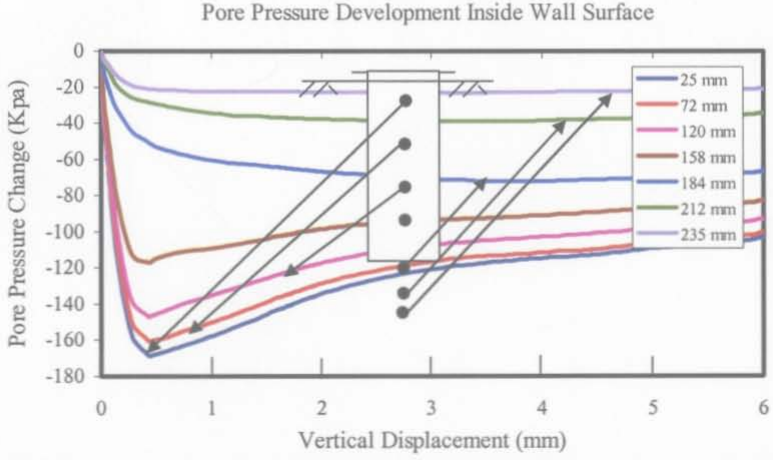

Figure 5.28: Excess pore pressure development along inside wall surface (model scale)

As the caisson's top was sealed and a very low permeability in its wall ($1.0x10^{-14}$ mm/second) was assumed in the finite element analysis, very little seepage occurred between the inside soil and the outside soil through the caisson's top and wall (as shown in Figures 5.29 and 5.30) during pullout. Therefore, the excess pore pressures in the inside soil were higher than those in the outside soil at the same elevation in the FEA. This was also confirmed at mudline by comparing the readings of the PPT mounted inside caisson top with these of the PPT embedded in top soil outside the caisson in the centrifuge tests of this study (see Figure 4.26).

Seepage between the outside soil and the inside soil will occur during the pullout of the caisson due to the generation of passive suction inside the caisson. This seepage in return affected the EPPs in the inside soil. The faster the seepage occurs, the faster the EPPs are dissipated. Generally, the seepage rate depends on the seepage path length, and the influence of the seepage on the EPP dissipation rate decreases with increase of its path distance. As shown in Figure 5.30, the only way for the occurrence of seepage between the outside soil and the inside soil during the pullout is around the caisson's tip. The seepage path distance for the soil inside the caisson increases with their elevation from the tip to the mudline. Therefore, the EPPs in the soil inside the caisson obtained by FEA decreased with depth from the mudline to the caisson's tip.

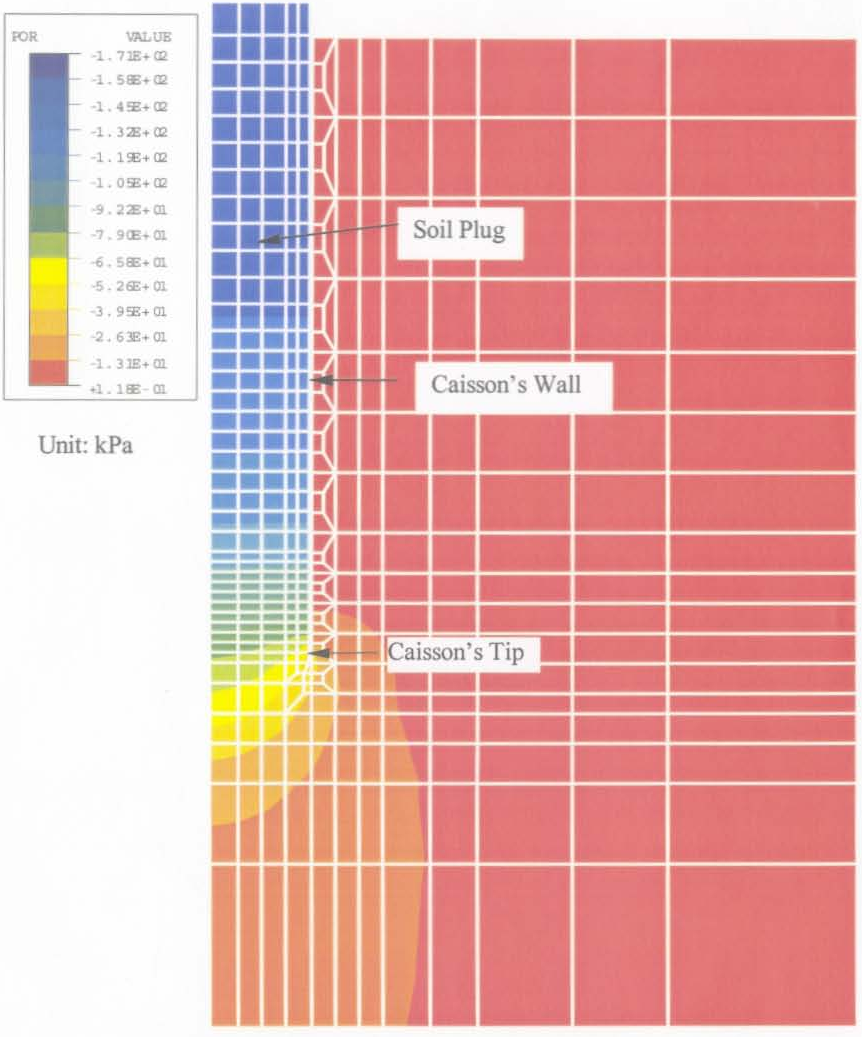

Figure 5.29: Distribution of the EPPs in the soil at 0.5 mm displacement (model scale)

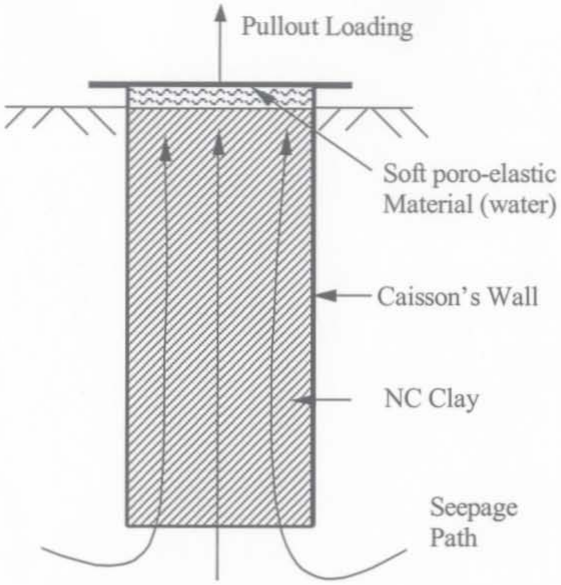

Figure 5.30: Seepage from the tip to the inside soil

Figure 5.31 presents the distribution and development of the excess pore pressures in the soil along the caisson's outside wall. The excess pore pressure increased from about 1 kPa at 25 mm below mudline to approximate 70 kPa at 184 mm, and then decreased to 20 kPa at about one diameter below the tip (235 mm below mudline). The EPPs increased with depth in the outside soil from mudline to the caisson's tip and then decreased with depth in the soil below the tip. However, as shown in Figure 5.28, the EPPs inside the caisson decreased from about 168 kPa at 25 mm below mudline to 20 kPa at about one diameter belop caisson's tip (232 mm below mudline). The distribution of the excess pore pressures in the soil outside the caisson is different from that in the soil inside the caisson. This difference was due to the change of the seepage gradient. As shown in

Figure 5.30, the seepage path in the soil was from mudline outside caisson to the caisson's tip and finally to the inside caisson top, resulting in an increase of seepage gradient with depth from mudline to the caisson's tip outside the caisson, and a decrease of seepage gradient with depth inside caisson from mudline to its tip.

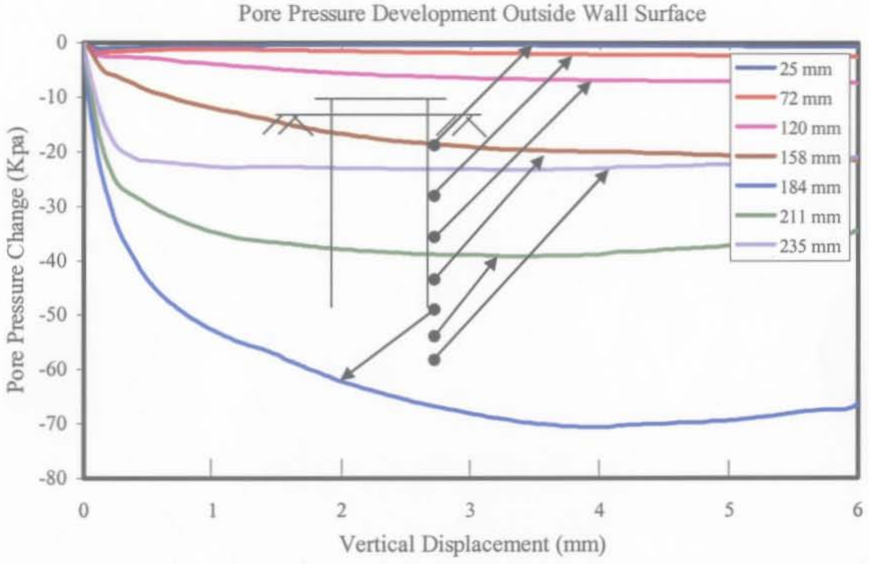

Figure 5.31: Excess pore pressure development along outside wall surface (model scale)

Figure 5.32 presents the EPPs in the soil along the outside caisson wall obtained in the FEA during pullout. The mobilized EPPs in the soil outside caisson increased with depth from mudline to the caisson's tip and followed a decrease with depth below. This also indicated that the passive suction was mobilized in the soil at the caisson tip during pullout phase of the caisson.

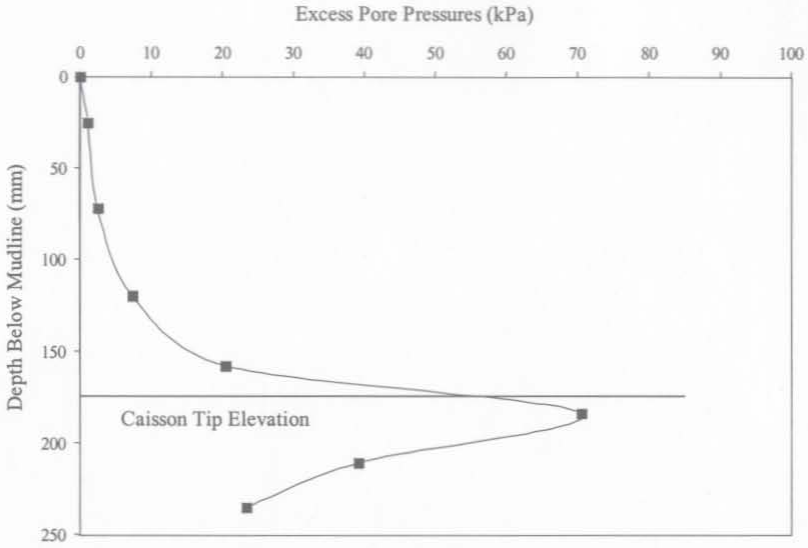

Figure 5.32: EPPs in the soil along outside caisson wall during pullout from FEA (model scale)

Figure 5.33 presents the distribution and development of the excess pore pressures in the soil, 20 mm away from the outside wall of the caisson and different depths below mudline in the finite element analysis. The excess pore pressures increased from 1 kPa at 25 mm below mudline to 25 kPa at 206 mm, and then decreased to 16 kPa at one diameter below the tip (232 mm below mudline).

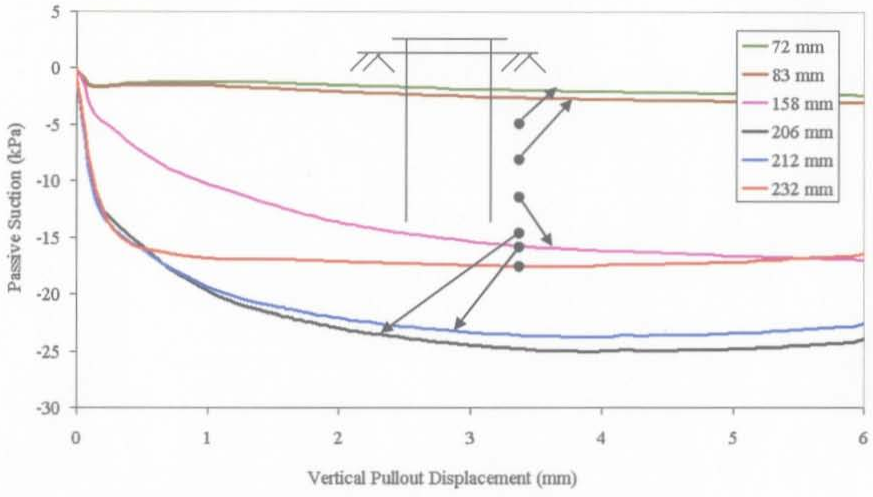

Figure 5.33: EPP development from FEA analysis
-20 mm away from outside caisson wall (model scale)

The distribution and development of the excess pore pressures at those positions were also monitored in the centrifuge tests. Figures 5.34 and 5.35 present the results of Test SAT06. The EPPs recorded by the top two PPTs (i.e., 72 and 83 mm below mudline) are small positive values, which are different from the FEA results. Generally, the distribution and development of the excess pore pressures obtained in finite element analyses had the same tendency with the centrifuge test results: the EPPs in the soil outside the caisson increased with depth from mudline to approximate the caisson's tip, then they decreased with depth. The passive suction inside caisson top predicted by FEA is reasonably close to that measured in centrifuge tests. However, the FEA predicted a very large gradient of EPP through the base of the soil plug inside the caisson and local to caisson's tip (see Figure 5.29). A different EPP distribution is inferred from one

measurement at 158 mm with high EPP of 120 kPa. Other measured values of EPPs seem reasonably close to those predicted by the FEA.

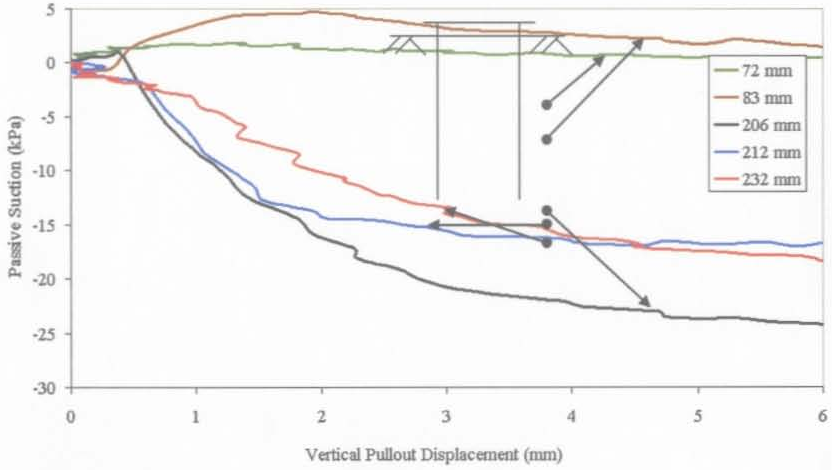

Figure 5.34: Excess Pore pressure development from centrifuge test - I (model scale)

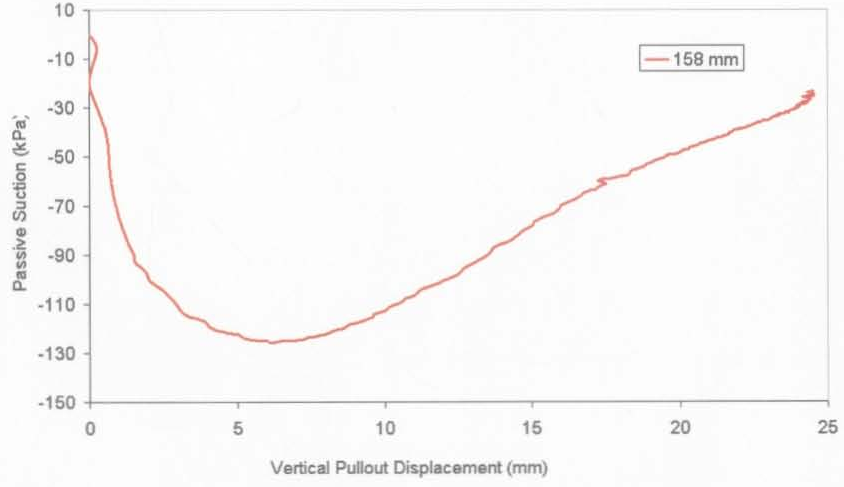

Figure 5.35: Excess Pore pressure development from centrifuge test - II (model scale)

5.5 Summary

A finite element analysis was performed to simulate passive suction that was generated in the soil inside and below the caisson during pullout of a suction caisson in this study. Three aspects were considered:

1. The water inside the caisson top was replaced by a soft porous-elastic material through which passive suction was applied at the top of caisson.

2. Perfect contact between soft porous-elastic material and the caisson cap was assumed. The top surface of the soft porous-elastic material didn't have any relative movement with the respect to the caisson cap during pulling out.

3. The soil surface inside the caisson was constrained from horizontal movement, resulting in the elimination of cavity development between soil and caisson's inside wall.

Based on the finite element analysis conducted in this study, the following is concluded:

1. The finite element analysis verified that a confined shear failure mechanism was the most appropriate one to describe the failure of suction caissons under an undrained loading condition (fast loading rate) in NC or SOC clay. The reverse end bearing (passive suction) developed fast with the displacement.

2. When the water inside the caisson top was replaced by a soft porous-elastic material, passive suction could be transferred to the caisson top by this material.

3. Although the passive suction versus pullout displacement curve obtained in the finite element analysis was different from that measured in the centrifuge tests, the maximum values of the suction were very close.

4. The total pullout force versus pullout displacement curve obtained from the finite element analysis was in agreement with those from centrifuge tests.

Chapter 6
Conclusions and Future Work

Suction caissons have been used as mooring systems for offshore structures since the mid-1980s due to their competitive technical and economical advantages over driven piles and drag embedment anchors. Over the last five years, suction caissons have become the foundation of choice for anchoring deepwater floating structures (e.g. SPARs, DDCVs, semis) or supporting seabed founded systems (e.g., well heads, SDUs, UTAs). However, several working principles are still not fully understood. The main aim of the work described in this thesis was to investigate the behavior of suction caissons installed in clay using both centrifuge model tests and finite element analyses, including penetration resistance during both self-weight and suction penetration, the distribution of the excess pore pressures induced by installation in clay and their dissipation with time, the failure mechanism of suction caissons in clay, the development of passive suction during pullout of the caisson, and the setup development after installation.

The research program was predominantly experimentally oriented, with a series of centrifuge model tests performed to obtain accurate and detailed data regarding the behavior of suction caissons in NC or SOC clay under an undrained loading condition (fast loading rate). Three sizes of caissons were used. Experimental data obtained from the centrifuge tests were analyzed to investigate the penetration resistance, gain insight into the physical mechanism that governs the response in uplift loading of the caisson.

The excess pore pressures in clay around the caisson due to the installation and the uplift loading were examined. A setup curve describing the development of the external friction with time after the installation of the caisson was obtained. The numerical work associated with this research programme was mainly focused on one of the centrifuge model tests, i.e., a model caisson with 51.7 mm out-diameter and an embedment of about 184 mm. The pullout behavior of the caisson under a vertical loading on its top was investigated. The generation of the passive suction was simulated through replacing the water at inside top of the caisson using a soft porous-elastic material. A detailed summary has been given at the end of each chapter, and following conclusions are drawn:

1. The penetration resistance had a sudden increase from the end of self-weight penetration to the beginning of suction penetration, resulting in an increase of $\alpha_{pe.}$ When active suction was applied, a different "soil flow" pattern from that during self-weight penetration has been caused. On the other hand, the EPPs in the soil outside the caisson were dissipated during this time interval and the effective stress in the soil also increased, leading to an increase of the outside skin friction. Centrifuge test results showed that the value of friction coefficient α_{pe} could have an increase by 0.2 or more during this time. In order to reduce the penetration resistance, the stopping time from the end of self-weight penetration to the beginning of suction penetration should be minimized.

2. The penetration friction coefficient was affected by the wall thickness. The larger the ratio of diameter to wall thickness (D/Δ), the smaller the friction coefficient.

3. For caissons with D/Δ ratio (diameter to wall thickness) from 64 to 79 and H/D ratio (embedment to diameter) from 1.8 to 3.5, the penetration resistance can be predicted by using a friction coefficient α_{pe} = 0.2 for self-weight penetration and α_{pe} = 0.3 for suction penetration. For caissons with a D/Δ ratio of about 28 and a H/D ratio of about 5.5, the penetration resistance can be calculated using α_{pe} = 0.3 for self-weight penetration and α_{pe} = 0.5 for suction penetration.

4. The excess pore pressures (EPPs) generated in the soil during installation increased with depth from mudline to the maximum penetration depth (i.e., tip of the caisson). Then, the EPPs in the soil quickly decreased to a small value at a distance equal to 0.5 times the caisson diameter below the caisson's tip. Cylindrical cavity expansion theory (Eq. 2.5), developed initially for driven piles, can also be used to well estimate the distribution of the initial EPPs in the soil induced during installation of a suction caisson.

5. Centrifuge tests showed that, after installation of the caisson, 50, 80 and 90% EPPs dissipated at time factors (T) of about 4, 16 and 26, respectively. Even though those results are local measurements, as discussed in Section 4.3.2, it may be appropriate when they are used to estimate the EPP dissipation in suction caisson design.

6. Radial consolidation theory (Eq. 4.10) can be used to predict the dissipation of the EPPs in the soil induced by installation of a suction caisson. The theoretical time factor (T) values are larger than the test results for a given degree of consolidation. This

difference is attributed to the vertical dissipation at the seafloor and caisson's tip in the model test.

7. Modified Bogard and Matlock method (initially derived for driven piles) can also be used to predict the dissipation of the EPPs in clay soils for suction caissons, provided adjustments are made to the diameter or the wall thickness of the caisson, so as to keep the ratio of diameter to wall thickness (D/Δ) to a maximum value of 48.

8. Both centrifuge tests and finite element analysis verified that a confined shear failure mechanism was the most appropriate one to describe the failure of suction caissons in NC and SOC clay under the conditions of this study (i.e., caisson geometries and fast loading condition). The pullout capacity of a suction caisson can be predicted using Eq. 4.23. The reverse end bearing (passive suction) developed fast with the pullout displacement. A displacement of approximately 4 to 10% caisson diameter was required to mobilize both the passive suction and the maximum pullout capacity of the caisson. The reverse end bearing (passive suction force) was in range of 40 to 60% of the maximum pullout capacity, resulting in the reverse end bearing factor varying from 6.5 to 10.8, with an average of 8.7.

9. Centrifuge test results showed that, the friction coefficient during pullout of the caisson increased with time from 0.65 to 0.95 with the time factor T from 3.5 to 46 after installation. Compared with the values of the friction coefficient during installation (i.e., 0.15 to 0.6 during self-weight penetration and 0.25 to 0.35 during suction penetration), the friction coefficient during pullout of the caisson is much bigger than that during

installation. This is due to the increase of the effective stress with the dissipation of the excess pore pressures in the soil during the time period from the end of installation to the beginning of pullout test.

10. The setup of the soil and caisson increased with the time after installation. 60 to 75%, 75 to 85 % and at least 95% wall skin friction could be mobilized in a time with a time factor (T) of 3.5, 11.4, and 46 after the caisson was installed. The setup development with time can be predicted using Eq. 4.28.

11. The behavior of suction caissons subjected to uplift loading can be investigated using finite element analysis when some aspects are taken into consideration. The passive suction could be reasonably simulated by the change of the excess pore pressures in the soil, and the suction was transferred to the caisson top by a soft porous-elastic material replacing the water inside the caisson top. Contact surface elements were used to well model the behavior of the caisson-soil interaction. The total pullout force versus pullout displacement curve obtained from finite element analysis was in agreement with those measured in the centrifuge tests. Although the passive suction versus pullout displacement curve generated by the finite element analyses is slightly different from that obtained using the results of the centrifuge tests, the values of the maximum developed suction are very close.

This research has been primarily concerned with the penetration resistance, EPP development, failure mechanism and setup development of suction caissons in clay. The present work can be extended to include many other aspects for further research. Some of

the further work that could be carried out for a better understanding of the behavior of suction caissons includes:

1. Suction caissons are usually subjected to inclined loading and dynamic loading. Their long term pullout capacity depends on both the cable angle and the loading characteristics, and more studies are required.

2. More work is required to extend the finite element model in this study so that it can simulate the behavior of suction caissons, including their installation, the environmental loading, and the soil conditions.

3. As caissons with internal ring stiffeners are widely used, the geotechnical consequences of those stiffeners are one of the design issues. More studies are needed to fully understand these.

References

Airhart, T.P., Coyle, H.M., Hirsch, T.J. and Buchanan, S.J. (1969). "Pile-Soil System Response In A Cohesive Soil," ASTM, STP 444, pp264-294.

Albertsen, N.D, and Beard, R.M. (1982). "State-of-the–art Assessment of High Capacity Sea Floor Anchors," ICE, Offshore Moorings, Thomas Telford Ltd, Landon, pp 129-142.

Al-Tabbaa, A. (1987). "Permeability and Stress-Strain Response of Speswhite Kaolin," Ph. D. Thesis, Cambridge University, England.

Al-Tabbaa, A. and Muir Wood, D. (1987). "Some Mesurements of the Permeability of Kaolin," *Géotechnique*, 37, No.4, pp 499-503.

Al-Tabbaa, A. and Muir Wood, D. (1991). "Horizontal Drainage during Consolidation: Insights Gained from Analyses of a Simple Problem," *Géotechnique*, 41, pp 571-585.

American Petroleum Institute (API), (1993). "Recommended Practice for Planning, Designing, and Constructing Fixed Offshore Platforms-Load and Resistance Factor Design, API Recommended Practice 2A-LRFD (RP 2A-LRFD)," 1st Ed., API, Washington, D.C.

Andersen, K.H., and Jostad, H.P. (2002). "Shear Strength Along Outside Wall of Suction Anchors in Clay After Installation," Proceedings of 12th International Offshore and Polar Engineering Conference, Kitayushu, Japan, ISOPE, Vol. 2, pp 785-794.

Andréasson, B., Christophersen, H.P., and Kvalstad, T.J. (1988). "Field Model Tests and Analyses of Suction Installed Long-Skirted Foundations," Proceedings of the International Conference on Behavior of Offshore Structures, pp 243-257.

Audibert, J.M.E., Nyman, D.J., and O'Rourke, T.D. (1984). "Differential Ground Movement Effects on Buried Pipeline," Part Five of "Guidelines for the Seismic Design of Oil and Gas Pipeline Systems", prepared by the Committee on Gas and Liquid Fuel Lifelines of the ASCE Technical Council on Lifeline Earthquake Engineering, published by the American Society of Civil Engineers, New York.

Audibert, J.M.E, Huang, J. and Clukey E. (2003). "Suction Caisson Installation at Horn Mountain – A Case History," Proceedings of 13th International Offshore and Polar Engineering Conference, Honolulu, USA.

Bezuijen, A. and Hjortnaes-Pedersen, A.G.I. (1992). "Offshore Skirt Penetration in the Geo-centrifuge," Proceedings of the Second(1992) International Offshore and Polar Engineering Conference", pp 463-469.

Bogard J.D. and Matlock H. (1990). "Application of Model Pile Tests to Axial Pile Design," Proceedings, 22nd Offshore Technology Conference, Houston, Texas, Paper No. 6376.

Bolton, M.D., Gui, M.W., and Phillips, R. (1993). "Review of Miniature Soil Probes for Model Tests," Proceeding of 11th SEAGC, Singapore.

Bowles, J.E. (1992). "Engineering Properties of Soils and Their Measurement," Fourth Edition, Irwin/McGraw-Hill Company.

Bransby, M.F. (1993). "Centrifuge Test Investigation of the Buttonhole Foundation Technique," Data Report, Cambridge University, England.

Brown, G.A., and Nacci, V.A. (1971). "Performance of Hydrostatic Anchors in Granular Soils," Offshore Technology Conference, OTC 1472, pp II533-II537.

C-CORE (1999). "Finite Element Analysis of Pipe/Soil Interaction; Phase 1 – Two-dimensional Plane Strain Analyses," Contract Report for the Geological Survey of Canada, C-CORE Publication No.99-C23.

C-CORE (2001). "3D Finite Element Analysis of Pipe/Soil Interaction," Contract Report for the Geological Survey of Canada, Minerals Management Services, Chevron Petroleum Technology, and Petro-Canada Resources, C-CORE Publication 01-C08.

Cao, J., Phillips, R. and Popescu, R. (2001). "Physical and Numerical Modelling on Suction Caissons in Clay," 18th Canadian Congress of Applied Mechanics CANCAM 2001 Memorial University of Newfoundland June 3-7, pp 217-218.

Cao, J., Phillips, R., Popescu, R., Al-Khafaji, Z. and Audibert J.M.E. (2002). "Penetration Resistance of Suction Caissons in Clay," Proceedings of 12th International Offshore and Polar Engineering Conference, Kitayushu, Japan, ISOPE, Vol. 2, pp 800-806.

Chicata, L.F.G.V. (2000). "Computational Procedure for the Estimation of Pile Capacity Including Simulation of the Installation Process," Ph. D. thesis, The University of Texas at Austin.

Christensen, N.H., Haahr, F., and Rasmussen, J.L. (1991). "Breakout Resistance of Large Suction Piles," 1991 OMAE-Volume I-B, Offshore Technology, pp 617-622.

Christensen, N.H. and Haahr, F. (1992). "A Computer Program to Analyze Suction Effects," Offshore Technology Conference, OTC 6845, pp 331-338.

Clukey, E.C., and Morrison, M.J. (1993). "A Centrifuge and Analytical Study to Evaluate Suction Caissons for TLP Applications in the Gulf of Mexico," Design and Performance of Deep Foundations: Piles and Piers in Soil and Soft Rock, Proceedings, Dallas, Texas, PP 141-156.

Clukey, E.C. and Phillips, R. (2002). "Centrifuge Model Test to Verify Suction Caisson Capacities for Taut and Semi-Taut Legged Mooring Systems," Deep Offshore Technology International Conference, New Orleans, November 13-15.

Colliat, J-L., Boisard, P., Gramet, J-C., and Sparrevik, P. (1996). "Design and Installation of Suction Anchor Piles at a Soft Clay Site," Offshore Technology Conference, OTC 8150, pp 325-335.

Das, B.M., Shin, E.C., Dass, R.N., and Omar, M.T. (1994). "Suction Force Below Plate Anchors in Soft Clay," Marine Georesources and Geotechnology", Vol. 12, pp 71-81.

Das, B.M. (1997). "Principles of Geotechnical Engineering," Fourth Edition, PWS Publishing Company.

Datta, M., and Kumar, P. (1996). "Suction Beneath Cylindrical Anchors in Soft Clay," Proceedings of the Sixth (1996) – International Offshore and Polar Engineering Conference, pp 544-548.

Dendani, H. and Colliat, J.L. (2002). "Girassol: Design Analysis and Installation of the Suction Anchors," Offshore Technology Conference, Houston ,OTC14209.

Deng, W. and Carter, J.P. (2000a). "Inclined Uplift Capacity of Suction Caissons in Sand," 2000' OTC 12196, Houston, Texas, May 1-4.

Deng, W. and Carter, J.P. (2000b). "Uplift Capacity of Suction Caissons in Uniform Soil," Personal Communication.

Deng, W., Carter, J. P. and Taiebat (2000). "Prediction of the Lateral Capacity of Suction Caissons," Personal Communication.

Deng, W. and Carter, J.P. (2002). "A Theoretical Study of the Vertical Uplift Capacity of Suction Caissons," International Journal of Offshore and Polar Engineering, Vol.12, No.2, pp 89-97.

Desai, C.S., and Christian, J.T. (1977). "Numerical Methods in Geotechnical Engineering," McGraw-Hill, Inc., New York.

El-Gharbawy, S., and Olson, R. (1998). "The Pullout Capacity of Suction Caisson Foundations for Tension Leg Platforms," Proceedings of the Eighth(1998) – International Offshore and Polar Engineering Conference, pp 531-536.

Ellis, E.A. (1993). "Lateral Loading of Bridge Abutment Piles due to Soil Movement," First Year Report, Cambridge University, England.

Erbrich, C., and Hefer, P. (2002). "Installation of the Laminaria Suction Piles – A Case History," Offshore Technology Conference, OTC 14240.

Eslami, A. and Fellenius, B.H. (1997). "Pile Capacity by Direct CPT and CPTU Methods Applied to 102 Case Histories," *Canadian Geotechnical Journal*, Vol.34, pp886 – 904.

Fines, S., Stove, O.J., and Guldberg, F. (1991). "Snorre TLP Tethers and Foundation," Offshore Technology Conference, OTC 6623, pp 587-597.

Fuglsang, L.D., and Steensen-Bach, J.O. (1991). "Breakout Resistance of Suction Piles in Clay," Centrifuge 91, pp 153-159.

Guo, W.D. (2000). "Viso-elastic Consolidation Subsequent to Pile Installation," *Computers and Geotechnics*, 26, pp113-144.

Handayanu, Swamidas A.S.J. and Booton M., (2000). "Ultimate Strength of Offshore Tension Foundations under Vertical and Inclined Loads," Proceedings of OMAE 2000, 19th International Conference on Offshore Mechanics and Artic Engineering, February 14-17, New Orleans, Lpuisiana, USA.

Hibbitt, Karlsson & Sorensen, Inc. (1998). "ABAQUS/Standard User's Manuals," Version 5.8.

Hight, D.W., Potts, D.M., and Tjelta, T.I. (1988). "Finite Element Analyses of a Deep Skirted Gravity Base," Proc. of International Conference on Behavior of Offshore Structure, pp 209-220.

Hjortnaes-Pedersen, A.G.I., and Bezuijen, A. (1992). "Offshore Skirt Penetration in Clay in the Geo-centrifuge," Proceedings of 6th International On Behavior of Offshore Foundation, London, 1-15.

Hogervorst, J.R. (1980). "Field Trails with Large Diameter Suction Piles," Offshore Technology Conference, OTC3187, pp 217-224.

House A.R. and Randolph M.F. (2001). "Centrifuge Modelling of Caisson Capacity Under Uplift Loading," Constitutive and Centrifuge Modeling: Two extremes. Monte Verita, Centro Stefano Franscini, July 8 – 13.

Jones, W.C., Iskander, M.G., Olson, R.E., and Goldberg, A.D. (1994). "Axial Capacity of Suction Piles in Sand," The 7th International Conference on the Behavior of Offshore Structures".

Koizumi, Y. and Ito, (1967). "Field Test with Regard to Pile Driving and Bearing Capacity of Piled Foundations," Soils and Foundations, No. 3, 30.

Kolk, H.J. and Kay, S. (2002). "North Nemba Flare Bucket Foundations," Offshore Technology Conference, Houston ,OTC13057.

Lacasse, S. (1999). "Ninth OTRC Honors Lecture: Geotechnical Contributions to Offshore Development," Offshore Technology Conference, Houston, OTC10822.

Larsen, P. (1989). "Suction Anchors as an Anchoring System for Floating offshore Constructions," Offshore Technology Conference, OTC 6029, pp 535-540.

Lo, K.Y. and Stermac, A.G. (1965). "Induced Pore Pressures During Pile Driving Operations," Proceedings of the 6th International Conference, S.M. & F.E., Vol.2, 285.

Lunne, T. and Kleven, A, (1981). "Role of CPT in North Sea Foundation Engineering," Proceedings of the 1981 Offshore Technology Conference, Houston, Texas, Vol.4, pp 305-317.

Lunne, T., Roberston, P.K. and Powell, J.T.M., (1991). "Cone Penetration Test in Geotechnical Practice," Balackie Academic and professional, an inprint of Chapman and Hall.

Morrison, M.J., and Clukey, E.C. (1994). "Behavior of Suction Caissons under Static Uplift Loading," International Conference Centrifuge 94, Singapore, pp 823-828.

Norwegian Geotechnical Institute, NGI (1999). "Set-up effects outside skirt wall," Joint industry project.

Nunez, L. (1989). "Tension Piles in Clay," Ph. D. Thesis, Cambridge University, England.

Orrie, O. and Broms, B.B., (1967). "Effects of Pile Driving on Soil Properties," J.S.M.F.D., ASCE, Vol. 93, SM5, pp 59-73.

Phillips, R. (1986). "Ground Deformations in the Vicinity of a Trench Heading," Ph.D. Thesis, Cambridge University.

Phillips, R. (1988). "Lynxvale Limited Centrifuge Lateral Pile Tests in Clay (Exhibit A – PR – 10582) Tasks 2 and 3 - Final Report".

Phillips, R. (1989). "Centrifuge Lateral Pile Tests in Clay (Exhibit A – PR – 10592) Task 1 - Final Report," prepared by the Soil Mechanics Group at Cambridge University for Lynxvale Limited, June.

Phillips, R. (1995). "Practical considerations in centrifuge modeling," Chapter 3, Geotechnical Centrifuge Technology edited by Taylor, Blackie Academic & Professional, McGraw-Hill, London.

Phillips, R. (1998). "Relationship of *e* and Effective Vertical Stress of Clay," Personal Communication.

Phillips, R., Clark, J.I., Paulin, M.J., Meaney, R., Millan, D.E.L., and Tuff, K., (1994). "Canadian National Centrifuge Center With Cold Regions Capabilities," Centrifuge 94, pp 57-61.

Poorooshasb, F. (1991). "Centrifuge Modeling of laterally Loaded Pipelines," Contract Report for NOVA Corporation of Alberta, C-CORE Contact Number 91-C14.

Popescu R., Konuk, I., Guo, P. and Nobahar, A. (2002). "Some Aspects in Numerical Analysis of Pipe-Soil Interaction," Proceedings of 2nd Canadian Specialty Conference on Computer Applications in Geotechnique, pp 290-297.

Randolph and Wroth, C.P. (1979). "An Analytical Solution For The Consolidation Around A Driven Pile," Internal Journal for Numerical and Analytical methods in Geomechnics. Vol. 3, pp.217-229.

Randolph, M. F., Carter, J. P., and Wroth, C. P. (1979). "Driven Piles in Clay – the Effects of Installation and Subsequent Consolidation," *Géotechnique* 19, No. 4, pp 361-393.

Randolph, M.F. and Houlsby, G.T. (1984). "The limiting Pressure on a Circular Pile Loaded laterally in Cohesive Soil," *Géotechnique* 34, No. 4, pp 613-623.

Randolph, M.F. and House, A.R. (2002). "Analysis of Suction Caisson Capacity in Clay," Offshore Technology Conference, OTC 14236.

Rao, S.N., Ravi, R., and Ganapathy, C. (1997). "Pullout behavior of Model Suction Anchors in Soft Marine Clays," Proceedings of the Seventh – International Offshore and Polar Engineering Conference, pp 740-744.

Reese, L.C. and Seed, H.B. (1955). "Pressure Distribution Along Friction Piles," Proceedings, American Society for Testing and Materials, Philadelphia, PA, Vol. 55, pp1156-1182.

Renzi, R., Maggioni, W., and Smits, F. (1991). "A Centrifuge Study on the Behavior of Suction Piles," Centrifuge 91, pp 169-176.

Rognlien, B., Eriksen, K., Sparrevik,P., and Baerheim, M. (1991). "Caisson Foundations for Jacket Structures," Proceedings of the First (1991) International Offshore and Polar Engineering Conference, Edinburgh, UK, August 11 – 16.

Schofield, A.N. (1980). "Cambridge geotechnical centrifuge operations," *Géotechnique*, 20, PP. 227-268.

Senpere, D. and Auvergne, G.A. (1982). "Suction Anchor Piles – A Proven Alternative to Driving or Drilling," Offshore Technology Conference, OTC 4206, pp 483-493.

Sharma, J.S. (1994). "Behavior of Reinforced Embankments on Soft Clay," Ph. D. Thesis, Cambridge University, England.

Soderberg, L.O. (1962). "Consolidation theory applied to foundation pile time effects," *Géotechnique*, 12, No.3, pp 217-225.

Sparrevik, P. (1998). "Suction Anchor – A Versatile Foundation Concept Finding Its Place in the Offshore Market," Proceedings of 17th International Conference on Offshore Mechanics and Arctic Engineering, OMAE 98-3096.

Sparrevik, P. (2002). "Suction Pile Technology and Installation in Deep Waters," Offshore Technology Conference, OCT 14241.

Springman, S.M. (1989). "Lateral Loading of Piles due to Simulated Embankment Construction," Ph. D. Thesis, Cambridge University, England.

Springman, S.M. (1993). "Centrifuge Modeling in Clay: Marine Applications," Proceedings of the 4th Canadian Conference on Marine Geotechnical Engineering, Vol. 3, pp 853-896.

Stas, C.V. and Kulhawy, F.H. (1983). "Critical Evaluation of Design Methods for Foundations Under Axial Uplift and Compression Loading," Report on Research Project 1493-1, EPRI, Cornell University, Ithaca, New York.

Steensen-Bach, J.O. (1992), "Recent Model Tests with Suction Piles in Clay and Sand," Offshore Technology Conference, OCT 6844, pp 323-330.

Stove, O.J., Bysveen, S., and Christophersen, H.P. (1992). "New Foundation for Snorre Development," Offshore Technology Conference, OCT 6882, pp 78-83.

Taylor, R.N. (1995). "Geotechnical Centrifuge Technology," Blackie Academic & Professional, McGraw-Hill, London.

Templeton J.S. (2002). "The Role of Finite Elements in Suction Foundation Design Analysis," Offshore Technology Conference, OTC 14235.

Tjelta, T.I., Guttormsen, T.R., and Hermstad, J. (1986). "Large-Scale Penetration Tests at a Deepwater Site," Offshore Technology Cenference, OTC 5103, pp 201-212

Tjelta, T.I., Aas, P.M., Hermstad, J., and Andenaes, E. (1990). "The Skirt Piled Gullfaks C Platform Installation," Offshore Technology Conference, OTC 6743, pp 453-462.

Tomlinson, M.J. (1957). "The Adhesion of Piles Driven into Clay Soils," Proceedings, Fourth International Conference on Soil Mechanics and Foundation Engineering, London, England, Vol. 2, pp 66-71.

Vanapalli, S.K. Fredlund, D.G, Pufahl, D.E. and Clifton, A.W. (1996). "Model for the prediction of shear strength with respect with soil suction," Canadian Geotechnical Journal, Vol.33, pp 379-392.

Walter, D. and Phillips, R. (1998). "Reduced Scale Centrifuge Modeling of Suction Anchors in Normally Consolidated Clay, Test SAT_01," C-CORE Publication 98-21.

Woodward, R. and Boitano, J. (1961). "Pile Loading Tests in Syiff Clays," Proceedings of the 5th International Conference, S.M. & F.E., Vol.2, 177.

Zdravkovic L., Potts D.M. and Jardine R.J. (1998). "Pull-out Capacity of Bucket Foundations in Soft Clay," Offshore Site Investigation and Foundation Behaviour '98, pp 301-324.

Zdravkovic L., Potts D.M. and Jardine R.J. (2001). "A parametric study of the pull-out capacity of bucket foundations in soft clay," *Géotechnique* 51, No. 1, pp 55-67.

Zhu, F. (1998). "Centrifuge Modelling and Numerical Analysis of Bearing Capacity of Ring Foundations on Sand," Ph. D. thesis, Memorial University of Newfoundland.

Zhu, G and Yin J-H. (2001). "Consolidation of Soil with Vertical and Horizontal Drainage under Ramo Load," *Géotechnique* 51, No. 4, pp. 361-367.